# Critical quantum liquids and the cuprate high temperature superconductors

### **Subir Sachdev**

Department of Physics, Harvard University, Cambridge MA 02138, USA. Center for Computational Quantum Physics, Flatiron Institute, 162 5th Avenue, New York, NY 10010, USA.

E-mail: sachdev@g.harvard.edu

13 July 2025

Abstract. We present a unified theoretical framework for the cuprate superconductors, rooted in a fractionalized Fermi liquid (FL\*) description of the intermediate-temperature pseudogap phase at low doping. In this approach, the FL\* state hosts small Fermi surfaces of electron-like quasiparticles that violate the conventional Luttinger count, which requires the presence of additional fractionalized excitations characteristic of a quantum spin liquid. Building on the proposal by Christos et al. (arXiv:2302.07885), we consider a critical spin liquid lacking quasiparticle excitations, one of whose low energy descriptions is an SU(2) gauge theory with  $N_f=2$  flavors of massless Dirac fermions.

This FL\* theory predicted hole pockets each of fractional area p/8 at hole doping p, in contrast to the area p/4 in a spin density wave state or its thermal fluctuation. A recent magnetotransport observation of the Yamaji angle is in good agreement with area p/8. We review a systematic method, based on the square lattice Hubbard model supplemented by ancilla qubits, to describe thermal fluctuations of the SU(2) gauge theory in the pseudogap, and explore multiple routes to confinement of the fractionalized excitations upon lowering temperature. A Monte Carlo study of the thermal SU(2) gauge theory models the Fermi arc spectra observed in photoemission and scanning tunneling microscopy. One route to confinement yields a d-wave superconductor via a Kosterlitz-Thouless transition of h/(2e) vortices, with nodal Bogoliubov quasiparticles featuring anisotropic velocities and vortices surrounded by charge order halos. An alternative route produces a charge-ordered metallic state that exhibits quantum oscillations in agreement with experimental data.

Increasing doping from the FL\* phase drives a transition to a conventional Fermi liquid at large doping, passing through an intermediate quantum-critical regime. We formulate a theory of this quantum-critical metal using a critical quantum 'charge' liquid of mobile electrons, developed via an extension of the Sachdev-Ye-Kitaev (SYK) model

This comprehensive perspective connects the pseudogap, superconducting, chargeordered, and strange metal phases within a single theoretical landscape.

## Contents

1	Introduction		
2	Critical spin liquid on the square lattice  2.1 Bosonic partons  2.1.1 Mean-field theory  2.1.2 Low energy U(1) gauge theory  2.1.3 Quantum criticality  2.2 Fermionic partons  2.2.1 Low energy SU(2) gauge theory.  2.3 SO(5) non-linear $\sigma$ -model	6 7 9 11 12 14 16	
3	Confinement to $d$ -wave superconductivity and charge order at half-filling	17	
4	Fractionalized Fermi liquids 4.1 Kondo lattice	22 23 25	
5	From the pseudogap to $d$ -wave superconductivity and competing orders  5.1 Anisotropic velocities in the $d$ -wave superconductor	30 31 32 34 34 35	
6	The SYK model 6.1 The WES-SYK model	<b>35</b>	
7	From the SYK model to strange metals 7.1 Universal model	42 43 48 48	

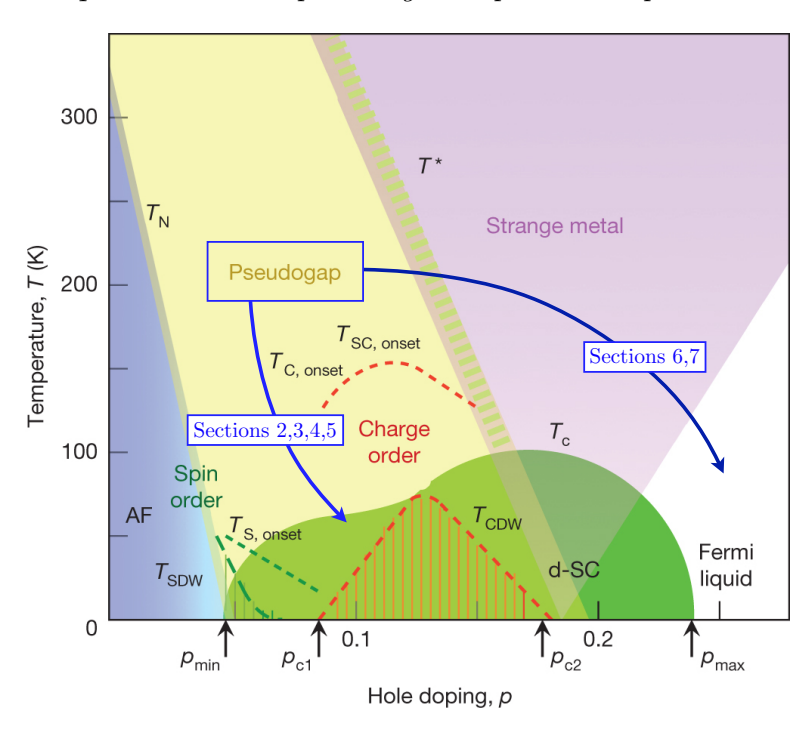


**Figure 1.** Cuprate phase diagram from Ref. [1]. Annotations in blue have been added. We use a theory of a fractionalized Fermi liquid (FL\*) of the pseudogap to connect to the other phases in the sections noted.

### 1. Introduction

This article presents a theoretical framework for the complex and rich phase diagram of the cuprate materials, see Fig. 1. Complex many-electron entanglement, which can give rise to quantum states of matter that lack any well-defined particle-like excitations, will play a central role. One such critical state is a particular quantum spin liquid, described in Section 2, in which the charge of some electrons is localized, while their spins remain entangled in a scale-invariant manner; it leads to a description of the pseudogap region of Fig. 1 and its low temperature instabilities. Another distinct critical state is associated with the collective dynamics of electron charge, a critical quantum 'charge' liquid, characteristic of the strange metal regime of Fig. 1; its theoretical description builds on concepts from the Sachdev-Ye-Kitaev (SYK) model, introduced in Section 6.

At large doping, p, where the  $T_c$  is relatively low, it is reasonable to apply the theory of spin-fluctuation mediated pairing of Fermi liquids (FL), leading to Cooper pairs around the Fermi surface, and the formation of a BCS-type superconductor. It is known that the spin fluctuations are antiferromagnetic, and antiferromagnetic spin fluctuations indeed lead to the observed d-wave pairing [2].

But this powerful paradigm runs into difficulty at lower p, and especially in the regime of the pseudogap, where there is no complete Fermi surface above  $T_c$  upon which the Cooper pairs can form. Nevertheless, below  $T_c$ , there is no dramatic change in the nature of the superconductivity with varying p, and so it is clear that the superconductor

itself is always adiabatically connected to a d-wave BCS state.

We shall address the low p phases here using a 'fractionalized Fermi liquid' [3, 4, 5, 6] (FL\*) theory of the pseudogap metal. The FL\* is a state with Fermi surfaces which do not enclose the Luttinger area, and this is possible if there is a 'background' spin liquid, as is reviewed in Section 4. With the remarkable progress in understanding and classifying spin liquids in recent decades, it is now legitimate to ask 'which spin liquid?'. Following the proposal by Christos et al. [7], we employ the FL\* state with the critical square lattice spin liquid, without quasiparticle excitations, which has dual [8] formulations in terms of a U(1) gauge theory of bosonic spinons [9, 10, 11, 12] (see Eq. (2.27)), or as a SU(2) gauge theory of fermionic spinons in the  $\pi$ -flux phase [13, 14, 15] (see Eq. (2.43)). We review the properties of this critical spin liquid in Section 2.

Sections 3 and 5 show that this critical spin liquid satisfies a key constraint: as the temperature is lowered, the emergent gauge fields are confined by a transition to a d-wave superconductor which is adiabatically connected to the BCS state [7]. The onset of superconductivity at low p is not a BCS-type Cooper-pairing transition, but a confinement/Higgs transition of a gauge theory. This is a specific realization of an early suggestion by Anderson [16], that cuprate superconductivity appears by exploiting the pre-existing pairing of electrons in a resonating valence bond state.

There were several earlier proposals [17, 18, 19, 20, 21] for a transition from a spin liquid to a d-wave superconductor. In these theories, gapless fermionic spinons of the spin liquid directly transmute into the Bogoliubov quasiparticles of the d-wave superconductor with a massless Dirac dispersion. However, these proposals had a significant problem as they predict a nearly isotropic velocity dispersion, with the velocities along the Brillouin zone diagonals ( $v_F$ , see Fig. 17B) and the orthogonal direction ( $v_{\Delta}$ ) being nearly equal to each other. Experimentally, we have  $v_F/v_{\Delta} \sim 14$  to 19 [22]. Section 5.1 shows how this problem is resolved [23, 24] by instead considering the transition from a FL\* state to a d-wave superconductor. In such a theory, the spinons do not transmute into Bogoliubov quasiparticles; instead, they mutually annihilate with extraneous Bogoliubov quasiparticles from the 'backside' of the hole pockets.

Sections 4 and 5 also review how the critical spin liquid FL\* theory is connected to a number of other experiments on the underdoped cuprates:

- Recent observations [25] of the Yamaji effect in the pseudogap state above  $T_c$  show hole pockets of area close to the FL\* predicted value of p/8 [3, 4, 26], and not the value p/4 expected in a theory of spin density wave fluctuations [27, 28, 29, 30]. This observation is therefore direct evidence for the presence of fractionalization in the cuprates.
- Quantum oscillations at low p and low T show small electron pockets in the presence of charge density wave order [31]. This can be explained as arising from the charge density wave acting on hole pockets only upon including the influence of the spinons of the FL\* state [32].

- The 'Fermi arcs' observed in photoemission [33, 34, 35, 36, 37, 38] and scanning tunneling microscopy (STM) [39, 40] are realized by thermal fluctuations of the SU(2) lattice gauge theory describing the FL\* state [41].
- The thermal SU(2) gauge theory [41] also describes the onset of superconductivity as a Kosterlitz-Thouless transition of vortices with flux h/(2e) [42]. As a consequence of the competing charge order instability of the critical spin liquid [7], each vortex carries a charge order halo, similar to observations [43].

As indicated in Fig. 1, Sections 6 and 7 address the strange metal phase as a crossover between the pseudogap metal and the large p Fermi liquid. Here a different critical quantum liquid plays an important role, one in which the electrons are mobile. Two solvable zero-dimensional models, the SYK model and the WES-SYK model (also known as the Yukawa-SYK model), yield much insight and their properties are reviewed in Section 6.

Section 7 extends the zero-dimensional models of Section 6 to the two-dimensional case of interest. We begin by the general description of a quantum phase transition in a two-dimensional metal. For quantum phase transitions without spatial disorder, we do find the breakdown of well-defined quasiparticles *i.e.* a non-Fermi liquid. However, such clean non-Fermi liquids have an emergent continuous translational symmetry which precludes the observed singular behavior in transport properties (see Section 7.2).

We can imagine a situation, which we do not review here, where the continuous translational symmetry emerges only at very low temperatures, because of the dominance of umklapp processes. In this case, we can study zero-dimensional SYK-type solutions of the dynamic mean-field theory of a 'Kondo breakdown' quantum phase transition [44, 45, 46, 47, 48, 49, 50, 51, 52, 53, 54, 55, 56, 57]. However, we do expect that there is eventually a momentum conserving theory at low energies for clean lattice models, but it is possible that the crossover to such behavior is strongly suppressed in Kondo lattice models where the couplings between the Kondo spins are weak.

Instead, Section 7 examines the role of impurities, which are ubiquitous in experiments, and which will prevent the emergent continuous translational symmetry. Section 7.3 examines the generic situation where impurities lead to spatial randomness in the position of the quantum critical point. We describe a self-averaging treatment of the spatial disorder, inspired by the structure of the solution of the SYK model. This leads to a set of universal predictions at low temperatures (T) in the quantum-critical 'fan', which are largely independent of the particular quantum phase transition under consideration [58, 59]. These properties include a linear-in-T resistivity, a  $T \ln(1/T)$  specific heat, a  $\sim 1/\omega$  tail in the optical conductivity at frequency  $\omega$ , and marginal Fermi liquid behavior in the electronic spectrum. These are in good agreement with observations across a wide range of correlated electron materials.

However, there is a particular feature that is special to the underlying FL\* to FL transition illustrated in Fig. 1. Such transitions have a singular particle-hole asymmetry, and this leads to singular behavior in the thermopower [60]. This is also consistent with

observations on the cuprates [61, 62] and heavy-fermion compounds [63].

Finally, we note that at sufficiently low T, the self-averaging treatment of disorder described above breaks down, and the contributions of regions where collective bosonic modes localize become important. This is addressed in other works [64, 65], has been reviewed elsewhere [66], and will not be discussed further here. These rare region effects lead to Griffiths phases [67], and the 'foot' in the strange metal region, observed in transport [68, 69] and neutron scattering [70].

### 2. Critical spin liquid on the square lattice

$$\mathcal{H}_J = \sum_{i < j} J_{ij} \, \mathbf{S}_i \cdot \mathbf{S}_j \,. \tag{2.1}$$

We consider the general case of  $S_i$  being spin S quantum spin operators on the sites, i, of a square lattice. The  $J_{ij}$  are short-ranged antiferromagnetic exchange interactions. We will mainly consider here the square lattice with nearest neighbor interactions, but the methods generalize to a wide class of lattices and interaction ranges.

We will begin in Section 2.1 by employing a method which fractionalizes the spin operator into bosonic partons. This leads to the low energy U(1) gauge theory with complex scalars in Eq. (2.27), and to the phase diagram in Fig. 3. Section 2.2 fractionalizes the spin operator into fermionic partons. This leads ultimately to a seemingly different low energy theory: a SU(2) gauge theory with massless Dirac fermions in Eq. (2.43). But we will argue, following Wang et al. [8], that the bosonic and fermionic theories are equivalent. This equivalence is powerful, as it yields a toolbox of different approaches to study spin liquids.

### 2.1. Bosonic partons

A careful examination of the non-magnetic 'spin-liquid' phases requires an approach which is designed explicitly to be valid in a region well separated from Néel long range order, and preserves SU(2) symmetry at all stages. It should also be designed to naturally allow for neutral S=1/2 excitations. To this end, we introduce the Schwinger boson description [71], in terms of elementary S=1/2 bosons. For the group SU(2) the complete set of (2S+1) states on site  $\boldsymbol{i}$  are represented as follows

$$|S,m\rangle \equiv \frac{1}{\sqrt{(S+m)!(S-m)!}} (b_{i\uparrow}^{\dagger})^{S+m} (b_{i\downarrow}^{\dagger})^{S-m} |0\rangle, \tag{2.2}$$

where m = -S, ... S is the z component of the spin (2m is an integer). We have introduced two flavors of Schwinger bosons on each site, created by the canonical operator  $b_{i\alpha}^{\dagger}$ , with  $\alpha = \uparrow, \downarrow$ , and  $|0\rangle$  is the vacuum with no Schwinger bosons. The total number of Schwinger bosons,  $n_b$ , is the same for all the states; therefore

$$b_{i\alpha}^{\dagger}b_{i\alpha} = n_b \tag{2.3}$$

with

$$n_b = 2S. (2.4)$$

The above representation of the states is completely equivalent to the operator identity between the spin and Schwinger boson operators

$$S_{i} = \frac{1}{2} b_{i\alpha}^{\dagger} \, \sigma_{\alpha\beta} \, b_{i\beta} \tag{2.5}$$

where  $\ell = x, y, z$  and the  $\sigma$  are the usual  $2 \times 2$  Pauli matrices.

The spin-states on two sites i, j can combine to form a singlet in a unique manner - the wavefunction of the (unnormalized) singlet state is particularly simple in the boson formulation:

$$\left(\varepsilon_{\alpha\beta}b_{i\alpha}^{\dagger}b_{j\beta}^{\dagger}\right)^{2S}|0\rangle\tag{2.6}$$

Also, using the constraint in Eq. (2.3), the following Fierz-type identity can be established

$$\left(\varepsilon_{\alpha\beta}b_{i\alpha}^{\dagger}b_{j\beta}^{\dagger}\right)\left(\varepsilon_{\gamma\delta}b_{i\gamma}b_{j\delta}\right) = -2\boldsymbol{S}_{i}\cdot\boldsymbol{S}_{j} + n_{b}^{2}/2 + \delta_{ij}n_{b}$$
(2.7)

where  $\varepsilon$  is the totally antisymmetric  $2 \times 2$  tensor

$$\varepsilon = \begin{pmatrix} 0 & 1 \\ -1 & 0 \end{pmatrix} . \tag{2.8}$$

This implies that  $\mathcal{H}_J$  can be rewritten in the form (apart from an additive constant)

$$\mathcal{H}_{J} = -\frac{1}{2} \sum_{i < j} J_{ij} \left( \varepsilon_{\alpha\beta} b_{i\alpha}^{\dagger} b_{j\beta}^{\dagger} \right) \left( \varepsilon_{\gamma\delta} b_{i\gamma} b_{j\delta} \right) \tag{2.9}$$

This form makes it clear that  $\mathcal{H}$  counts the number of singlet bonds.

2.1.1. Mean-field theory We begin by the coherent state path integral of  $\mathcal{H}_J$  in imaginary time  $\tau$  at a temperature  $\beta = 1/T$ 

$$\mathcal{Z}_{J} = \int \mathcal{D}\mathcal{Q}\mathcal{D}b\mathcal{D}\lambda \exp\left(-\int_{0}^{\beta} \mathcal{L}_{J} d\tau\right), \qquad (2.10)$$

where

$$\mathcal{L}_{J} = \sum_{i} \left[ b_{i\alpha}^{\dagger} \left( \frac{d}{d\tau} + i\lambda_{i} \right) b_{i\alpha} - i\lambda_{i} n_{b} \right]$$

$$+ \sum_{\langle i,j \rangle} \left[ \frac{J_{ij} |\mathcal{Q}_{i,j}|^{2}}{2} - \frac{J_{ij} \mathcal{Q}_{i,j}^{*}}{2} \varepsilon_{\alpha\beta} b_{i\alpha} b_{j\beta} + H.c. \right].$$
(2.11)

Here the  $\lambda_i$  fix the boson number of  $n_b$  at each site;  $\tau$ -dependence of all fields is implicit;  $\mathcal{Q}$  was introduced by a Hubbard-Stratonovich decoupling of  $\mathcal{H}$ .

This procedure is similar to that employed in deriving the Landau-Ginzburg theory of superconductivity from electron pairing, with the crucial difference that now the Lagrangian  $\mathcal{L}$  has a U(1) gauge invariance under which

$$b_{i\alpha}^{\dagger} \rightarrow b_{i\alpha}^{\dagger} \exp(i\rho_{i}(\tau))$$

$$Q_{i,j} \rightarrow Q_{i,j} \exp(-i\rho_{i}(\tau) - i\rho_{j}(\tau))$$

$$\lambda_{i} \rightarrow \lambda_{i} + \frac{\partial \rho_{i}}{\partial \tau}(\tau).$$
(2.12)

The functional integral over  $\mathcal{L}_J$  faithfully represents the partition function, but does require gauge fixing. This gauge invariance leads to emergent gauge field degrees of freedom, as we will see below.

We begin with mean-field saddle point of  $\mathcal{Z}_J$  over the path integrals of  $\mathcal{Q}$  and  $\lambda$ . The saddle-point approximation is valid in the limit of a large number of spin flavors, but we do not explore this here. With the saddle point values  $\mathcal{Q}_{ij} = \bar{\mathcal{Q}}_{ij}$ ,  $i\lambda_i = \bar{\lambda}_i$  we obtain a mean-field Hamiltonian for the  $b_{i\alpha}$ 

$$\mathcal{H}_{J,MF} = \sum_{\langle i,j \rangle} \left( \frac{J_{ij} |\bar{\mathcal{Q}}_{ij}|^2}{2} - \frac{J_{ij} \bar{\mathcal{Q}}_{ij}^*}{2} \varepsilon_{\alpha\beta} b_i^{\alpha} b_j^{\beta} + H.c. \right) + \sum_{i} \bar{\lambda}_{i} (b_{i\alpha}^{\dagger} b_{i\alpha} - n_b).$$
(2.13)

This Hamiltonian is quadratic in the boson operators and all its eigenvalues can be determined by a Bogoluibov transformation. This leads in general to an expression of the form

$$\mathcal{H}_{J,MF} = E_{J,MF}[\bar{\mathcal{Q}}, \bar{\lambda}] + \sum_{\mu} \omega_{\mu}[\bar{\mathcal{Q}}, \bar{\lambda}] \gamma^{\dagger}_{\mu\alpha} \gamma_{\mu\alpha}$$
 (2.14)

The index  $\mu$  extends over 1...number of sites in the system,  $E_{J,MF}$  is the ground state energy and is a functional of  $\bar{Q}$ ,  $\bar{\lambda}$ ,  $\omega_{\mu}$  is the eigenspectrum of excitation energies which is also a function of  $\bar{Q}$ ,  $\bar{\lambda}$ , and the  $\gamma_{\mu}^{\alpha}$  represent the bosonic eigenoperators. The excitation spectrum thus consists of non-interacting spinor bosons. The ground state is determined by minimizing  $E_{J,MF}$  with respect to the  $\bar{Q}_{ij}$  subject to the constraints

$$\frac{\partial E_{MF}}{\partial \bar{\lambda}_i} = 0 \tag{2.15}$$

The saddle-point value of the  $\bar{Q}$  satisfies

$$\bar{\mathcal{Q}}_{ij} = \langle \varepsilon_{\alpha\beta} b_{i\alpha} b_{j\beta} \rangle \tag{2.16}$$

Note that  $\bar{Q}_{ij} = -\bar{Q}_{ji}$  indicating that  $\bar{Q}_{ij}$  is a directed field - an orientation has to be chosen on every link.

These saddle-point equations have been solved for the square lattice with nearest neighbor exchange J, and they lead to stable and translationally invariant solutions for  $\bar{\lambda}_{i}$  and  $\bar{Q}_{ij}$ . The only saddle-point quantity which does not have the full symmetry of the lattice is the orientation of the  $\bar{Q}_{ij}$ . Note that although it appears that such a choice of orientation appears to break inversion or reflection symmetries, such symmetries are actually preserved: the  $\bar{Q}_{ij}$  are not gauge-invariant, and all gauge-invariant observables do preserve all symmetries of the underlying Hamiltonian. For the square lattice, we have  $\bar{\lambda}_{i} = \bar{\lambda}$ ,  $\bar{Q}_{i,i+\hat{x}} = \bar{Q}_{i,i+\hat{y}} = \bar{Q}$ .

We can also compute the dispersion  $\omega_{\mathbf{k}}$  of the  $\gamma_{\mathbf{k}}$  excitations. These are bosonic particles which carry spin S = 1/2 ('spinons'). Their dispersion is

$$\omega_{\mathbf{k}} = \left(\bar{\lambda}^2 - J^2 \bar{\mathcal{Q}}^2 (\sin k_x + \sin k_y)^2\right)^{1/2} . \tag{2.17}$$

We plot the dispersion in Fig. 2. Note the minima at  $\mathbf{k} = \pm (\pi/2, \pi/2)$  with an energy gap of  $(\bar{\lambda}^2 - 4J^2\bar{\mathcal{Q}}^2)^{1/2}$ .

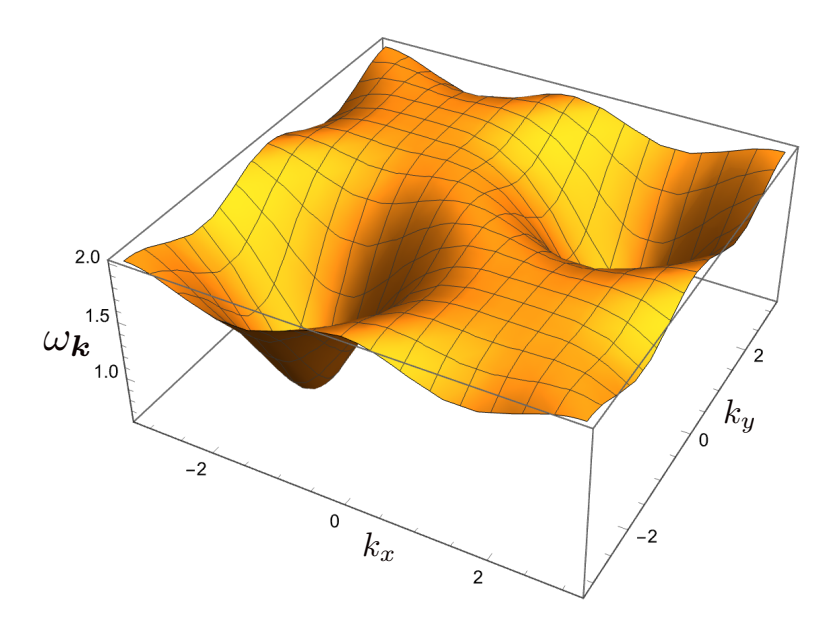


**Figure 2.** Dispersion of bosonic spinons in a square lattice spin liquid, from Eq. (2.17).

2.1.2. Low energy U(1) gauge theory We now examine the low energy theory in the regime where the energy gap of the spinon excitations is small. Here, we can take a continuum limit for the spinons, and also account for the fluctuations of  $\mathcal{Q}$  and  $\lambda$ . For the spinons, we introduce the wavevector at the minimum spinon gap  $\mathbf{k}_0 = (\pi/2, \pi/2)$  and parameterize on the checkerboard A and B sublattices (with  $\mathbf{i}_x + \mathbf{i}_y$  even and odd)

$$b_{Ai\alpha} = \psi_{1\alpha}(\mathbf{r}_i)e^{i\mathbf{k}_0\cdot\mathbf{r}_i}$$

$$b_{Bi\alpha} = -i\varepsilon_{\alpha\beta}\psi_{2\beta}(\mathbf{r}_i)e^{i\mathbf{k}_0\cdot\mathbf{r}_i}.$$
(2.18)

For Q and  $\lambda$ , we anticipate that the fluctuations will be un-important unless associate with the gauge symmetry in Eq. (2.12). So we focus only on the phases of the  $Q_{ij}$  and parameterize

$$Q_{i,i+\hat{x}} = \bar{Q} \exp(i\Theta_{ix})$$

$$Q_{i,i+\hat{y}} = \bar{Q} \exp(i\Theta_{iy}) , \qquad (2.19)$$

and express the phases in terms of continuum field  $(a_{\tau}, a_{x}, a_{y})$  via

$$\Theta_{ix}(\tau) = \eta_i a_x(\mathbf{r}, \tau) 
\Theta_{iy}(\tau) = \eta_i a_y(\mathbf{r}, \tau) 
\lambda_i = -i\bar{\lambda} - \eta_i a_\tau(\mathbf{r}, \tau)$$
(2.20)

where

$$\eta_i = (-1)^{i_x + i_y} \tag{2.21}$$

identifies the checkerboard sublattices. Next, we insert these parameterizations into the spinon action, perform a gradient expansion, and transform the Lagrangian  $\mathcal{L}_J$  into (a is the lattice spacing)

$$\mathcal{L}_z = \int \frac{d^2r}{2a^2} \left[ \psi_{1\alpha}^* \left( \frac{d}{d\tau} + ia_\tau \right) \psi_{1\alpha} + \psi_{2\alpha}^* \left( \frac{d}{d\tau} - ia_\tau \right) \psi_{2\alpha} \right]$$

$$+ \bar{\lambda} \left( |\psi_{1\alpha}|^2 + |\psi_{2\alpha}|^2 \right) - 2J \bar{\mathcal{Q}} \left( \psi_{1\alpha} \psi_{2\alpha} + \psi_{1\alpha}^* \psi_{2\alpha}^* \right)$$

$$+ (J/2) \bar{\mathcal{Q}} a^2 \left[ (\boldsymbol{\nabla} + i\boldsymbol{a}) \, \psi_{1\alpha} \left( \boldsymbol{\nabla} - i\boldsymbol{a} \right) \psi_{2\alpha} \right]$$

$$+ (\boldsymbol{\nabla} - i\boldsymbol{a}) \, \psi_{1\alpha}^* \left( \boldsymbol{\nabla} + i\boldsymbol{a} \right) \psi_{2\alpha}^* \right].$$

$$(2.22)$$

We now introduce the fields

$$z_{\alpha} = (\psi_{1\alpha} + \psi_{2\alpha}^*)/\sqrt{2}$$
  
$$\pi_{\alpha} = (\psi_{1\alpha} - \psi_{2\alpha}^*)/\sqrt{2},$$

to map Eq. (2.22) to

$$\mathcal{L}_{z} = \int \frac{d^{2}r}{2a^{2}} \left[ \pi_{\alpha}^{*} \left( \frac{d}{d\tau} + ia_{\tau} \right) z_{\alpha} - \pi_{\alpha} \left( \frac{d}{d\tau} - ia_{\tau} \right) z_{\alpha}^{*} + \bar{\lambda} \left( |z_{\alpha}|^{2} + |\pi_{\alpha}|^{2} \right) - 2J\bar{\mathcal{Q}} \left( |z_{\alpha}|^{2} - |\pi_{\alpha}|^{2} \right) + (J/2)\bar{\mathcal{Q}}a^{2} \left[ |(\boldsymbol{\nabla} + i\boldsymbol{a}) z_{\alpha}|^{2} - |(\boldsymbol{\nabla} + i\boldsymbol{a}) \pi_{\alpha}|^{2} \right] \right].$$
 (2.23)

From Eq. (2.23), it is clear that the the  $\pi$  fields have 'mass'  $\bar{\lambda} + 2J\bar{Q}$ , while the z fields have a mass  $\bar{\lambda} - 2J\bar{Q}$  which vanishes at a quantum phase transition where the  $z_{\alpha}$  condense, leading to Néel order. The  $\pi$  fields can therefore be safely integrated out, and  $\mathcal{L}_z$  yields the following effective action, valid at distances much larger than the lattice spacing [9, 10]:

$$S_{\text{eff}} = \int \frac{d^2r}{4\sqrt{2}a} \int d\tau \left\{ |(\partial_{\mu} - ia_{\mu})z_{\alpha}|^2 + \frac{\Delta^2}{c^2} |z^{\alpha}|^2 \right\}.$$
 (2.24)

Here  $\mu$  extends over  $x, y, \tau$ ,  $c = \sqrt{2}J\bar{\mathcal{Q}}a$  is the spin-wave velocity, we have rescaled  $\tau \to \tau/c$ , and  $\Delta = (\bar{\lambda}^2 - 4J^2\bar{\mathcal{Q}}_1^2)^{1/2}$  is the gap towards spinon excitations. Thus the long-wavelength theory describes a spin liquid with of a massive, spin-1/2, relativistic, boson  $z_{\alpha}$  (spinon) excitation coupled to a U(1) gauge field  $a_{\mu}$ .

The continuum theory also makes it easy to determine the fate of the antiferromagnet when the spin energy gap vanishes. We expect that  $z_{\alpha}$  will bose condense, and this will break the spin rotation symmetry; a term quartic in  $z_{\alpha}$  will be needed to stabilize the condensate. But  $z_{\alpha}$  carries a U(1) gauge charge, and so is not directly observable. Following the definitions of the underlying spin operators, it is not difficult to show that the gauge-invariant composite

$$\mathcal{N} = z_{\alpha}^* \sigma_{\alpha\beta} z_{\beta} \sim \eta_i S_i \tag{2.25}$$

is just the Néel order parameter.

However, there is an important ingredient that our low energy theory has not yet considered. These are non-perturbative fluctuations of  $a_{\mu}$  which are Dirac monopoles in 2+1 dimensional spacetime. We will not carry out a full analysis here, and merely summarize some important consequences. An important result is that the spin liquid noted above is ultimately not a spin liquid. It is unstable to proliferation of monopoles, and ultimately confines a valence bond solid. But monopoles do not have a significant effect on the Néel state.

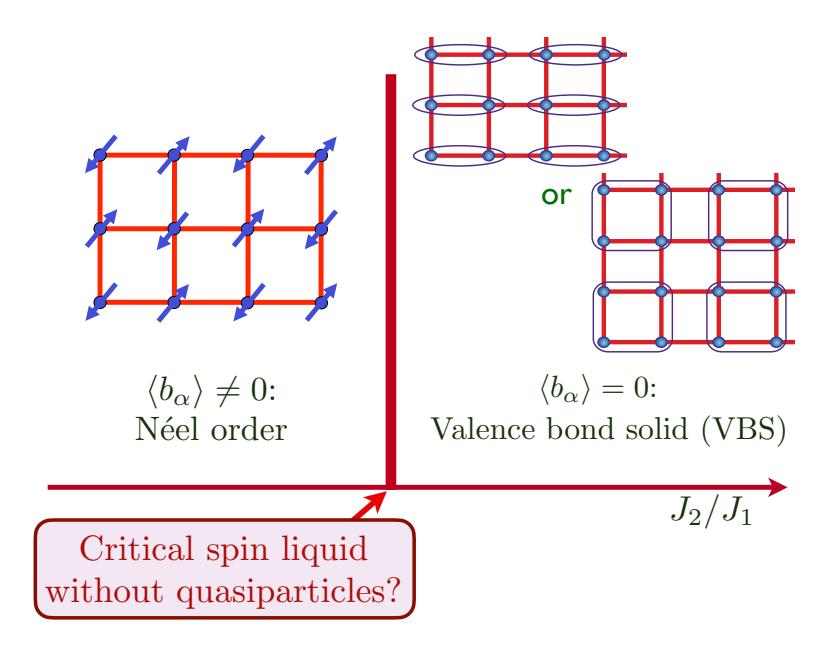


Figure 3. Phase diagram of the U(1) gauge theory with bosonic spinons, Eq. (2.27. The Néel order appears in a Higgs phase where the bosonic spinons are condensed. The VBS order appears in the confining phase, and is induced by the Berry phases of the confining monopoles. The same phase diagram applies to the fermionic spinon theory in Eq. (2.50), and the SO(5)  $\sigma$ -model with the WZW term in Eq. (2.57).

2.1.3. Quantum criticality On general symmetry grounds, we extend Eq. (2.24) to a theory for the vicinity of the quantum critical point at which the spinon gap vanishes [72]:

$$S_{U(1)} = \int d^3x \left( \mathcal{L}_z + \mathcal{L}_{\text{monopole}} \right) + S_B$$

$$\mathcal{L}_z = |(\partial_\mu - ia_\mu)z_\alpha|^2 + g|z_\alpha|^2 + u\left(|z_\alpha|^2\right)^2 + K(\epsilon_{\mu\nu\lambda}\partial_\nu a_\lambda)^2$$

$$\mathcal{L}_{\text{monopole}} = -y\left(\mathcal{M}_a + \mathcal{M}_a^{\dagger}\right)$$

$$S_B = i2S \sum_{i} \eta_i \int d\tau \, a_{i\tau} \,. \tag{2.26}$$

The theory  $\mathcal{L}_z$  is also known as the  $\mathbb{CP}^1$  model. We have included monopoles  $\mathcal{M}_a$  in the gauge field  $a_{\mu}$ , and also the Berry phase of the spinons in the ground state. As we tune the coupling g in Eq. (2.26), we can expect the 2 phases shown in Fig. 3:

- (i) Néel phase,  $g < g_c$ : the spinon  $z_{\alpha}$  condenses in a Higgs phase with  $\langle z_{\alpha} \rangle \neq 0$ . The  $a_{\mu}$  gauge field is Higgsed, and spin rotation symmetry is broken by opposite polarization of the spins on the two sublattices.
- (ii) Valence bond solid (VBS),  $g > g_c$ : the spinons are gapped. For half-integer spin S, there is broken translational symmetry by the crystallization of valence bonds in the pattern shown in Fig. 3.

We now obtain a potential gapless spin liquid if there is a continuous quantum phase transition at  $g = g_c$ . For half-integer spin S, the single monopole terms in Eq. (2.26) average to zero at long wavelengths from the Berry phases, and only quadrupoled

monopole terms survive. So we can simplify the continuum theory for the vicinity of the quantum critical point to [11, 12]

$$\mathcal{L}_z = |(\partial_\mu - ia_\mu)z_\alpha|^2 + g|z_\alpha|^2 + u\left(|z_\alpha|^2\right)^2 + K(\epsilon_{\mu\nu\lambda}\partial_\nu a_\lambda)^2 - y_4\left(\mathcal{M}_a^4 + \mathcal{M}_a^{\dagger 4}\right), (2.27)$$

where  $y_4$  is the quadrupoled monopole fugacity. There is ample numerical evidence that  $y_4$  is irrelevant near a possible critical point, and so the question reduces to whether the theory  $\mathcal{L}_z$  at  $y_4 = 0$  exhibits a critical point which realizes a conformal field theory in 2+1 dimensions. This is a question that has been studied extensively in numerics, and it is clear that a 'deconfined critical' description is suitable over a substantial length scale: with fractionalized spinons interacting with a U(1) gauge field in the absence of monopoles.

### 2.2. Fermionic partons

We now present an alternative analysis of the square lattice antiferromagnet in Eq. (2.1), replacing the bosonic partons in Eq. (2.5) by fermionic partons. This will ultimately lead to the same phase diagram as in Fig. 3, but with a dual description of the phases and the criticality. This dual fermionic description turns out to be the most efficient way to describe the connection between the critical spin liquid and d-wave superconductivity in the doped antiferromagnet, as we will see in Section 3.

The following Schwinger fermion representation applies only for S=1/2

$$S_{i} = \frac{1}{2} f_{i\alpha}^{\dagger} \sigma_{\alpha\beta} f_{i\beta}$$
 (2.28)

where  $f_{i\alpha}$  are canonical fermions obeying the constraint

$$\sum_{\alpha} f_{i\alpha}^{\dagger} f_{i\alpha} = 1 \quad , \quad \text{for all } i.$$
 (2.29)

While the bosonic parton representation led to the U(1) gauge symmetry in Eq. (2.12), it turns out the Eqs. (2.28) and (2.29) have a larger SU(2) gauge invariance, and this will be crucial to our results. The analysis is clearest upon introducing a matrix notation for the fermions

$$\mathcal{F}_{i} \equiv \begin{pmatrix} f_{i\uparrow} & -f_{i\downarrow} \\ f_{i\downarrow}^{\dagger} & f_{i\uparrow}^{\dagger} \end{pmatrix}$$
 (2.30)

This matrix obeys the 'reality' condition

$$\mathcal{F}_{i}^{\dagger} = \sigma^{y} \mathcal{F}_{i}^{T} \sigma^{y}. \tag{2.31}$$

Now we can write Eq. (2.28) as

$$\mathbf{S}_{i} = -\frac{1}{4} \text{Tr}(\mathcal{F}_{i} \sigma^{z} \boldsymbol{\sigma}^{T} \sigma^{z} \mathcal{F}_{i}^{\dagger}). \tag{2.32}$$

The SU(2) gauge symmetry is now associated with a SU(2) matrix  $V_i$  under which

$$\mathcal{F}_i \to V_i \, \mathcal{F}_i \,, \tag{2.33}$$

which is easily seen to leave the spin operator in Eq. (2.32) invariant. The global spin rotation symmetry is however

$$\mathcal{F}_{i} \to \mathcal{F}_{i} \, \sigma^{z} \Omega_{i}^{T} \sigma^{z}$$
. (2.34)

where  $\Omega$  is the S=1/2 spin rotation matrix defined by

$$\begin{pmatrix} f_{i\uparrow} \\ f_{i\downarrow} \end{pmatrix} \to \Omega \begin{pmatrix} f_{i\uparrow} \\ f_{i\downarrow} \end{pmatrix} . \tag{2.35}$$

Next we insert Eq. (2.32) into Eq. (2.1), and perform Hubbard-Stratonovich transformation to obtain an effective Hamiltonian for the spinons, following the same procedure as for bosonic spinons. We skip the intermediate steps, and focus directly on the fermion bilinear Hamiltonian on symmetry grounds. From the gauge transformations in Eq. (2.33), and the global spin rotation in Eq. (2.34), we anticipate a spinon hopping term of the form

$$\operatorname{Tr}\left(\mathcal{F}_{i}^{\dagger}U_{ij}\mathcal{F}_{j}\right) \tag{2.36}$$

which is invariant under both transformations. Here we have introduced a SU(2) gauge field  $U_{ij} = U_{ji}^{\dagger}$  on each lattice link upon which the SU(2) gauge transformation acts as

$$U_{ij} \to V_i U_{ij} V_i^{\dagger}$$
 (2.37)

However, the identity

$$\operatorname{Tr}\left(\mathcal{F}_{i}^{\dagger}\mathcal{F}_{j}\right) = -\operatorname{Tr}\left(\mathcal{F}_{j}^{\dagger}\mathcal{F}_{i}\right) \tag{2.38}$$

implies that we need a pure-imaginary hopping in a hermitian Hamiltonian in the mean-field with  $U_{ij} = 1$ . So we have the mean-field nearest-neighbor spin liquid Hamiltonian for the spinons of the  $\pi$ -flux phase [13]:

$$\mathcal{H}_{SLf} = \frac{iJ}{2} \sum_{\langle ij \rangle} e_{ij} \left[ \text{Tr} \left( \mathcal{F}_{i}^{\dagger} \mathcal{F}_{j} \right) - \text{Tr} \left( \mathcal{F}_{j}^{\dagger} \mathcal{F}_{i} \right) \right]$$

$$= iJ \sum_{\langle ij \rangle} e_{ij} \left( \Psi_{i}^{\dagger} \Psi_{j} - \Psi_{j}^{\dagger} \Psi_{i} \right); \quad \Psi_{i} \equiv \begin{pmatrix} f_{i\uparrow} \\ f_{i\downarrow}^{\dagger} \end{pmatrix}, \qquad (2.39)$$

where  $e_{ij} = \pm 1$  represents  $\pi$ -flux on the fermions as shown in Fig. 4. We choose  $e_{ij} = -e_{ji}$  and

$$e_{i,i+\hat{x}} = 1, \quad e_{i,i+\hat{y}} = (-1)^x,$$
 (2.40)

where  $\mathbf{i} = (x, y), \, \hat{\mathbf{x}} = (1, 0), \, \hat{\mathbf{y}} = (0, 1).$ 

If we had not used the pure imaginary hopping in Eq. (2.39), then the mean-field Hamiltonian would break ('Higgs') the SU(2) gauge symmetry to a smaller symmetry. A 'staggered flux' ansatz which breaks the SU(2) down to U(1) has commonly been used in the literature [21]. However, it is now known that this U(1) spin liquid allows single monopole perturbations [73, 74] (unlike the quadrupole monopole perturbations in Eq. (2.27)), and such single monopole terms are expected to drive a strong instability to confinement. So we don't consider this U(1) spin liquid here.

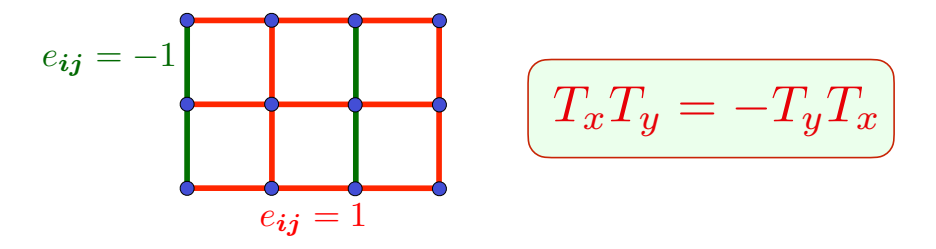


**Figure 4.** Background  $\pi$  flux acting on the spinons f, and also on the chargens B.

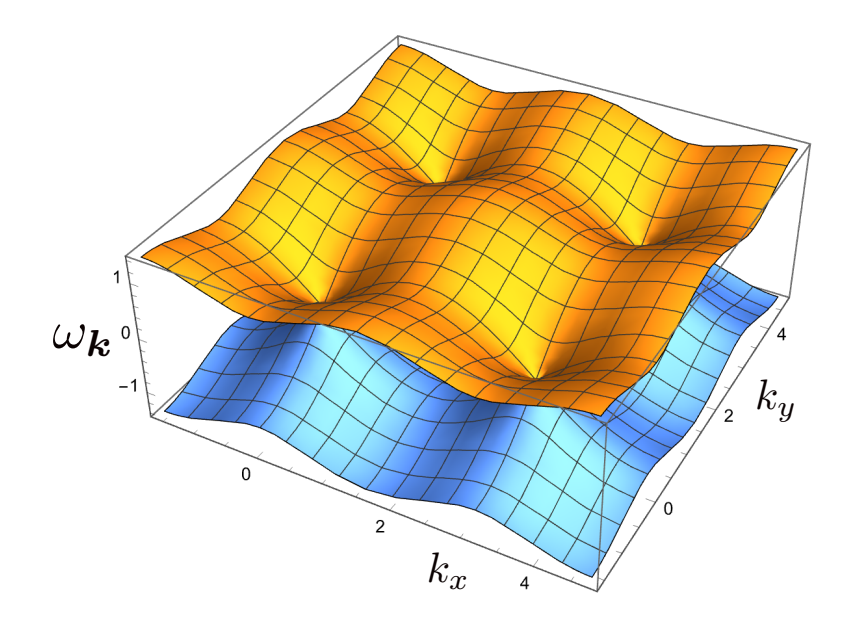


**Figure 5.** Dispersion of fermionic spinons in Eq. (2.41).

We can now easily diagonalize the Hamiltonian in Eq. (2.39), and obtain the fermionic dispersion spectrum analogous to Eq. (2.17)

$$\omega_{k} = \pm 2J \left( \sin^{2} k_{x} + \sin^{2} k_{y} \right)^{1/2} . \tag{2.41}$$

We show a plot of this analogous to Fig. 2 in Fig. 5. Unlike the bosonic spinons, the energy of the fermionic spinons is allowed to be negative, and the negative energy fermion states are occupied in the ground state. The constraint in Eq. (2.29) is then automatically satisfied. Notice the two independent nodal Dirac points at  $\mathbf{k}_v$ , v = 1, 2 with

$$\mathbf{k}_1 = (0,0) \quad , \quad \mathbf{k}_2 = (0,\pi) \,.$$
 (2.42)

The index v is the 'valley'.

2.2.1. Low energy SU(2) gauge theory. Going beyond mean field theory, while still remaining on the lattice, we extend the mean field Hamiltonian in Eq. (2.39) by adding the gauge field  $U_{ij}$  as in Eq. (2.36). Then, by gauge invariance, we extend Eq. (2.39) to

$$\mathcal{H}_{SLf} = \frac{iJ}{2} \sum_{\langle ij \rangle} e_{ij} \left[ \text{Tr} \left( \mathcal{F}_{i}^{\dagger} U_{ij} \mathcal{F}_{j} \right) - \text{Tr} \left( \mathcal{F}_{j}^{\dagger} U_{ji} \mathcal{F}_{i} \right) \right]$$

$$= iJ \sum_{\langle ij \rangle} e_{ij} \left( \Psi_{i}^{\dagger} U_{ij} \Psi_{j} - \Psi_{j}^{\dagger} U_{ji} \Psi_{i} \right); \quad \Psi_{i} \equiv \begin{pmatrix} f_{i\uparrow} \\ f_{i\downarrow}^{\dagger} \end{pmatrix}, \quad (2.43)$$

The first form in terms of  $\mathcal{F}$  makes both the SU(2) gauge invariance and the SU(2) spin rotation invariance explicit, while in the second form in terms of  $\Psi$  only the gauge invariance is explicit.

The continuum formulation of this theory can be obtained by following the same procedure as in Section 2.1.2, but we have to carefully account for the SU(2) gauge symmetry. First, neglecting gauge fluctuations of  $U_{ij}$  for now, let us write Eq. (2.39) in momentum space, in terms of the fermions  $\mathcal{F}_s(\mathbf{k})$ , where s = A, B is a sublattice index. Now the sublattices refer to sites with  $\mathbf{i}_x$  even and odd, which are the two sites in the unit cell. We obtain

$$\mathcal{H}_{SLf} = -J \sum_{\mathbf{k}} \operatorname{Tr} \left( \mathcal{F}^{\dagger}(\mathbf{k}) \left[ \rho^{x} \sin(k_{x}) + \rho^{z} \sin(k_{y}) \right] \mathcal{F}^{\dagger}(\mathbf{k}) \right) , \qquad (2.44)$$

where  $\rho^{\ell}$ , with  $\ell = x, y, z$ , are Pauli matrices in sublattice space. Next, analogous to Eq. (2.18), we take the continuum limit near the valley momenta in terms of  $\mathcal{X}_{sv}(\mathbf{r}, \tau)$ 

$$\mathcal{F}_{Ai} = \sum_{v} \mathcal{X}_{Av}(\boldsymbol{r}, \tau) e^{i\boldsymbol{k}_{v} \cdot \boldsymbol{r}_{i}}$$

$$\mathcal{F}_{Bi} = \sum_{v} \mathcal{X}_{Bv}(\boldsymbol{r}, \tau) e^{i\boldsymbol{k}_{v} \cdot \boldsymbol{r}_{i}}$$
(2.45)

for i on the A and B sublattices respectively. This yields the imaginary time Lagrangian density

$$\mathcal{L}_{\mathcal{X}} = \frac{1}{2} \text{Tr} \left( \mathcal{X}^{\dagger} \left[ \partial_{\tau} + 2Ji \rho^{x} \partial_{x} + 2Ji \rho^{z} \mu^{z} \partial_{y} \right] \mathcal{X} \right) , \qquad (2.46)$$

where  $\mu^{\ell}$  are the Pauli matrices in valley space. We recall that the fermion  $\mathcal{X}_{sv}$  has four-components, and each component is a  $2 \times 2$  matrix which obeys the reality condition in Eq. (2.31). We can write this in a relativistic Dirac form

$$\mathcal{L}_{\mathcal{X}} = \frac{i}{2} \operatorname{Tr} \left( \bar{\mathcal{X}} \gamma^{\mu} \partial_{\mu} \mathcal{X} \right) , \qquad (2.47)$$

with the definitions

$$\bar{\mathcal{X}} = -i\mathcal{X}^{\dagger}\gamma^{0}$$
 ,  $\gamma^{0} = \rho^{y}\mu^{z}$  ,  $\gamma^{x} = \rho^{z}\mu^{z}$  ,  $\gamma^{y} = -\rho^{x}$  , (2.48)

where we have absorbed factor of c = 2J for the velocity of light. Finally, it is a simple matter to include the SU(2) gauge field by taking the continuum limit by writing

$$U_{ii} = \exp\left(-iA_{ii}^{\ell}\sigma^{\ell}\right) \tag{2.49}$$

(where  $\sigma^{\ell}$  are the Pauli matrices in SU(2) gauge space) and expanding the exponential. We then obtain

$$\mathcal{L}_{\mathcal{X}} = \frac{i}{2} \operatorname{Tr} \left( \bar{\mathcal{X}} \gamma^{\mu} \left[ \partial_{\mu} - i A_{\mu}^{\ell} \sigma^{\ell} \right] \mathcal{X} \right) . \tag{2.50}$$

The theory in Eq. (2.50) is the analog of the  $\mathcal{L}_z$  in Eq. (2.26) for bosonic spinons. The latter theory was a U(1) gauge theory with two relativistic complex scalars  $z_{\alpha}$ . In the present case, we have a SU(2) gauge theory with  $N_f = 2$  massless Dirac fermions, associated with valley index v. The global symmetry of  $z_{\alpha}$  was just spin rotations  $z \to \Omega z$ . In contrast, here we have emergent global symmetry which combines spin and valley rotations. A first guess is a SU(4) symmetry generalizing Eq. (2.34)

$$\mathcal{X} \to \mathcal{X}L$$
, (2.51)

where L acts on spin and valley space with  $L^{\dagger}L = 1$ . However, imposition of the reality condition Eq. (2.31) shows that we also need

$$L^T = \sigma^y L^\dagger \sigma^y \,, \tag{2.52}$$

and so the symmetry is only  $\operatorname{Sp}(4)=\operatorname{SO}(5)/\mathbb{Z}_2$  [75, 8]. In terms of the Hermitian Lie algebra elements M, with  $L=e^{iM}$ , the reality condition is

$$M^T = -\sigma^y M \sigma^y \,. \tag{2.53}$$

Requiring that M commute with the  $\gamma^{\mu}$ , we can now write down the 10 elements of the Lie algebra of  $\operatorname{Sp}(4)=\operatorname{SO}(5)/\mathbb{Z}_2$ 

$$M = \{ \sigma^x, \sigma^y, \sigma^z, \mu^z \sigma^x, \mu^z \sigma^y, \mu^z \sigma^z, \rho^x \mu^y, \rho^x \mu^x \sigma^x, \rho^x \mu^x \sigma^y, \rho^x \mu^x \sigma^z \}. \tag{2.54}$$

The remaining 5 SU(4) generators which commute with the  $\gamma^{\mu}$  are (t=1...5)

$$\Gamma^t = \{ \mu^z, \rho^x \mu^x, \rho^x \mu^y \sigma^x, \rho^x \mu^y \sigma^y, \rho^x \mu^y \sigma^z \}.$$
(2.55)

The  $\Gamma^t$  all anti-commute with each other, and transform as a SO(5) vector under the generators in Eq. (2.54). It is now straightforward to check by working back to the lattice operators from the information above that the vector  $i\text{Tr}(\bar{\mathcal{X}}\Gamma^t\mathcal{X})$  corresponds precisely to the 5 components of the orders parameters shown in Fig. 3: the first two components are the VBS order, and the last 3 components are the Néel order  $\mathcal{N}$  in Eq. (2.25) [75, 8].

Wang et al. [8] have argued that the likely fate of the SU(2) gauge theory upon confinement is a state which the SO(5) symmetry is spontaneously broken with  $\langle \Gamma^t \rangle \neq 0$ . The lattice model does not have exact SO(5) symmetry, and the choice between the Néel and VBS components of  $\Gamma^t$  is made by additional 4-fermi terms that can be added to Eq. (2.50). So the ultimate fate of the theory is essentially identical to the fate of the bosonic spinon theory in Section 2.1, as illustrated in Fig. 3. This is essentially the reason for the duality between the theories in Section 2.1.3 and 2.2.1, and Wang et al. have provided additional topological arguments.

### 2.3. SO(5) non-linear $\sigma$ -model

There is a third formulation of the theories in Section 2.1.3 and 2.2.1 which is useful for some purposes. This is obtained most simply by coupling Eq. (2.50) to the SO(5) vector order parameter, and integrating out the fermions. Introducing the SO(5) fundamental unit length field  $n_t$ ,  $n_t n_t = 1$  to Eq. (2.50)

$$\mathcal{L}_{\mathcal{X}n} = \frac{i}{2} \operatorname{Tr} \left( \bar{\mathcal{X}} \gamma^{\mu} \left[ \partial_{\mu} - i A_{\mu}^{\ell} \sigma^{\ell} \right] \mathcal{X} \right) - i n_{t} \operatorname{Tr} \left( \bar{\mathcal{X}} \Gamma^{t} \mathcal{X} \right) , \qquad (2.56)$$

we integrate out the Dirac fermions following the analysis of Ref. [76] and obtain

$$\mathcal{L}_n = \frac{1}{2q} \left( \partial_\mu n_t \right)^2 + 2\pi i \Gamma[n_t] \tag{2.57}$$

The last term is the Wess-Zumino-Witten (WZW) term at level 1: it is a Berry phase associated with spacetime textures of  $n_t$ , a higher dimensional analog of the Berry phase of a single spin which is proportional to area enclosed by a spherical path [77, 8]: an explicit expression of  $\Gamma[n_t]$  requires 4+1 dimensions with an emergent spatial direction. Upon reduction to a O(3) non-linear sigma model for the Néel order parameter  $\mathcal{N}$  in Eq. (2.25), the WZW term reduces [78] to the Berry phases of the monopoles noted near Eq. (2.27).

Also, note that while the SO(5) symmetry is explicit in the fermionic spinon theory in Eq. (2.50), it is not explicit in the bosonic spinon theory in Eq. (2.27), but expected to be emergent [79].

The form in Eq. (2.57) has been exploited in recent numerical work on the fuzzy sphere [80]. Their results, and those of a number of other numerical works [81, 82, 83, 84, 85, 86, 87] show that the critical spin liquid defined by Eq. (2.27), Eq. (2.50), or (2.57) is stable over a substantial intermediate energy and length scales, before ultimately confining into a Néel or VBS state. This intermediate range stability is not a bug, but a feature ideal for our purposes of defining a FL\* state at intermediate temperatures, which ultimately confines to variety of other states at low temperatures.

### 3. Confinement to d-wave superconductivity and charge order at half-filling

We have so far considered the square lattice antiferromagnet as an insulator with an essentially infinite gap to electrically charged excitations. In the follow discussion, we will build on the low energy theory of such an antiferromagnet as a SU(2) gauge theory coupled to fermionic spinons in Eq. (2.43). We have argued that the phase diagram of such a theory is as in Fig. 3 *i.e.* except possibly in a critical region, the SU(2) gauge theory confines at low energies, and we obtain either the Néel or VBS states.

We now wish to consider a more general situation in which the gapped to charged excitations can vanish [88]. In the cuprates, gapless charged excitations appear when we dope the antiferromagnet. We will consider this important situation in the following sections. But for now we consider the simpler case where the charge gap vanishes while the electronic density remains the same as in an insulator; the resulting particle-hole symmetry simplifies the analysis. We can do this by describing the insulator by an underlying Hubbard model with on-site repulsion U, and reducing the value of U, or by adding additional off-site interactions. Such models have been considered in numerical studies [89, 90]. We will now show that the SU(2) gauge theory of Eq. (2.43) has other possible fates once charged excitations are included, the most interesting of which is a d-wave superconductor with gapless nodal quasiparticles. In terms of adiabatic continuity, this is precisely the superconductor observed in the cuprates. However, the d-wave superconductor obtained in this section has one significant quantitative difference

from the observations: it has a Lorentz-invariant form of its dispersion, with the two velocities only the square lattice diagonals,  $v_F$  and  $v_{\Delta}$ , being equal to each other (see Fig. 17B). The cuprates instead have  $v_F \gg v_{\Delta}$ . We will resolve this problem in an interesting manner in Section 5.1 when we consider the transition from FL\* to a d-wave superconductor in the doped case.

The only matter field in Section 2.2 is the fermion  $\mathcal{F}$ , which has electrical charge 0, spin 1/2, and is a gauge SU(2) fundamental. As we are allowing for charged fluctuations, we need to define an electron operator, which has charge -e, spin 1/2, and is a gauge SU(2) singlet. This directly leads us to introducing a boson B which has charge +e, spin 0, and is a gauge SU(2) fundamental, so that a composite of  $\mathcal{F}$  and B will have the same quantum numbers as the electron. We now show that this information is basically sufficient to deduce an effective action for B, and to reach our main conclusions. We will give a more microscopic definition of the field B in the doped case later near Eq. (5.3).

Similar to Eq. (2.30), we introduce a matrix notation for the electron  $\mathcal C$  and the boson B:

$$C_{i} \equiv \begin{pmatrix} c_{i\uparrow} & -c_{i\downarrow} \\ c_{i\downarrow}^{\dagger} & c_{i\uparrow}^{\dagger} \end{pmatrix} , \quad B_{i} \equiv \begin{pmatrix} B_{1i} \\ B_{2i} \end{pmatrix} , \quad \mathcal{B}_{i} \equiv \begin{pmatrix} B_{1i} & -B_{2i}^{*} \\ B_{2i} & B_{1i}^{*} \end{pmatrix} (3.1)$$

Then the generalization of the SU(2) gauge transformation in Eq. (2.33) is

$$C_i \to C_i$$
 ,  $F_i \to V_i F_i$   
 $\mathcal{B}_i \to V_i \mathcal{B}_i$  ,  $U_{ij} \to V_i U_{ij} V_i^{\dagger}$  , (3.2)

while the generalization of the global SU(2) spin rotation in Eq. (2.34) is

$$C_{i} \to C_{i} \sigma^{z} \Omega^{T} \sigma^{z} \quad , \quad \mathcal{F}_{i} \to \mathcal{F}_{i} \sigma^{z} \Omega^{T} \sigma^{z}$$

$$\mathcal{B}_{i} \to \mathcal{B}_{i} \quad , \quad U_{ij} \to U_{ij} . \tag{3.3}$$

Finally, the U(1) charge conservation symmetry acts as

$$C_i \to \Theta C_i \quad , \quad \mathcal{F}_i \to \mathcal{F}_i$$
  
 $\mathcal{B}_i \to \mathcal{B}_i \Theta^{\dagger} \quad , \quad U_{ij} \to U_{ij} ,$  (3.4)

where

$$\Theta = \begin{pmatrix} e^{i\theta} & 0\\ 0 & e^{-i\theta} \end{pmatrix}. \tag{3.5}$$

By matching these gauge, spin rotation, and charge conservation symmetries we deduce that the operator correspondence between the electrons, the Higgs boson B, and the fermionic spinons must be

$$C_i \sim \mathcal{B}_i^{\dagger} \mathcal{F}_i$$
. (3.6)

In terms of the matrix components, we can write Eq. (3.6) as

$$c_{i\alpha}^{\dagger} \sim B_{1i} f_{i\alpha}^{\dagger} + B_{2i} \varepsilon_{\alpha\beta} f_{i\beta},$$
 (3.7)

where  $\varepsilon_{\alpha\beta}$  is the unit antisymmetric tensor for spin SU(2).

Symmetry	$f_{\alpha}$	$B_a$
$T_x$	$(-1)^y f_\alpha$	$(-1)^y B_a$
$T_y$	$f_{lpha}$	$B_a$
$P_x$	$(-1)^x f_{\alpha}$	$(-1)^x B_a$
$P_y$	$(-1)^y f_\alpha$	$(-1)^y B_a$
$P_{xy}$	$(-1)^{xy}f_{\alpha}$	$(-1)^{xy}B_a$
$\mathcal{T}$	$(-1)^{x+y} \varepsilon_{\alpha\beta} f_{\beta}$	$(-1)^{x+y}B_a$

**Table 1.** Projective transformations of the f spinons and B chargons on lattice sites i = (x, y) under the symmetries  $T_x : (x, y) \to (x + 1, y)$ ;  $T_y : (x, y) \to (x, y + 1)$ ;  $P_x : (x, y) \to (-x, y)$ ;  $P_y : (x, y) \to (x, -y)$ ;  $P_{xy} : (x, y) \to (y, x)$ ; and time-reversal  $\mathcal{T}$ . The indices  $\alpha, \beta$  refer to global SU(2) spin, while the index a = 1, 2 refers to gauge SU(2).

We now obtain an energy functional for B in a Landau-type expansion [7]. Such a functional must also involve the gauge field U to maintain gauge invariance. The fermion f experiences a  $\pi$  flux with pure imaginary hopping, while the electron c has purely real hopping with zero flux (in the absence of an applied physical magnetic field). From these facts and Eq. (3.6) we reach the important conclusion that the boson B must also have purely imaginary hopping with  $\pi$ -flux (the iw term in Eq. (3.9) below). So the relation

$$T_x T_y = -T_y T_x \,, \tag{3.8}$$

realizing the  $\pi$ -flux applies both to the spinons and to B. We can also reach these conclusions, and obtain other constraints, by examining the action of all symmetry operators of f, and use Eq. (3.6) to deduce the action of symmetry operations on B: the results are summarized in Table 1. These considerations lead to the energy functional  $\mathcal{E}_2[B,U] + \mathcal{E}_4[B,U]$  with terms quadratic and quartic in B respenctively:

$$\mathcal{E}_{2}[B,U] = r \sum_{\mathbf{i}} B_{\mathbf{i}}^{\dagger} B_{\mathbf{i}} + iw \sum_{\langle ij \rangle} e_{ij} \left( B_{\mathbf{i}}^{\dagger} U_{ij} B_{\mathbf{j}} - B_{\mathbf{j}}^{\dagger} U_{ji} B_{\mathbf{i}} \right)$$

$$+ \kappa \sum_{\square} \left\{ 1 - \frac{1}{2} \operatorname{ReTr} \prod_{ij \in \square} U_{ij} \right\}$$

$$\mathcal{E}_{4}[B,U] = \frac{u}{2} \sum_{\mathbf{i}} \rho_{\mathbf{i}}^{2} + V_{1} \sum_{\mathbf{i}} \rho_{\mathbf{i}} \left( \rho_{\mathbf{i}+\hat{\mathbf{x}}} + \rho_{\mathbf{i}+\hat{\mathbf{y}}} \right) + g \sum_{\langle ij \rangle} |\Delta_{ij}|^{2} + J_{1} \sum_{\langle ij \rangle} Q_{ij}^{2}$$

$$+ K_{1} \sum_{\langle ij \rangle} J_{ij}^{2} + V_{11} \sum_{\mathbf{i}} \rho_{\mathbf{i}} \left( \rho_{\mathbf{i}+\hat{\mathbf{x}}+\hat{\mathbf{y}}} + \rho_{\mathbf{i}+\hat{\mathbf{x}}-\hat{\mathbf{y}}} \right)$$

$$+ V_{22} \sum_{\mathbf{i}} \rho_{\mathbf{i}} \left( \rho_{\mathbf{i}+2\hat{\mathbf{x}}+2\hat{\mathbf{y}}} + \rho_{\mathbf{i}+2\hat{\mathbf{x}}-2\hat{\mathbf{y}}} \right). \tag{3.9}$$

The quartic terms are expressed as products of bilinears of B which are associated with various gauge-invariant observables as identified below

site charge density: 
$$\left\langle c_{i\alpha}^{\dagger}c_{i\alpha}\right\rangle \sim \rho_{i}=B_{i}^{\dagger}B_{i}$$

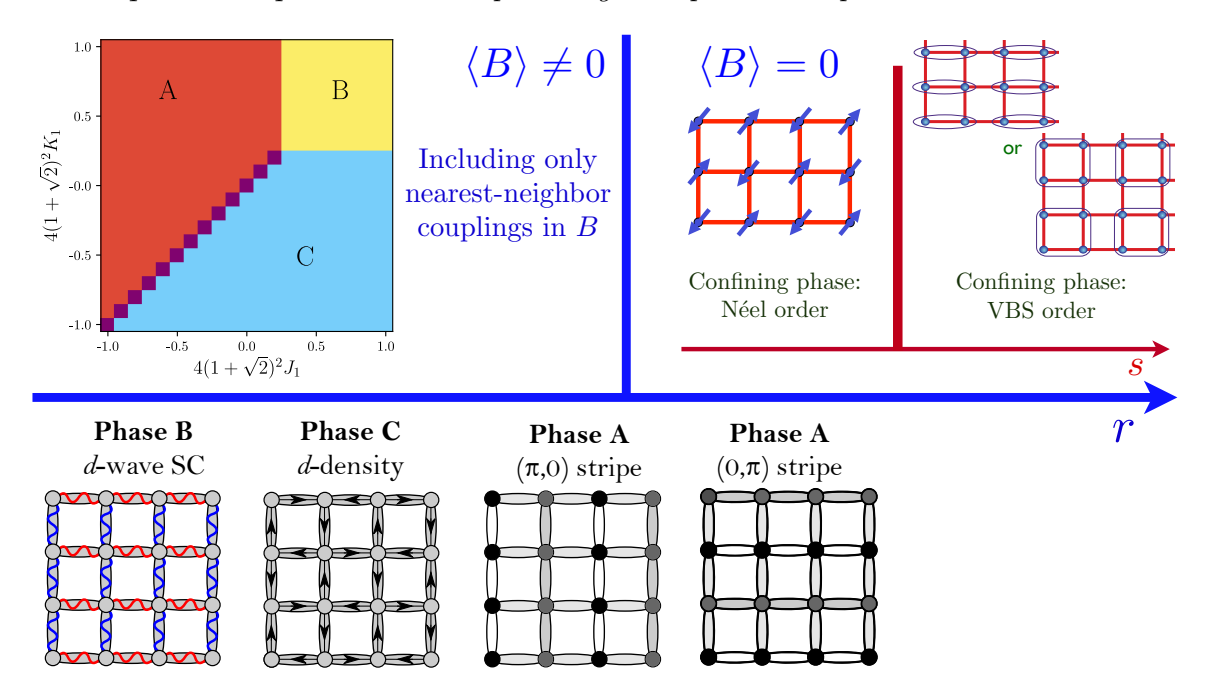


**Figure 6.** Mean field phase diagram obtained by minimized the Higgs potential of B,  $\mathcal{E}_2 + \mathcal{E}_4$  (from Ref. [7]).

bond density: 
$$\left\langle c_{i\alpha}^{\dagger} c_{j\alpha} + c_{j\alpha}^{\dagger} c_{i\alpha} \right\rangle \sim Q_{ij} = Q_{ji} = \operatorname{Im} \left( B_{i}^{\dagger} e_{ij} U_{ij} B_{j} \right)$$
  
bond current:  $i \left\langle c_{i\alpha}^{\dagger} c_{j\alpha} - c_{j\alpha}^{\dagger} c_{i\alpha} \right\rangle \sim J_{ij} = -J_{ji} = \operatorname{Re} \left( B_{i}^{\dagger} e_{ij} U_{ij} B_{j} \right)$   
Pairing:  $\left\langle \varepsilon_{\alpha\beta} c_{i\alpha} c_{j\beta} \right\rangle \sim \Delta_{ij} = \Delta_{ji} = \varepsilon_{ab} B_{ai} e_{ij} U_{ij} B_{bj}$ . (3.10)

We have retained terms involving nearest neighbor sites, and a few terms with longerrange density-density interactions.

Fig. 6 shows a phase diagram obtained by minimizing the energy functional with nearest-neighbor interactions only  $(V_{11} = V_{22} = 0)$ . Three phases are found, also illustrated in Fig. 6:

- A. This state A charge stripe order with period 2, centered on the sites.
- B. A d-wave superconductor, with  $\Delta_{i,i+\hat{x}} = -\Delta_{i,i+\hat{y}}$ .
- C. A "d-density wave" state which has a staggered pattern of spontaneous current.

Our primary interest for now is phase B. The remarkable fact is that it is the structure of the  $\pi$ -flux spin liquid, and consequent  $\pi$ -flux on B which has led to the d-wave pairing, and not s-wave pairing. Also, once B is condensed, we can identify  $c \sim f$  via Eq. (3.6), and so the electron spectral function will inherit nodal Bogoliubov quasiparticles from the massless Dirac spinons. The main phenomenological difficulty, as noted earlier, is that the Bogoliubov quasiparticles will have isotropic dispersion, as in Eq. (2.41) and Fig. 5. However, other features of the d-wave state obtained from the energy functional in Eq. (3.9) do match observations, including vortices with flux h/(2e) (despite the boson B having charge e), and competing charge order halos of vortex cores.

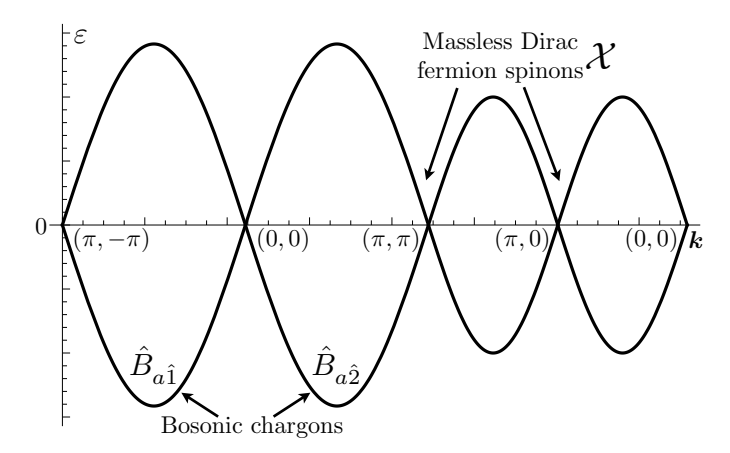


**Figure 7.** Common dispersion of the fermionic spinons f, and the bosonic chargens B. The continuum fermionic fields  $\mathcal{X}$  are defined at zero energy, while the continuum bosonic fields  $\hat{B}$  are defined at the minimum energy.

As these features apply also to the doped case, we defer their discussion to Section 5, where we will also fix the difficulty with the anisotropic velocities in Section 5.1.

We now discuss more global aspects of the phase diagram shown in Fig. 6, as a function of the tuning parameter r, which is the 'mass' of B.

- When r is large and positive, then we can ignore the B sector, and revert to the spinon only theory of Section 2.2. The low energy theory is Eq. (2.50), and we expect a confining insulator with either Néel or VBS order as the ground state.
- When r is negative, B condenses, and this has the salutary effect of making the gauge field A massive, as in the Higgs phenomenon. So a mean-field treatment is qualitatively valid, and we obtain one of three states A,B,C listed above.

It is also interesting to consider the nature of the low energy theory when we approach the Higgs condensation transition [88]. The dispersion of the B bosons is the same as that of the f fermions, apart from an overall constant - see Fig. 7. And while the low energy fermions are near the middle of the band, the low energy bosons are near the bottom of the band. In this manner, we identify two valleys  $v = \hat{1}, \hat{2}$ , and we introduce a continuum field  $\hat{B}_{av}$  for the low energy theory, where a = 1, 2 is a SU(2) gauge space index (this is similar to Section 2.1.2). From the lattice transformations in Table 1, we can also relate the order parameters A,B,C to gauge-invariant bilinears of  $\hat{B}$ 

$$\begin{array}{lll} d\text{-wave superconductor}: & \varepsilon_{ab} \hat{B}_{a\hat{1}} \hat{B}_{b\hat{2}} \equiv \Delta \\ & x\text{-CDW} & : & \hat{B}_{a\hat{1}}^* \hat{B}_{a\hat{1}} - \hat{B}_{a\hat{2}}^* \hat{B}_{a\hat{2}} \equiv \hat{B}^\dagger \mu^z \hat{B} \\ & y\text{-CDW} & : & \hat{B}_{a\hat{1}}^* \hat{B}_{a\hat{2}} + \hat{B}_{a\hat{2}}^* \hat{B}_{a\hat{1}} \equiv \hat{B}^\dagger \mu^x \hat{B} \\ & d\text{-density wave} & : & i \left( \hat{B}_{a\hat{1}}^* \hat{B}_{a\hat{2}} - \hat{B}_{a\hat{2}}^* \hat{B}_{a\hat{1}} \right) \equiv -\hat{B}^\dagger \mu^y \hat{B} \end{array} . \tag{3.11}$$

Here  $\mu^{\ell}$  are the Pauli matrices acting in the boson valley space of Fig. 7.

We now assume that the quartic couplings of B are such that the ground state in the Higgs phase is a d-wave superconductor. Then, we can sketch the phase diagram in

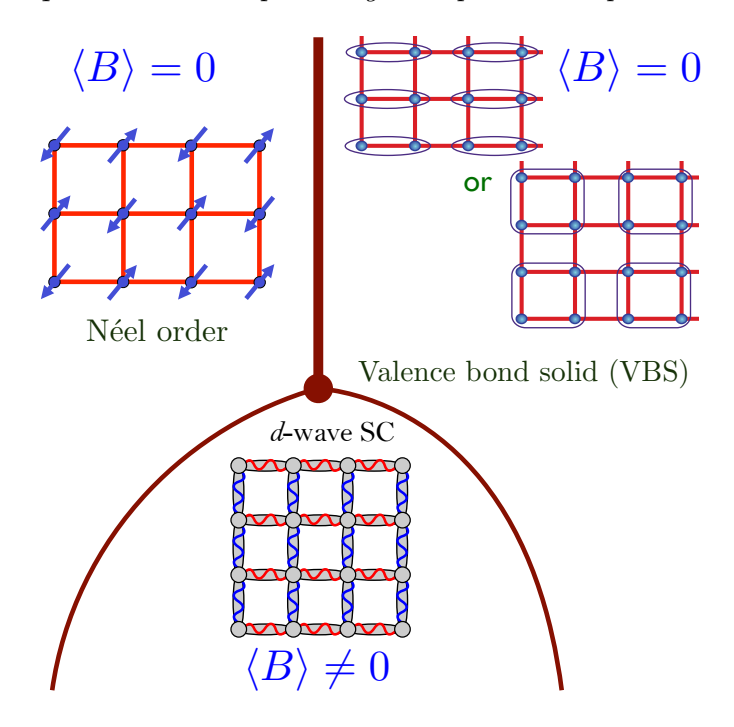


**Figure 8.** Proposed phase diagram of  $\mathcal{L}_{\chi\hat{B}}$ .

Fig. 8 with the 3 important phases - Néel, VBS, and d-wave superconductivity. Near the onset of the B condensate, we extend the spinon continuum theory of Eq. (2.50) to also include phases A,B,C by adding a continuum Lagrangian for  $\hat{B}$ :

$$\mathcal{L}_{\mathcal{X}\hat{B}} = \mathcal{L}_{\mathcal{X}} + \left| \left( \partial_{\mu} - iA_{\mu}^{\ell} \sigma^{\ell} \right) \hat{B} \right|^{2} + r|\hat{B}|^{2} + \bar{u}|\hat{B}|^{4}$$

$$+ v_{1} \left( \hat{B}^{\dagger} \mu^{z} \hat{B} \right)^{2} + v_{1} \left( \hat{B}^{\dagger} \mu^{x} \hat{B} \right)^{2} + v_{2} \left( \hat{B}^{\dagger} \mu^{y} \hat{B} \right)^{2} + v_{3} \left| \varepsilon_{ab} \hat{B}_{a1} \hat{B}_{b2} \right|^{2} . (3.12)$$

We have added only a relativistic time derivative term for  $\hat{B}$ , which is the allowed term at half-filling with particle-hole symmetry.

### 4. Fractionalized Fermi liquids

We now turn our discussion to metallic systems. Almost all metals are well described at low temperatures by the principles of Fermi liquid theory. This is a theory of nearly free fermionic quasiparticle excitations with the same spin and charge as an electron. The energy of these quasiparticles vanishes on a d-1 dimensional surface in momentum space (d is the spatial dimension) known as the Fermi surface. A crucial feature for our purposes is the Luttinger constraint on the volume enclosed by the Fermi surface in momentum space. Luttinger established by a perturbative diagrammatic analysis that the enclosed volume is independent of the strength of the interactions and is determined only by the electron density  $\rho$  [91]. A more precise statement is that the volume enclosed by the Fermi surface is the same as that of a free electron system with the same symmetry and the same density.

An important step forward was Oshikawa's proof of the Luttinger constraint using a 't Hooft anomaly matching argument [92]. Oshikawa identified a mixed anomaly between translations and global U(1) symmetry of charge conservation. The value of the anomaly can be computed exactly from a knowledge of the density of electrons in the lattice Hamiltonian. Matching this anomaly with that of the low energy Fermi liquid theory, Oshikawa established the Luttinger constraint in a non-perturbative manner [6, 93, 94].

Soon after, the idea of a 'fractionalized Fermi liquid' (FL\*) was introduced [3, 4], as a metallic state in which the Fermi surface did *not* obey the Luttinger constraint. In the simplest case, the volume enclosed by the Fermi surface in FL\* was the same as free electrons with density  $\rho - 1$  (we are assuming a spin S = 1/2 degeneracy). The central point was that it was possible to satisfy Oshikawa's anomaly by combining the anomaly of a Fermi surface (which contributes an amount equivalent to a density  $\rho - 1$ ) with that of a fractionalized spin liquid of the type studied in Section 2 (which contributes an amount equivalent to a density 1).

We will illustrate these ideas by explicit constructions of FL\*, first in a two-band Kondo lattice model in Section 4.1, and then a single band Hubbard-like model in Section 4.2.

### 4.1. Kondo lattice

The Kondo lattice is illustrated in Fig. 9. A Kondo exchange interaction couples the

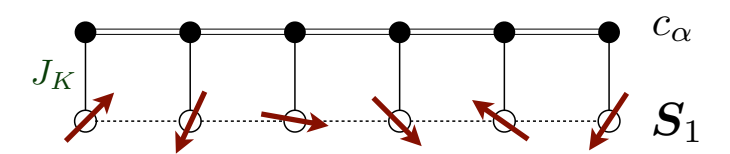


**Figure 9.** A Kondo lattice of conduction electrons c coupled to S = 1/2 spins  $S_1$ . All lattices are two-dimensional, although only one-dimensional projections are shown.

spin model of Section 2 in Eq. (2.1) with a Fermi surface of free electrons  $c_{\alpha}$  of density p in a second band:

$$\mathcal{H}_{KL} = \sum_{i < j} J_{1,ij} S_{1i} \cdot S_{1j} - \sum_{i,j} t_{ij} c_{i\alpha}^{\dagger} c_{j\alpha} + \sum_{i} \frac{J_K}{2} S_{1i} \cdot c_{i\alpha}^{\dagger} \boldsymbol{\sigma}_{\alpha\beta} c_{i\beta}$$
(4.1)

We have now written the spins as  $S_{1i}$ , rather than  $S_i$ , in anticipation of a second set of spins,  $S_{2i}$ , to be introduced in the next subsection. While  $\mathcal{H}_{KL}$  can have a wide variety of phases, we focus on two phases which have no broken symmetries. We proceed with the fermionic parton method of Section 2.2, replacing Eq. (2.28) by

$$S_{1i} = \frac{1}{2} f_{1,i\alpha}^{\dagger} \boldsymbol{\sigma}_{\alpha\beta} f_{1i\beta} . \tag{4.2}$$

# Fermi-volume-changing QPT in the Kondo lattice $\langle \Phi \rangle = 0$ $\langle \Phi \rangle = 0$ Higgs boson $\Phi \sim f_{1\alpha}^{\dagger} c_{\alpha}$ $\Phi > 0$ $\Phi > 0$ $\Phi > 0$ $\Phi > 0$ Higgs boson $\Phi > f_{1\alpha}^{\dagger} c_{\alpha}$ $\Phi > 0$ $\Phi > 0$

**Figure 10.** Phase diagram of the Kondo lattice. Neither phase has any symmetry breaking, but there is nevertheless a quantum phase transition (a Higgs transition in an emergent gauge theory) associated with Fermi volume change [3, 4].

Then, as in Section 2.2, we decouple both sets of exchange interactions to obtain a mean-field fermion Hamiltonian [95, 96, 97, 98]

$$\mathcal{H}_{\text{KLmf}} = \sum_{i,j} \left[ -t_{ij} c_{i\alpha}^{\dagger} c_{j\alpha} - t_{1,ij} f_{1i\alpha}^{\dagger} f_{1j\alpha} \right] - \sum_{i} (\Phi c_{i\alpha}^{\dagger} f_{1i\alpha} + \Phi^* f_{1i\alpha}^{\dagger} c_{i\alpha}) . (4.3)$$

The  $\Phi$  is the decoupling field for the  $J_K$  interaction, while the  $t_{1,ij}$  are the decoupling fields for the  $J_{1,ij}$  interactions. Unlike Section 2.2, we do not assume any flux in the  $t_{1,ij}$ , and make the simplest possible choice in which the  $t_{1,ij}$  have the same symmetry as the lattice. With these choices, our Kondo lattice theory only has an emergent U(1) gauge symmetry under which

$$f_{1i\alpha} \to e^{i\phi_i} f_{1i\alpha} \quad , \quad t_{1,ij} \to t_{1,ij} e^{i\phi_i - i\phi_j}$$
 $c_{i\alpha} \to c_{i\alpha} \quad , \quad \Phi_i \to \Phi_i e^{-i\phi_i}$  (4.4)

This is distinct from the global charge conservation symmetry, under which only maps  $c_{i\alpha} \to e^{i\theta} c_{i\alpha}$ , while all other fields remain invariant.

We can now identify two distinct phases of the Kondo lattice model, neither with any symmetry breaking [3, 4], as illustrated in Fig. 10.

•  $\langle \Phi \rangle \neq 0$ , FL. This is the conventional 'heavy Fermi liquid' phase, observed in numerous heavy fermion compounds. The Fermi surface obeys the Luttinger constraint. The condensation of the Higgs boson  $\Phi$  quenches the gauge fluctuations associated with Eq. (4.4). The Fermi surface is described by the simple two-band model of Eq. (4.3), in which  $\Phi$  hybridizes the two bands. The total density of electrons is 1+p, and if all the fermions are in the lower energy band, we obtain a Fermi surface of size 1+p, as illustrated in Fig. 10. The heavy quasiparticle mass arises in cases where there is little direct interactions between the  $S_1$  spins: then the  $J_{ij}$  and hence the  $t_{1,ij}$  are very small, and we have a nearly flat band  $f_1$  band hybridizing with the conduction band of c near the Fermi level.

•  $\langle \Phi \rangle = 0$ ,  $FL^*$ . This is the novel phase, in which the  $f_1$  and c fermions are decoupled to leading order in  $\mathcal{H}_{KLmf}$ . The  $f_{1\alpha}$  form a spin liquid, in this case one with a spinon Fermi surface. But any other spin liquid with the same anomaly is allowed *i.e.* any other spin liquid with unit density of spinons in the ground state. The conduction electrons now form a 'small' Fermi surface of size p, and this is not the Luttinger value. At higher order, the  $f_1$  and c fermions will couple with each other, and in general, because of the absence of particle-hole symmetry in the underlying electronic model with a large but finite U on the  $f_1$  sites (often called the lattice Anderson model), the density of electrons in the  $f_1$  band will deviate from unity. Nevertheless, a crucial point is that the size of the Fermi surface will remain pinned at p, because the anomaly of the spin liquid is pinned at unity.

### 4.2. Single band model

We now turn to a construction of the FL\* phase in a single band model, such as the square lattice Hubbard model (possibly with longer range interactions) of interest for the cuprates. Now the situation is more complicated than in the Kondo lattice model, as there is no natural distinction between electrons that form a spin liquid, and electrons that form a Fermi surface.

Nevertheless, at the level of cartoon pictures, we can illustrate the structure of a FL\* state in Fig. 11 [99]. This figure describes three distinct metallic phases in a Hubbard time model with electron density 1 - p. Note that in the absence of a broken symmetry, the Luttinger constraint on hole Fermi surfaces is that they have a fractional area of 1 + p, relative to the area of the full square lattice Brillouin zone.

- AF Metal. This is a state with antiferromagnetic long-range order. We can understand the Fermi surface by considering free electrons moving in a background with the same symmetry *i.e.* in a background spin-dependent potential which has a modulation at the wavevector  $(\pi, \pi)$ . This leads to the magnetic Brillouin zone boundary shown by the dashed line, and 4 hole pocket Fermi surfaces. Only two of these pockets are independent within the magnetic Brillouin zone. After accounting for a factor of 2 from spin, we conclude that the fractional area of each pocket is p/4. This Fermi surface area obeys the Luttinger constraint. Thermal fluctuations do not move Fermi surfaces, only broaden them, and so we expect that a fluctuating spin density wave state will also have pockets of area p/4 [27, 28, 29, 30].
- Holon metal. This is a state with no broken symmetry, in which the electrons have paired up in singlet bonds which resonate with each other. The dopants are realized by spinless mobile vacancies of charge +e, known as holons. The density of holons is p, and if the holons are fermions, they will form Fermi surfaces corresponding to spinless free fermions of density p. If there are four distinct Fermi surfaces in the Brillouin zone (as is the case in many computations), then the fractional area of each pocket will be p/4. Although this area is the same as that for the AF metal, the reason is very different. Now there is no broken symmetry, and the

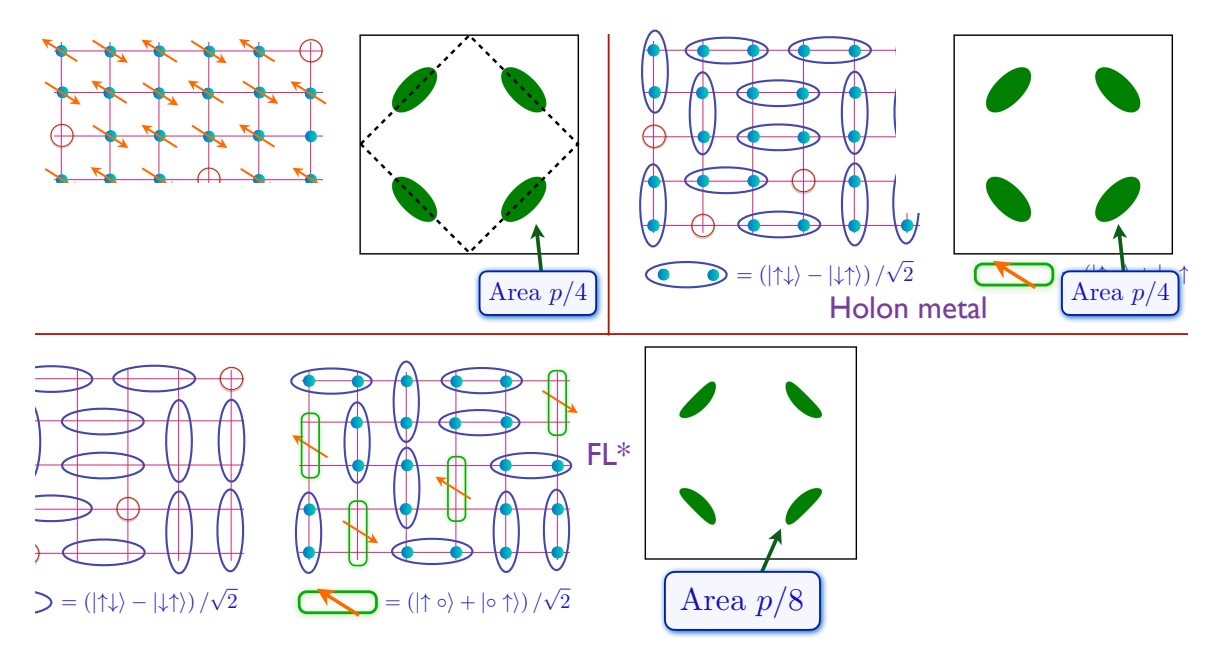


Figure 11. Cartoon pictures of different states of doped antiferromagnets; adapted from Ref. [99]. The AF metal has long-range antiferromagnetic order, and the reduced Brillouin zone is shown with the dashed line. The other phases do not break any symmetries. The open circles are holons, and these are assumed fermionic in the holon metal. The green dimers represent bound states of holons and spinons.

fermionic quasiparticles are spinless holons. This Fermi surface area does *not* obey the Luttinger constraint, and this is permitted because of the presence of the spin liquid.

•  $FL^*$ . Finally, we turn to the metallic state of interest. The holon metal state also has spinon excitations, which can be created out of the ground state. Now imagine a situation in which each holons gains energy by binding with a spinon, so that the system can pay the price for creating the spinons. Then the ground state will change into one in which the mobile charge carriers are holon-spinon bound states [26, 100, 101, 102, 103, 104, 105, 99, 106, 107, 108, 109, 110]. These are always fermions with charge +e, spin S=1/2, just like a hole. Treating these holes as free fermions, we conclude that the total area of the Fermi surface should be p/2. If there are 4 distinct pockets (as there in the computation below), then each pocket will have the distinctive area of p/8. This Fermi surface area also does not obey the Luttinger constraint.

Recent observations by Chan *et al.* [25] of the Yamaji effect in HgBa<sub>2</sub>CuO<sub>4+ $\delta$ </sub> show a fractional area of 'approximately 1.3%' at a doping p=0.1, close to the value p/8=1.25% predicted for FL\* [3, 4, 26, 111].

While much insight can be gained from the methods above, they fall short of providing a mean-field theory for the FL\* phase, which can then be used to study quantum phase transitions out of it. To this end, we now describe the ancilla method [112, 113], which is designed to do so, while also easily ensuring consistency with anomaly

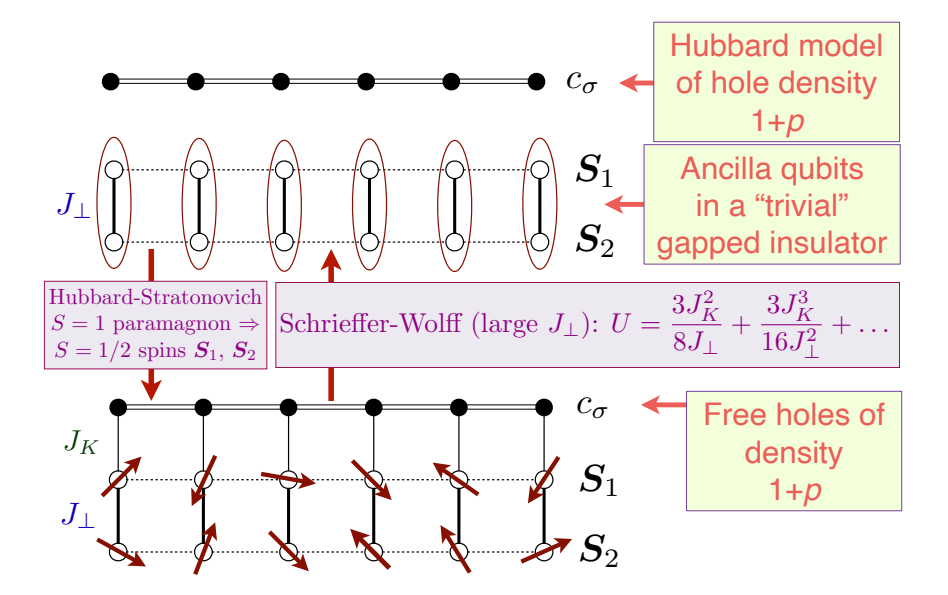


**Figure 12.** Illustration of the mapping from a single band Hubbard model with decoupled ancilla qubits, to a single band with free fermions coupled to a bilayer antiferromagnet. The Schrieffer-Wolff transformation is derived in Ref. [117].

arguments. The ancilla method can also be used to write down variational wavefunctions for the FL\* phase, which can then be studied numerically: such numerical analyses [114, 115, 116] are in good agreement with cold atom experiments measuring local, multi-point spin and charge correlations.

The key idea is to "integrate in" ancilla quantum degrees of freedom, similar to a Hubbard-Stratonovich transformation, see Fig. 12. It is important that the new degrees of freedom have a trivial ground state with an energy gap, so that its extra excited states can be eliminated by a canonical transformation, similar to a Schrieffer-Wolff transformation. For the ancillas, we choose a pair of qubits associated with every site of the square lattice, which we identify as S = 1/2 spins  $S_{1i}$  and  $S_{2i}$ . There is an exchange interaction  $J_{\perp}$  between the two spins at each i, and so the ancillas form a bilayer square lattice antiferromagnet. We take  $J_{\perp}$  to be large enough so that the ground state of the bilayer is smoothly connected to the rung singlet state. This bilayer has a triplon excited state, which eventually connects to the paramagnon obtained by the Hubbard-Stratonovich transformation on the Hubbard model: so the spins  $S_{1i}$  and  $S_{2i}$ are S=1/2 fractionalizations of the S=1 paramagnon [118]. As illustrated in Fig. 12, we can perform an inverse Schrieffer-Wolff transformation to map to a model of free electrons coupled by a Kondo exchange  $J_K$  to the  $S_{1i}$  [117]. So the ancilla Hamiltonian is a simple augmentation of the Kondo lattice Hamiltonian  $\mathcal{H}_{KL}$  in Eq. (4.1) by the  $S_{2i}$ spins

$$\mathcal{H}_{\text{ancilla}} = \mathcal{H}_{\text{KL}} + J_{\perp} \sum_{i} S_{1i} \cdot S_{2i} + \sum_{i < i} J_{ij} S_{2i} \cdot S_{2j} + \dots$$
 (4.5)

We have also included a direct exchange interaction between the  $S_{2i}$  spins, and that will be important for our purposes below. The Schrieffer-Wolff transformation eliminates all

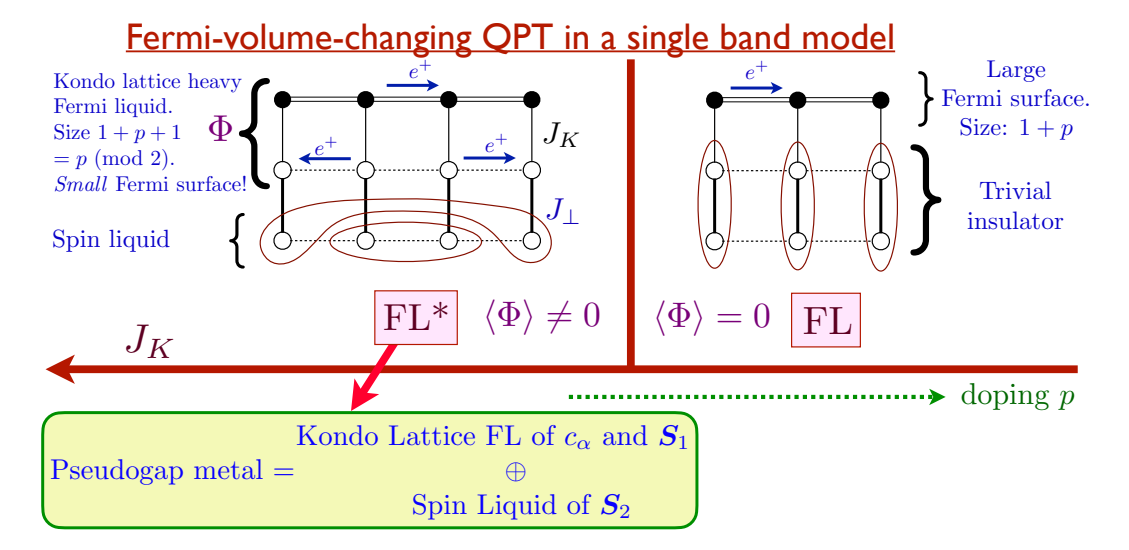


**Figure 13.** Phases of the ancilla theory. They are distinguished by the condensation of the boson  $\Phi$ , which hybridizes the conduction electrons in the top layer with the fermionic spinons in the middle layer.

the excited states of the ancilla spins in powers of  $1/J_{\perp}$ , and returns to the single band Hubbard model for the  $c_{i\alpha}$ , with the value of U shown in Fig. 12 [117].

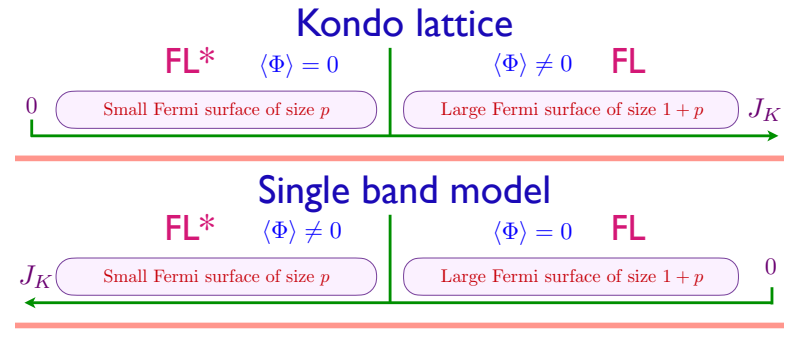
We are now ready to discuss the phase diagram of  $\mathcal{H}_{ancilla}$  shown in Fig. 13.

At small  $J_K$ , the ancilla spins decouple into rung singlets, and we are back to a  $c_{\alpha}$  state adiabatically connected to free electrons, which is the conventional Fermi liquid with a large hole pocket of area 1 + p.

At large  $J_K$ , we assume that the  $c_{\alpha}$  electrons and  $S_1$  spins realize the conventional FL phase of  $\mathcal{H}_{KL}$  in Fig. 10. With the present density  $c_{\alpha}$  equal to 1+p, the total density of the 'large' Fermi surface is 2+p. As a trivial filled band with density 2 can always be removed, we obtain 'small' Fermi surface of size p in the FL phase of  $\mathcal{H}_{KL}$ . While this is the Luttinger value for  $\mathcal{H}_{KL}$ , it is not for  $\mathcal{H}_{ancilla}$ . Indeed, we obtain a FL\* phase for  $\mathcal{H}_{ancilla}$  if the  $S_{2i}$  layer forms a spin liquid, and the effects of  $J_{\perp}$  in Eq. (4.5) can be treated perturbatively. This leads the identification in Fig. 13 of the FL\* pseudogap metal with the combination of a Kondo lattice FL state of  $c_{\alpha}$  and  $S_1$ , and a spin liquid of  $S_2$ .

In the remaining discussion of the present section, we ignore the  $S_2$  layer, and discuss the FL\* state of the single band model solely in terms of the Kondo lattice model  $\mathcal{H}_{KL}$  in Eq. (4.1). The coupling to the  $S_2$  is definitely needed for a complete theory, and we will include it in Section 5. For now, we proceed with parton decomposition of  $S_1$  in Eq. (4.2), and obtain the fermion Hamiltonian Eq. (4.3). When considered as a theory of the Kondo lattice model  $\mathcal{H}_{KL}$ , the FL state corresponds to the condensation of the decoupling field  $\Phi$ . On the other hand, for  $\mathcal{H}_{ancilla}$ , the  $\Phi$  condensed phase is the FL\* state, as we just discussed. This interesting inversion is highlighted in Fig. 14: the single band model has an 'inverted' Kondo lattice transition.

Mascot et al. [118] used  $\mathcal{H}_{KLmf}$  in Eq. (4.3) to model the photoemission spectra in



One-band model has an 'inverted' Kondo lattice transition in a theory using a bilayer of ancilla qubits

Figure 14. Comparison of the phases of the Kondo lattice model in Fig. 10, and the ancilla theory of the single band Hubbard model in Fig. 13. There is an inversion in the phase in which  $\Phi$  is condensed.

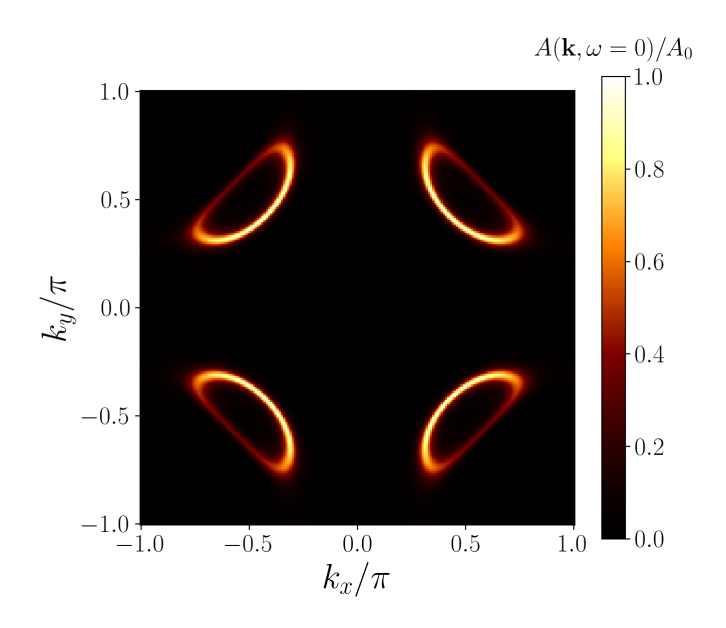


**Figure 15.** Zero energy electronic spectral weight (as would be measured in photoemission) in the ancilla mean field theory of the FL\* phase, from Ref. [118]. The corrections from thermal fluctuations of B are shown later in Fig. 19, where they lead to Fermi arcs.

the cuprates. The value  $\Phi$  was fixed by the magnitude of the fermion pseudogap near wavevectors  $(0, \pi)$ ,  $(\pi, 0)$ , the values of the  $t_{ij}$  are known from observations at large doping, and only the values of the  $t_{1,ij}$  were fitting parameters. The results provide a good fit to observations over a wide range of frequency across the Brillouin zone. We show the theory for the zero energy photoemission spectral weight in Fig. 15. There are 4 hole pockets, each of fractional area p/8, which are obtained from the hybridization of the  $c_{\alpha}$  band of density 1 + p and the  $f_{1\alpha}$  band of density 1 in Eq. (4.3). (In contrast, in spin density wave theory, we would hybridize the  $c_{\alpha}$  band of density 1 + p, with a  $(\pi, \pi)$  momentum-shifted  $c_{\alpha}$  band also of density 1 + p to obtain pockets of area p/4.) The

pockets of Fig. 15 do have faint, but visible, 'backsides'. In contrast, the observations how only 'Fermi arcs' corresponding to the front sides of the pockets (See Fig. 19 later), with no visible backsides. We will show in Section 5.3 how this issue is resolved by inclusion of the coupling to the  $S_2$  spin liquid.

### 5. From the pseudogap to d-wave superconductivity and competing orders

This section address the fate of the FL\* pseudogap as the temperature is lowered, upon including the coupling to the  $S_2$  spin liquid. We will specifically choose the  $\pi$ -flux spin liquid of Section 2.2 for the  $S_2$  layer. We will show that for this spin liquid there is a transition to a conventional BCS-type d-wave superconductor, with anisotropic nodal velocities for the Boboliubov quasiparticles, and h/(2e) vortices. Nevertheless the transition itself is not of the BCS type with a Cooper-pairing instability of a Fermi surface. Instead, the transition is driven by the confinement of the fractionalized excitations of the  $S_2$  spin liquid. We also find nearby instabilities to charge ordering, consistent with observations.

Our analysis proceeds from the Hamiltonian  $\mathcal{H}_{\text{ancilla}}$  in Eq. (4.5). We apply the parton decoupling to  $\mathcal{H}_{\text{KLmf}}$  in Eq. (4.3) as before. We write the parton decomposition of  $S_2$  as

$$S_{2,i} = \frac{1}{2} f_{i\alpha}^{\dagger} \boldsymbol{\sigma}_{\alpha\beta} f_{i\beta}$$
 (5.1)

and decouple the  $J_{ij}$  term in Eq. (4.5) to  $\mathcal{H}_{SLf}$  in Eq. (2.43) realizing a  $\pi$ -flux state with a SU(2) gauge field.

Finally, we have to decouple the  $J_{\perp}$  term coupling the  $f_1$  and f spinons. Given the SU(2) gauge structure of the  $S_2$  layer, it pays to decouple the  $J_{\perp}$  term in a manner which keeps the SU(2) gauge invariance explicit. In fact, the needed decoupling field is precisely the boson  $\mathcal{B}_i$  introduced in Eq. (3.1). We also introduce a matrix fermion operator  $\mathcal{F}_{1i}$ 

$$\mathcal{F}_{1i} \equiv \begin{pmatrix} f_{1i\uparrow} & -f_{1i\downarrow} \\ f_{1i\downarrow}^{\dagger} & f_{1i\uparrow}^{\dagger} \end{pmatrix}, \tag{5.2}$$

whose transformations under the symmetries in Eqs. (3.2,3.3,3.4) are the same as those of  $C_i$ . Then, from the  $J_{\perp}$  term, symmetry considerations are sufficient to constrain the structure of the Yukawa term between  $\mathcal{B}$  and the fermions [7], which is illustrated in Fig. 16:

$$\mathcal{H}_{Y} = -\frac{1}{2} \sum_{i} \left[ i \operatorname{Tr} \left( \mathcal{F}_{1i}^{\dagger} \mathcal{B}_{i}^{\dagger} \mathcal{F}_{i} \right) + i g \operatorname{Tr} \left( \mathcal{C}_{i}^{\dagger} \mathcal{B}_{i}^{\dagger} \mathcal{F}_{i} \right) + \operatorname{H.c.} \right]$$

$$= \sum_{i} \left[ i \left( B_{1i} f_{i\alpha}^{\dagger} f_{1i\alpha} - B_{2i} \varepsilon_{\alpha\beta} f_{i\alpha} f_{1i\beta} \right) + \operatorname{H.c.} \right]$$

$$+ i g \left( B_{1i} f_{i\alpha}^{\dagger} c_{i\alpha} - B_{2i} \varepsilon_{\alpha\beta} f_{i\alpha} c_{i\beta} \right) + \operatorname{H.c.} \right], \qquad (5.3)$$

We have also included a Yukawa coupling to  $c_{\alpha}$  from an allowed term  $\sim S_2 \cdot c_{i\alpha}^{\dagger} \sigma_{\alpha\beta} c_{i\beta}$ .

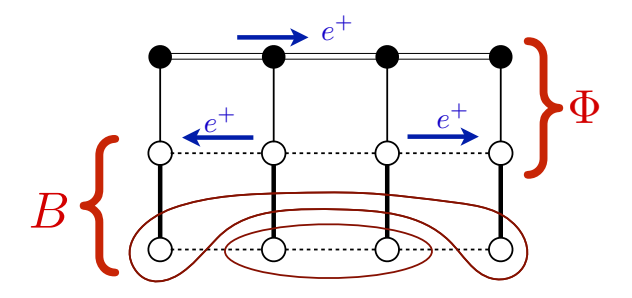


**Figure 16.** The two distinct Higgs fields in the ancilla theory of the single band Hubbard model.  $\Phi$  hybridizes conduction electrons in the top layer with spinons in the middle layer. B couples the spinons of the bottom layer to the upper layers.

We can now collect all terms to write down the complete Hamiltonian needed for our analysis of the pseudogap metal, and its low temperature instabilities.

$$\mathcal{H}_{\text{pseudogap}} = \mathcal{H}_{\text{KLmf}} + \mathcal{H}_{SLf} + \mathcal{H}_{Y} + \mathcal{E}_{2}[B, U] + \mathcal{E}_{4}[B, U]$$
 (5.4)

specified in Eqs. (4.3), (2.43), (5.3), (3.9). This Hamiltonian has 3 fermions  $c_{\alpha}$ ,  $f_{1\alpha}$ ,  $f_{\alpha}$  whose transformations under SU(2) gauge, spin rotation, and electromagnetic charge symmetries are in Eqs. (3.2), (3.3), (3.4), with  $f_{1\alpha}$  transforming just like  $c_{\alpha}$ . The boson  $\Phi$  will be treated as a c-number constant here, although we will consider its quantum and thermal fluctuations in Section 7. The boson B and the gauge field U will be treated as classical variables, with thermal fluctuations, analogous to nuclear positions in the Born-Oppenheimer approximation [41].

There is a remarkable similarity between Eq. (5.4), and the Weinberg-Salam theory of weak interactions [7]. Although the dispersions of the fermions and bosons have a lattice structure, the SU(2)× U(1) gauge structure (we treat the electromagnetic U(1) as global), and the Yukawa couplings between the Higgs and the fermions are similar, with the spinons mapping to neutrinos, and the electrons mapping to electrons.

The following subsections show how such a Born-Oppenheimer analysis of  $\mathcal{H}_{pseudogap}$  connects to a wide range of experimental observations in the underdoped cuprates.

### 5.1. Anisotropic velocities in the d-wave superconductor

We now show how the problem of isotropic quasiparticle velocities, noted in Section 3, is resolved by the presence of the pocket Fermi surfaces described by  $\mathcal{H}_{KLmf}$ . This discussion below is based on the detailed computations presented in Refs. [23, 24].

Given the pocket Fermi surfaces in Fig. 15, we imagine imposing a BCS type pairing on the Fermi surface excitations. If the pairing is d-wave, it would lead to 8 nodal Bogoliubov points as shown in Fig. 17A. However this state also has the 4 nodal quasiparticles of the  $S_2$  spin liquid, associated with the dispersion in Fig. 5. So strictly speaking, this state remains fractionalized, and is *not* a conventional d-wave superconductor. It would be appropriate to call it d-SC\*.

However, if we induce the pairing by the B condensate in Eq. (5.3), the SU(2) gauge field is higgsed. Morever, the Yukawa coupling allows the nodal quasiparticles of the  $S_2$ 

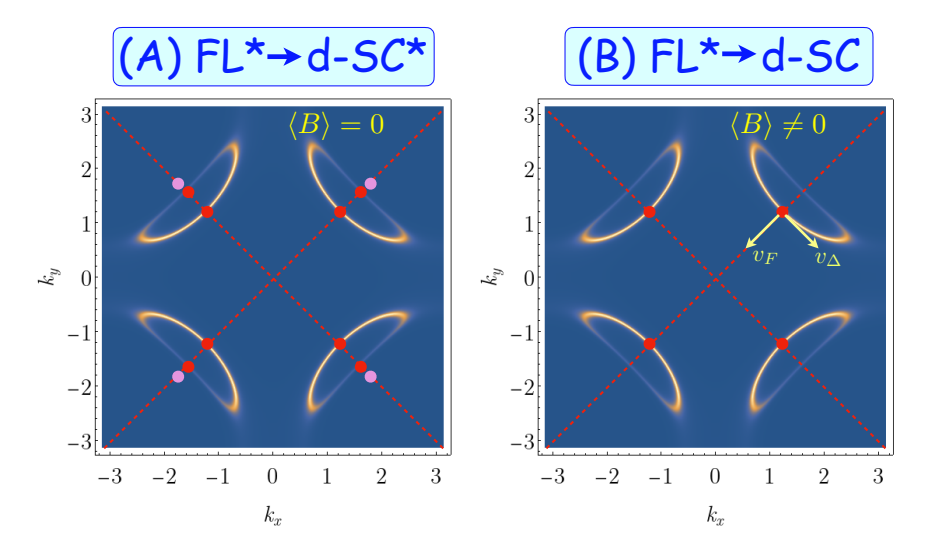


Figure 17. (A) Cooper pairing the Fermi surface quasiparticles in FL\* leads to d-SC\* state, with 8 nodal Bogoliubov quasiparticles (red), and 4 nodal spinons (pink). (B) Upon condensing B, the spinons mutually annihilate 4 of the Bogoliubov quasiparticles, leaving 4 Bogoliubov quasiparticles with  $v_F \gg v_{\Delta}$ .

spin liquid to hybridize with the Bogoliubov quasiparticles of the pocket Fermi surfaces. The net result, shown in Fig. 17B, is that the B condensate can enable the nodal points on the 'backsides' of the pocket Fermi surfaces to mutually annihilate with the spinons of the  $S_2$  spin liquid. We are then left with the 4 nodal quasiparticles on front sides of the pocket Fermi surfaces. The number of nodal points are the same as those obtained in conventional BCS theory from d-wave pairing of a Fermi liquid. These remaining nodal points are associated with pairing on the pocket Fermi surfaces, and these is no reason for their velocity to be isotropic (unlike the spinons). Indeed, computations which diagonalize  $\mathcal{H}_{KLmf} + \mathcal{H}_{SLf} + \mathcal{H}_{Y}$  with B fixed do indeed yield anisotropic velocities similar to those observed. Unlike the situation in Section 3, the spinons do not become the Bogoliubov quasiparticles in the doped case, although the spinons are needed to annihilate the extraneous Bogoliubov quasiparticles.

### 5.2. Vortices with flux h/(2e) and charge order halos

We have seen in Section 5.1 that d-wave superconductivity is induced by the condensation of B, a boson which carries electrical charge e. So we might worry that the elementary flux quantum of such a superconductor is h/e. However, that is not correct, and the SU(2) gauge field  $A^{\ell}_{\mu}$  (introduced in Eq. (2.49)) plays a central in establishing the presence of vortices with flux h/(2e) [42].

The argument only requires  $A^z_{\mu}$  to be non-zero. In terms of the two components of  $B = (B_1, B_2)$ , we can write the following gradient term in the action far from the vortex core

$$|(\boldsymbol{\nabla} - i\boldsymbol{A}^z - i\boldsymbol{a})B_1|^2 + |(\boldsymbol{\nabla} + i\boldsymbol{A}^z - i\boldsymbol{a})B_2|^2$$
(5.5)

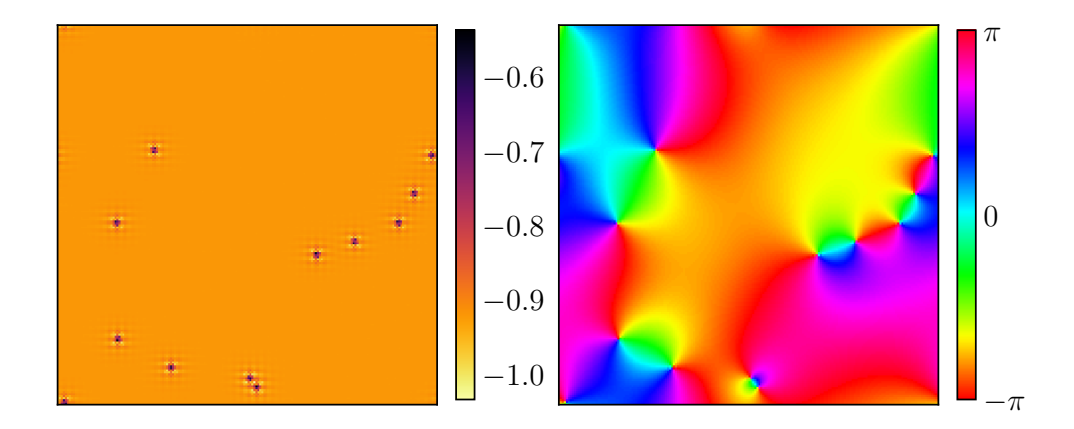


Figure 18. From Ref. [41]. The bond density (left panel) and the distribution of the phase of the superconducting order parameter (right panel) on a  $192 \times 192$  lattice at low temperature in the thermal ensemble defined by Eq. (5.7).

where  $\mathbf{A}^z$  is the spatial component of  $A^z_{\mu}$ , and  $\mathbf{a}$  is the electromagnetic vector potential (we are using units here with  $\hbar = e = 1$ ). Let us assume that the phases of  $B_{1,2}$  wind by  $2\pi n_{1,2}$  around the vortex core, where  $n_{1,2}$  are integers. Then, finiteness of the energy of the vortex requires

$$\int d^2r \, (\boldsymbol{\nabla} \times \boldsymbol{A}^z + \boldsymbol{\nabla} \times \boldsymbol{a}) \cdot \hat{\boldsymbol{z}} = 2\pi n_1$$

$$\int d^2r \, (\boldsymbol{\nabla} \times \boldsymbol{A}^z - \boldsymbol{\nabla} \times \boldsymbol{a}) \cdot \hat{\boldsymbol{z}} = 2\pi n_2$$
(5.6)

By choosing  $n_1 = 1$ ,  $n_2 = 0$ , we obtain a vortex with  $\int (\nabla \times \boldsymbol{a}) \cdot \hat{\boldsymbol{z}} = \pi$ , which corresponds to flux h/(2e).

There is an interesting feature of the vortex solution near its core. Recall from Eqs. (3.10,3.11) that different orientations of the complex vector  $(B_1, B_2)$  correspond to different local orders. At the vortex core, it is preferential for the orientation of B to rotate from that preferring d-SC, to one of the other orders [42]. Explicit solutions of the continuum theory Eq. (3.12) were obtained in Ref. [42] with period 2 charge order.

Recently, Bonetti et al [41] have carried out Monte Carlo simulations of the classical, thermal, lattice gauge theory for B and U defined by the partition function

$$\mathcal{Z}_{2+0} = \int \prod_{i} \mathcal{D}B_{i} \int \prod_{\langle ij \rangle} \mathcal{D}U_{ij} \exp\left(-\left(\mathcal{E}_{2}[B, U] + \mathcal{E}_{4}[B, U]\right)/T\right) , \qquad (5.7)$$

where the energy functionals are defined in Eq. (3.9). They observe a Kosterlitz-Thouless transition to a d-wave superconductor at low energies. The coupling constants in  $\mathcal{E}_4[B,U]$  were chosen so that the ground state is a d-wave superconductor, while the next best state had period 4 charge order. Fig. 18 shows a snapshot from the simulation at low T. Note the vortices with the phase winding of  $2\pi$  in the superconducting order parameter (corresponding to h/(2e) vortices), and the period 4 charge order halos around each vortex. These halos are remarkably similar to those observed by Hoffman  $et\ al.\ [43]$ .

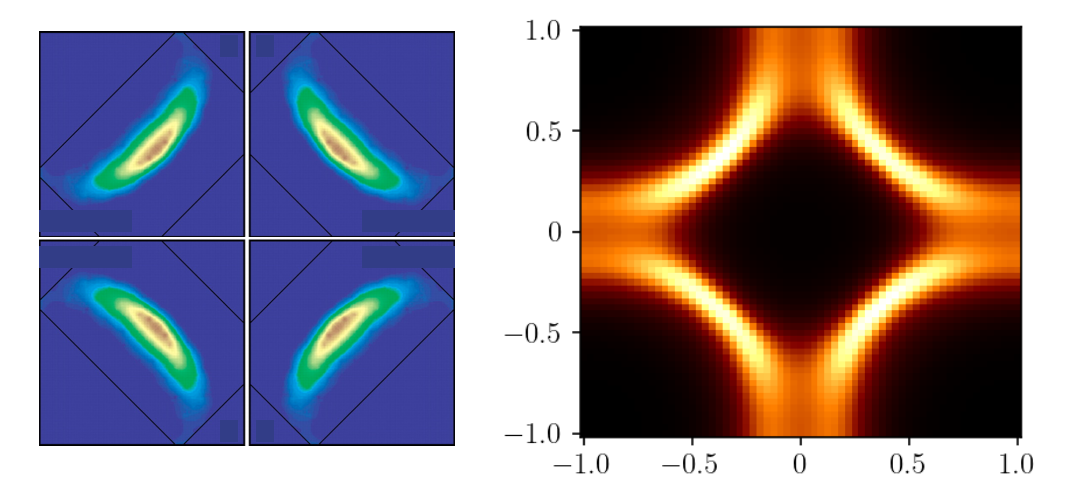


**Figure 19.** The right panel shows the electron spectral function computed in Ref. [41] from  $\mathcal{H}_{KLmf} + \mathcal{H}_{SLf} + \mathcal{H}_{Y}$  after averaging over the Monte Carlo simulation of B and U in Eq. (5.7); the spectrum with B = U = 0 was shown in Fig. 15. The left panel is experimental photoemission data from Ref. [119].

### 5.3. Fermi arc spectra

Fig. 15 showed the prediction for the photoemission spectrum in the pseudogap phase without the coupling to the  $S_2$  spin liquid. Bonetti et al. [41] included the coupling to thermal fluctuations of B via the Yukawa coupling in Eq. (5.3). The thermal fluctuations of B and U were included via the ensemble in Eq. (5.7). Here the Born-Oppenheimer procedure is to choose random samples of the  $B_i$  and  $U_{ij}$ , diagonalize  $\mathcal{H}_{KLmf} + \mathcal{H}_{SLf} + \mathcal{H}_Y$  for each sample, and average over the spectral functions. The results are shown in Fig. 19. Note that the back side of the pocket in Fig. 15 is now invisible, and the resulting spectrum is similar to the 'Fermi arc' observed in experiments.

### 5.4. Magnetotransport and Quantum oscillations

Observations at high magnetic fields provide the most sensitive probes of the Fermi surface configurations in the cuprates.

At large doping, the observed quantum oscillations are compatible with a 'large' Fermi surface of size 1 + p [120]. This is as expected, and well understood, and will not be discussed further.

At low doping and low temperatures, quantum oscillations show evidence for small electron pockets [31]. The formation of electron pockets is believed to be associated with the appearance of charge density wave order at high magnetic fields. Nevertheless, computations on charge density wave models had difficulty reproducing the observed spectrum. Zhang and Mei [121] worked with a model of pocket Fermi surfaces (similar to  $\mathcal{H}_{KLmf}$ ) in the presence of charge density wave order: in addition to the observed electron pocket, their results show an unobserved additional oscillation frequency from a Fermi surface arising from the backsides of the hole pockets completing the Fermi

arcs. Bonetti et al. [32] extended their computation to include spinons by working with  $\mathcal{H}_{KLmf} + \mathcal{H}_{SLf} + \mathcal{H}_{Y}$ , and found that the spinons annihilated the unobserved Fermi surface. This is rather analogous to the role of the spinons in Section 5.1.

More recently, compelling evidence for hole pockets has emerged at low doping in the higher temperature pseudogap metal phase [122, 25]. Chan et al [25] have observed the remarkable Yamaji effect, which allows deduction of pocket area only from a knowledge of the layer spacing and the value of the Yamaji angle at which there is peak in the magnetoresistance. At these higher temperatures there is no ordering, and the Hall effect is positive, indicating the absence of electron pockets. Their results are consistent with the FL\* prediction of hole pockets of area p/8 [3, 4, 26, 111], as we noted earlier near Fig. 11. This is to be constrasted with pockets of area p/4 in the fluctuating spin density wave state [27, 28, 29, 30]. The Yamaji angle observation of Chan et al [25] is therefore the long-sought direct signature of fractionalization in the cuprates.

But given the role of thermal B fluctuations in removing the pocket backsides in Fig. 19, it is legitimate to ask if the thermal B fluctuations will also wash out quantum oscillations. This question was investigated recently by Pandey  $et\ al.$  [41]: they averaged the quantum oscillations associated with  $\mathcal{H}_{KLmf} + \mathcal{H}_{SLf} + \mathcal{H}_{Y}$  over gaussian fluctations of B. They found that the quantum oscillations survived in regimes where the Fermi arc spectrum in Fig. 19 was well established.

### 5.5. Direct observation of spinons

The spinons  $f_{\alpha}$  in  $\mathcal{H}_{SLf}$  have played a crucial role the theory of the observed electronic spectrum in Sections 5.1, 5.3, and 5.4. It would therefore be a nice confirmation of the theoretical scenario to observe the spinons directly in the spin fluctuation spectrum, rather than indirectly through the electronic spectrum. It has recently been argued [32, 66] that RIXS measurements [123, 124] do indeed provide strong support for the presence of spinons. At filling, there is sharp spin wave excitation extending to high energy  $\sim 400$ meV. This excitation survives upon doping even at high energies, but becomes much broader. Now the spectrum has similarities to that expected from the  $\pi$ -flux spin liquid, as computed near the destruction of the Néel order in the insulating  $J_1$ - $J_2$  model by Ref. [125]. See Figs. 8 and 9 in Ref. [66] for a comparison.

More precise computations and observations should help settle this issue.

### 6. The SYK model

We now turn to a different critical quantum liquid, associated with mobile electrons, the SYK model. This is a zero-dimensional model for which the absence of quasiparticle excitations is well established. A direct and extensive application of the zero-dimensional SYK model has been to the low energy quantum theory of charged black holes, and this is reviewed elsewhere [126]. There are also connections to experiments on graphene

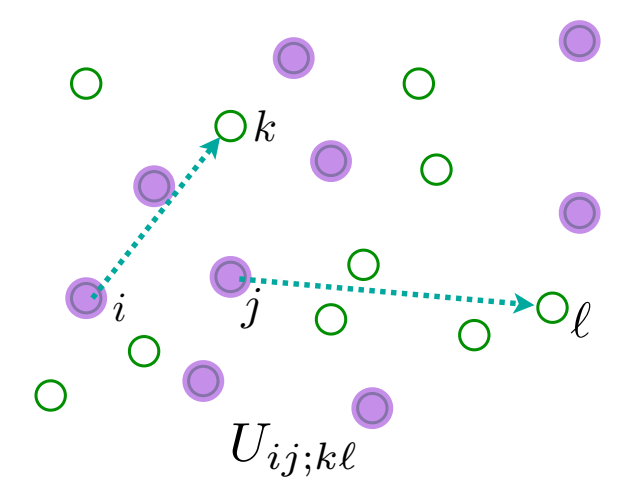
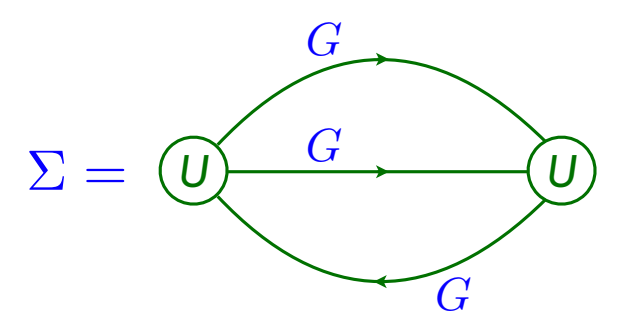


Figure 20. The SYK model: fermions undergo the transition ('collision') shown with quantum amplitude  $U_{ij;k\ell}$ .

flakes [127]. But our primary interest here will be extensions to two-dimensional models relevant to the strange metal state of the cuprates and other correlated electron materials—we will turn to this in Section 7.

The Hamiltonian of a version of a SYK model is illustrated in Fig. 20. A system with fermions  $c_i$ , i=1...N states is assumed. Depending upon physical realizations, the label i could be position or an orbital, and it is best to just think of it as an abstract label of a fermionic qubit with the two states  $|0\rangle$  and  $c_i^{\dagger}|0\rangle$ . QN fermions are placed in these states, so that a density  $Q \approx 1/2$  is occupied, as shown in Fig. 20. The quantum dynamics is restricted to only have a 'collision' term between the fermions, analogous to the right-hand-side of the Boltzmann equation. However, in stark contrast to the Boltzmann equation, statistically independent collisions are not assumed, and quantum interference between successive collisions is accounted for: this is the key to building up a many-body state with non-trivial entanglement. So a collision in which fermions move from sites i and j to sites k and  $\ell$  is characterized not by a probability, but by a quantum amplitude  $U_{ij:k\ell}$ , which is a complex number.

The model so defined has a Hilbert space of order  $2^N$  states, and a Hamiltonian determined by order  $N^4$  numbers  $U_{ij;k\ell}$ . Determining the spectrum or dynamics of such a Hamiltonian for large N seems like an impossibly formidable task. But with the assumption that the  $U_{ij;k\ell}$  are statistically independent random numbers, remarkable progress is possible. Note that an ensemble of SYK models with different  $U_{ij;k\ell}$  is not being considered, but a single fixed set of  $U_{ij;k\ell}$ . Most physical properties of this model are self-averaging at large N, and so as a technical tool, they can be rapidly obtained by computations on an ensemble of random  $U_{ij;k\ell}$ . In any case, the analytic results described below have been checked by numerical computations on a computer for a fixed set of  $U_{ij;k\ell}$ . Recall that, even for the Boltzmann equation, there was an ensemble average over the initial positions and momenta of the molecules that was implicitly



**Figure 21.** Self-energy for the fermions of  $\mathcal{H}$  in Eq. (6.1) in the limit of large N. The intermediate Green's functions are fully renormalized.

performed.

Specifically, the Hamiltonian in a chemical potential  $\mu$  is

$$\mathcal{H} = \frac{1}{(2N)^{3/2}} \sum_{i,j,k,\ell=1}^{N} U_{ij;k\ell} c_{i}^{\dagger} c_{j}^{\dagger} c_{k} c_{\ell} - \mu \sum_{i} c_{i}^{\dagger} c_{i}$$

$$c_{i} c_{j} + c_{j} c_{i} = 0 \quad , \quad c_{i} c_{j}^{\dagger} + c_{j}^{\dagger} c_{i} = \delta_{ij}$$

$$\mathcal{Q} = \frac{1}{N} \sum_{i} c_{i}^{\dagger} c_{i} ; \quad [\mathcal{H}, \mathcal{Q}] = 0 ; \quad 0 \leq \mathcal{Q} \leq 1 ,$$

$$(6.1)$$

and its large N limit is most simply taken graphically, order-by-order in  $U_{ij;k\ell}$ , and averaging over  $U_{ij;k\ell}$  as independent random variables with  $\overline{U_{ij;k\ell}} = 0$  and  $\overline{|U_{ij;k\ell}|^2} = U^2$ . This expansion can be used to compute graphically the Green's function in imaginary time  $\tau$ 

$$G(\tau) = -\frac{1}{N} \sum_{i} \overline{\left\langle \mathcal{T} \left( c_{i}(\tau) c_{i}^{\dagger}(0) \right) \right\rangle}, \qquad (6.2)$$

where  $\mathcal{T}$  is the time-ordering symbol, the angular brackets are a quantum average for any given  $U_{ij;k\ell}$ , and the over-line denotes an average over the ensemble of  $U_{ij;k\ell}$ . (It turns out that the last average is not needed for large N, because the quantum observable is self-averaging.) In the large N limit, only the graph for the Dyson self energy,  $\Sigma$ , in Fig. 21 survives, and the on-site fermion Green's function is given by the solution of the following equations

$$G(i\omega_n) = \frac{1}{i\omega_n + \mu - \Sigma(i\omega_n)}$$

$$\Sigma(\tau) = -U^2 G^2(\tau) G(-\tau)$$

$$G(\tau = 0^-) = \mathcal{Q},$$
(6.3)

where  $\omega_n$  is a fermionic Matsubara frequency. The first equation in Eq. (6.3) is the usual Dyson relation between the Green's function and self energy in quantum field theory, the second equation in Eq. (6.3) is the Feynman graph in Fig. 21, and the last determines the chemical potential  $\mu$  from the charge density Q. These equations can also be obtained as saddle-point equations of the following exact representation of the

disordered-averaged partition function, expressed as a ' $G-\Sigma$ ' theory [128, 129, 130, 131]:

$$\mathcal{Z} = \int \mathcal{D}G(\tau_{1}, \tau_{2}) \mathcal{D}\Sigma(\tau_{1}, \tau_{2}) \exp(-NI)$$

$$I = \ln \det \left[ \delta(\tau_{1} - \tau_{2})(\partial_{\tau_{1}} + \mu) - \Sigma(\tau_{1}, \tau_{2}) \right]$$

$$+ \int d\tau_{1} d\tau_{2} \left[ \Sigma(\tau_{1}, \tau_{2}) G(\tau_{2}, \tau_{1}) + (U^{2}/2) G^{2}(\tau_{2}, \tau_{1}) G^{2}(\tau_{1}, \tau_{2}) \right]$$
(6.4)

This is a path-integral over bi-local in time functions  $G(\tau_1, \tau_2)$  and  $\Sigma(\tau_1, \tau_2)$ , whose saddle point values are the Green's function  $G(\tau_1 - \tau_2)$ , and the self energy  $\Sigma(\tau_1 - \tau_2)$ . This bi-local G can be viewed as a composite quantum operator corresponding to an on-site fermion bilinear

$$G(\tau_1, \tau_2) = -\frac{1}{N} \sum_{i} \mathcal{T} \left( c_i(\tau_1) c_i^{\dagger}(\tau_2) \right)$$
(6.5)

that is averaged in Eq. (6.2).

For general  $\omega$  and T, the equations in Eq. (6.3) have to be solved numerically. But an exact analytic solution is possible in the limit  $\omega, T \ll U$ . At T = 0, the asymptotic forms can be obtained straightforwardly [132]

$$G(i\omega) \sim -i\operatorname{sgn}(\omega)|\omega|^{-1/2}$$
 ,  $\Sigma(i\omega) - \Sigma(0) \sim -i\operatorname{sgn}(\omega)|\omega|^{1/2}$ , (6.6)

and a more complete analysis of Eq. (6.3) gives the exact form at non-zero T ( $\hbar=k_B=1$ ) [133]

$$G(\omega) = \frac{-iCe^{-i\theta}}{(2\pi T)^{1/2}} \frac{\Gamma\left(\frac{1}{4} - \frac{i\omega}{2\pi T} + i\mathcal{E}\right)}{\Gamma\left(\frac{3}{4} - \frac{i\omega}{2\pi T} + i\mathcal{E}\right)} \qquad |\omega|, T \ll U.$$
(6.7)

Here,  $\mathcal{E}$  is a dimensionless number which characterizes the particle-hole asymmetry of the spectral function; both  $\mathcal{E}$  and the pre-factor C are determined by an angle  $-\pi/4 < \theta < \pi/4$ 

$$e^{2\pi\mathcal{E}} = \frac{\sin(\pi/4 + \theta)}{\sin(\pi/4 - \theta)} \quad , \quad C = \left(\frac{\pi}{U^2 \cos(2\theta)}\right)^{1/4} , \tag{6.8}$$

and the value of  $\theta$  is determined by a Luttinger relation to the density  $\mathcal{Q}$  [128]

$$Q = \frac{1}{2} - \frac{\theta}{\pi} - \frac{\sin(2\theta)}{4} \,. \tag{6.9}$$

A notable property of Eq. (6.7) at  $\mathcal{E}=0$  is that it equals the temporal Fourier transform of the spatially local correlator of a fermionic field of dimension 1/4 in a conformal field theory in 1+1 spacetime dimensions. A theory in 0+1 dimensions is considered here, where conformal transformations map the temporal circle onto itself, as reviewed in Appendices A and B of Ref. [134]; such transformations allow a non-zero  $\mathcal{E}$ . An important consequence of this conformal invariance is that Eq. (6.7) is a scaling function of  $\hbar\omega/(k_BT)$  (after restoring fundamental constants); in other words, the characteristic frequency scale of Eq. (6.7) is determined solely by  $k_BT/\hbar$ , and is independent of the value of  $U/\hbar$ . A careful study of the consequences of this conformal

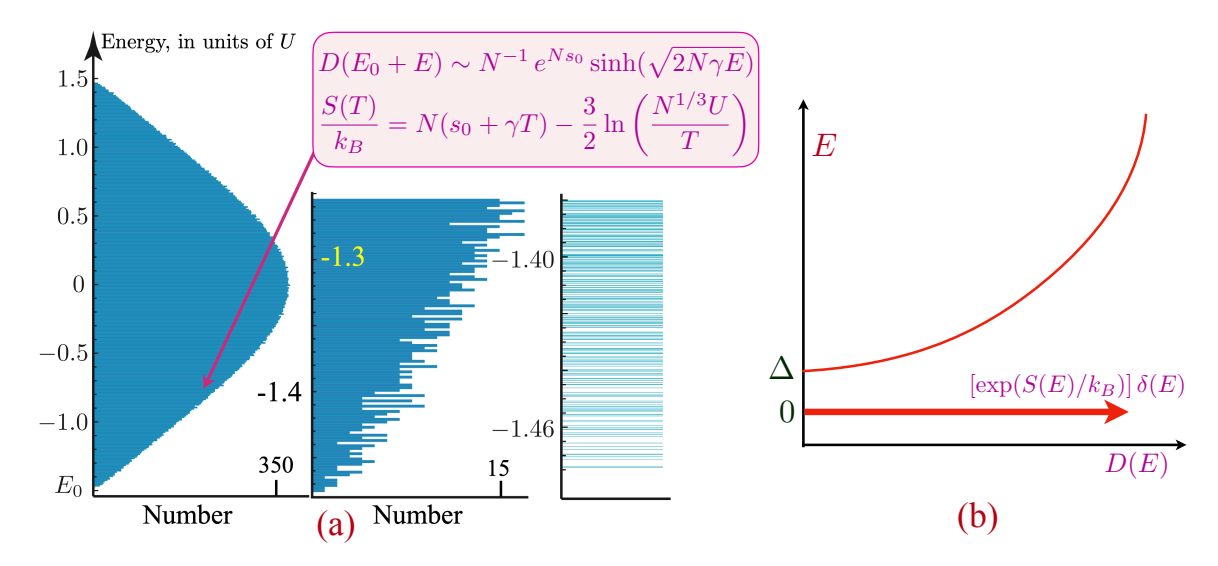


Figure 22. (a) Plot of the 65536 many-body eigenvalues of a N=32 Majorana SYK Hamiltonian; however, the analytical results quoted here are for the SYK model with complex fermions which has a similar spectrum. The coarse-grained low-energy and low-temperature behavior is described by Eq. (6.10) and Eq. (6.12). (b) Schematic of the lower energy density of states of a supersymmetric generalization of the SYK model [139, 137]. There is a delta function at E=0, and the energy gap  $\Delta$  is proportional to the inverse of S(E=0).

invariance have established the following properties of the SYK model (more complete references to the literature are given in other reviews [134, 94]):

- There are no quasiparticle excitations, and the SYK model exhibits quantum dynamics with a Planckian relaxation time of order  $\hbar/(k_BT)$  at  $T \ll U$ . In particular, the relaxation time is *independent* of U, a feature not present in any ordinary metal with quasiparticles. While the Planckian relaxation in Eq. (6.7) implies the absence of quasiparticles with the same quantum numbers as the c fermion, it does not rule out the possibility that c has fractionalized into some emergent quasiparticles; this possibility is ruled out by the exponentially large number of low energy states, as discussed below.
- At large N, the many-body density of states at fixed Q is [135, 136, 131, 130, 137, 138] (see Fig. 22a)

$$D(E) \sim \frac{1}{N} \exp(Ns_0) \sinh\left(\sqrt{2N\gamma E}\right),$$
 (6.10)

where the ground state energy has been set to zero. Here  $s_0$  is a universal number dependent only on  $\mathcal{Q}$  ( $s_0 = 0.4648476991708051...$  for  $\mathcal{Q} = 1/2$ ),  $\gamma \sim 1/U$  is the only parameter dependent upon the strength of the interactions, and the N dependence of the pre-factor is discussed in Ref. [138]. Given D(E), the partition function can be computed from

$$\mathcal{Z}(T) = \int dE D(E) e^{-E/(k_B T)}, \qquad (6.11)$$

and hence the low-T dependence of the entropy at fixed Q is given by

$$\frac{S(T)}{k_B} = N(s_0 + \gamma k_B T) - \frac{3}{2} \ln \left( \frac{U}{k_B T} \right) - \frac{\ln N}{2} + \dots$$
 (6.12)

The thermodynamic limit  $\lim_{N\to\infty} S(T)/N$  yields the microcanonical entropy

$$S(E)/k_B = Ns_0 + \sqrt{2N\gamma E}, \qquad (6.13)$$

and this connects to the extensive E limit of Eq. (6.10) after using Boltzmann's formula  $D(E) \sim \exp(S(E)/k_B)$ . The limit  $\lim_{T\to 0} \lim_{N\to\infty} S(T)/(k_BN) = s_0$  is non-zero, implying an energy-level spacing exponentially small in N near the ground state: the density of states Eq. (6.10) implies that any small energy interval near the ground state contains an exponentially large number of energy eigenstates (see Fig. 22a). This is very different from systems with quasiparticle excitations, whose energy level spacing vanishes with a positive power of 1/N near the ground state, as quasiparticles have order N quantum numbers. The exponentially small level spacing therefore rules out the existence of quasiparticles in the SYK model.

- However, it important to note that there is no exponentially large degeneracy of the ground state itself in the SYK model, unlike that in a supersymmetric generalization of the SYK model (see Fig. 22b) and the ground states in Pauling's model of ice [140]. Indeed, the SYK model is the first system to exhibit an extensive zero temperature entropy without an exponentially large ground state degeneracy. Obtaining the ground-state degeneracy requires the opposite order of limits between T and N, and numerical studies show that the entropy density does vanish in such a limit for the SYK model. The many-particle wavefunctions of the low-energy eigenstates in Fock space change chaotically from one state to the next, providing a realization of maximal many-body quantum chaos [141] in a precise sense. This structure of eigenstates is very different from systems with quasiparticles, for which the lowest energy eigenstates differ only by adding and removing a few quasiparticles.
- The E dependence of the density of states in Eq. (6.10) is associated with a time reparameterization mode, and Eq. (6.10) shows that its effects are important when  $E \sim 1/N$ . The low energy quantum fluctuations of Eq. (6.4) can be expressed in terms of a path integral which reparameterizes imaginary time  $\tau \to f(\tau)$ , in a manner analogous to the quantum theory of gravity being expressed in terms of the fluctuations of the spacetime metric. There are also quantum fluctuations of a phase mode  $\phi(\tau)$ , whose time derivative is the charge density, and the path integral in Eq. (6.4) reduces to the partition function

$$\mathcal{Z}_{SYK-TR} = e^{Ns_0} \int \mathcal{D}f \mathcal{D}\phi \exp\left(-\frac{1}{\hbar} \int_0^{\hbar/(k_B T)} d\tau \, \mathcal{L}_{SYK-TR}[f, \phi]\right) (6.14)$$

The Lagrangian  $\mathcal{L}_{SYK-TR}$  is known, and involves a Schwarzian of  $f(\tau)$ . Remarkably, despite its non-quadratic Lagrangian, the path integral in Eq. (6.14) can be performed exactly [137], and leads to Eq. (6.10).

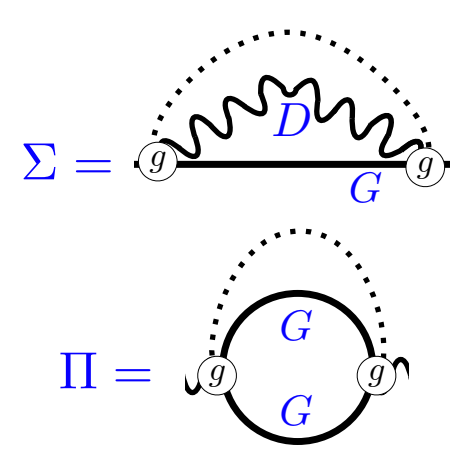


Figure 23. Self-energies of the fermions and bosons in the Hamiltonian  $\mathcal{H}_Y$  in Eq. (6.15). The intermediate Green's functions are fully renormalized.

### 6.1. The WES-SYK model

The SYK model defined above is a 0+1 dimensional theory with no spatial structure, and so cannot be directly applied to transport of strange metals in non-zero spatial dimensions. A great deal of work has been undertaken on generalizing the SYK model to non-zero spatial dimensions [134], but this effort has ultimately not been successful: although 'bad metal' states (see Section 7) have been obtained, low T strange metals have not. But another effort based upon a variation of the SYK model, the 0+1 dimensional 'WES-SYK' model [139, 142, 143, 144, 145, 146, 147, 148, 149, 150, 151, 152], has been a much better starting point for a non-zero spatial dimensional theory, as shown in Section 7. Here 'WES' stands for Wang-Esterlis-Schmalian from Refs. [145, 146], the for the simplest realization [146, 150, 151, 152] discussed below. But the name 'Yukawa-SYK' is more commonly used.

In the spirit of Eq. (6.1), a model of fermions  $c_i$  (i = 1...N) and bosons  $\phi_{\ell}$  ( $\ell = 1...N$ ) with a Yukawa coupling  $g_{ij\ell}$  between them is now considered

$$\mathcal{H}_Y = -\mu \sum_{\boldsymbol{i}} c_{\boldsymbol{i}}^{\dagger} c_{\boldsymbol{i}} + \sum_{\ell} \frac{1}{2} \left( \pi_{\ell}^2 + \omega_0^2 \phi_{\ell}^2 \right) + \frac{1}{N} \sum_{\boldsymbol{i}\boldsymbol{j}\ell} g_{\boldsymbol{i}\boldsymbol{j}\ell} c_{\boldsymbol{i}}^{\dagger} c_{\boldsymbol{j}} \phi_{\ell} , \qquad (6.15)$$

with  $g_{ij\ell}$  independent random numbers with zero mean and r.m.s. value g. The bosons are oscillators with the same frequency  $\omega_0$ , while the fermions have no one-particle hopping. The large N limit of Eq. (6.15) can be taken just as for the SYK model in Eq. (6.1). The self-energy graph in Fig. 21 is replaced by those in Fig. 23: the phonon Green's function is D, while the phonon self-energy is  $\Pi$ .

Continuing the parallel with the SYK model, the disorder-averaged partition function of the WES-SYK model is a bi-local G- $\Sigma$ -D- $\Pi$  theory, analogous to Eq. (6.4):

$$\mathcal{Z} = \int \mathcal{D}G \, \mathcal{D}\Sigma \, \mathcal{D}D \, \mathcal{D}\Pi \exp(-NS_{\text{all}})$$

$$S_{\text{all}} = -\ln \det(\partial_{\tau} - \mu + \Sigma) + \frac{1}{2} \ln \det(-\partial_{\tau}^{2} + \omega_{0}^{2} - \Pi)$$

$$+ \int d\tau \int d\tau' \left[ -\Sigma(\tau';\tau)G(\tau,\tau') + \frac{1}{2}\Pi(\tau',\tau)D(\tau,\tau') + \frac{g^2}{2}G(\tau,\tau')G(\tau',\tau)D(\tau,\tau') \right]. \tag{6.16}$$

The large N saddle-point equations replacing Eq. (6.3) are:

saddle-point equations replacing Eq. (6.3) are:  

$$G(i\omega_n) = \frac{1}{i\omega_n + \mu - \Sigma(i\omega_n)} , \quad D(i\omega_n) = \frac{1}{\omega_n^2 + \omega_0^2 - \Pi(i\omega_n)}$$

$$\Sigma(\tau) = g^2 G(\tau) D(\tau) , \quad \Pi(\tau) = -g^2 G(\tau) G(-\tau)$$
(6.17)

The solution of Eqs. (6.16) and (6.17) leads to a critical state with properties very similar to that of the SYK model [146, 150, 151, 152]. Only the low-frequency behavior of the Green's functions at T = 0, is quoted analogous to Eq. (6.6):

$$G(i\omega) \sim -i\operatorname{sgn}(\omega)|\omega|^{-(1-2\Delta)}$$
 ,  $D(i\omega) \sim |\omega|^{1-4\Delta}$  ,  $\frac{1}{4} < \Delta < \frac{1}{2}(6.18)$ 

Inserting the ansatz Eq. (6.18) into Eq. (6.17) fixes the value of the critical exponent  $\Delta$ .

$$\frac{4\Delta - 1}{2(2\Delta - 1)[\sec(2\pi\Delta) - 1]} = 1 \quad , \quad \Delta = 0.42037\dots$$
 (6.19)

Although the fermion Green's function has an exponent which differs from that of the SYK model, the thermodynamic properties have the same structure as that of the SYK model, including the presence of the Schwarzian mode and the form of the many-body density of states.

## 7. From the SYK model to strange metals

We now turn to the 'strange metal' regime of Fig. 1. A similar regime is found in numerous correlated electron materials, and we will present here a theory [58, 59] which applies to a wide variety of quantum phase transitions, and so can explain the universality in the observations.

Some of the key properties of strange metals, as observed in recent experiments, are first summarized [153]:

(i) The resistivity,  $\rho(T)$ , of strange metals has a linear-T dependence at low temperatures:

$$\rho(T) = \rho_0 + AT + \dots , \quad T \to 0. \tag{7.1}$$

Importantly, this resistivity is below the Mott-Ioffe-Regel bound [153], so  $\rho(T) < h/e^2$  in d=2 spatial dimensions. Metals with  $\rho(T) > h/e^2$  are bad metals, and are not discussed here. Bad metals can be described by lattice models of coupled SYK 'islands' [154, 155, 156], as reviewed elsewhere [134].

(ii) Ordinary metals have low T specific heat which vanishes linearly with T, but in a strange metal the specific heat is enhanced to  $\sim T \ln(1/T)$  as  $T \to 0$ .

(iii) Careful analyses of optical data in the cuprates over wide ranges of frequencies and temperatures [157, 158] has shown that the optical conductivity can be accurately described by the following form

$$\sigma(\omega) = \frac{K}{\frac{1}{\tau_{\text{trans}}(\omega)} - i\omega \frac{m_{\text{trans}}^*(\omega)}{m}} ; \frac{1}{\tau_{\text{trans}}(\omega)} \sim |\omega| \Phi_{\sigma} \left(\frac{\hbar \omega}{k_B T}\right), (7.2)$$

where K is a constant, and the transport scattering rate  $1/\tau_{\rm trans}$  scales linearly with the larger of  $|\omega|$  and  $k_BT/\hbar$ . The frequency dependence of the effective transport mass  $m_{\rm trans}^*$  is then determined by a Kramers-Kronig connection to that of  $1/\tau_{\rm trans}$ , which leads to a logarithmic frequency dependence in  $m_{\rm trans}^*(\omega)$ .

(iv) Photoemission experiments on the cuprates have measured the electron self-energy near the nodal point in the Brillouin zone. This was found to obey the scaling form [159]

$$\frac{1}{\tau_{\rm in}(\omega)} = 2 \operatorname{Im}\Sigma(\omega) \sim |\omega|^{2\alpha} \Phi_{\Sigma} \left(\frac{\hbar \omega}{k_B T}\right)$$
 (7.3)

with an exponent  $\alpha \approx 1/2$  near optimal doping. The value  $\alpha = 1/2$  corresponds to a 'marginal Fermi liquid' [160], at least as far as the self energy is concerned. But an important point is that there is no direct theoretical connection between the single-particle scattering rate  $1/\tau_{\rm in}(\omega)$  in Eq. (7.3), and the value of transport scattering rate  $1/\tau_{\rm trans}(\omega)$  in Eq. (7.2), although they are observed to have the same exponent. As seen below, the transport and single-particle scattering rates can be very different in some common models.

(v) In experimental observations [161, 162, 163], the value of the overall constant K in Eq. (7.2) is often fixed by writing the d.c. conductivity in the Drude form

$$\sigma = \frac{ne^2 \tau_{\text{trans}}}{m^*} \,, \tag{7.4}$$

where n is the known conduction electron density, and  $m^*$  is an electronic effective mass. In some experiments, the transport mass  $m_{\text{trans}}^*$  of Eq. (7.2) is used in Eq. (7.4), while other experiments use the  $m^*$  determined from thermodynamic measurements. In the form Eq. (7.4), the absolute value of  $\tau_{\text{trans}}$  can be deduced from experimental observations. In the strange metal, such a value is found to obey 'Planckian' behavior with [161, 162, 163]

$$\frac{1}{\tau_{\text{trans}}} = \alpha \, \frac{k_B T}{\hbar} \,, \tag{7.5}$$

with  $\alpha$  a numerical constant of order unity. Measurements of  $1/\tau_{\rm trans}$  in  ${\rm La_{1.6-}}_x{\rm Nd_{0.4}Sr_xCuO_4}$  in angle-dependent magnetotransport show  $\alpha=1.2\pm0.4$  [163] upon using the thermodynamic  $m^*$ .

#### 7.1. Universal model

This subsection will present a simple and universal generalization of the WES-SYK model of Section 6.1 to spatial dimension d=2 which reproduces all five of the above

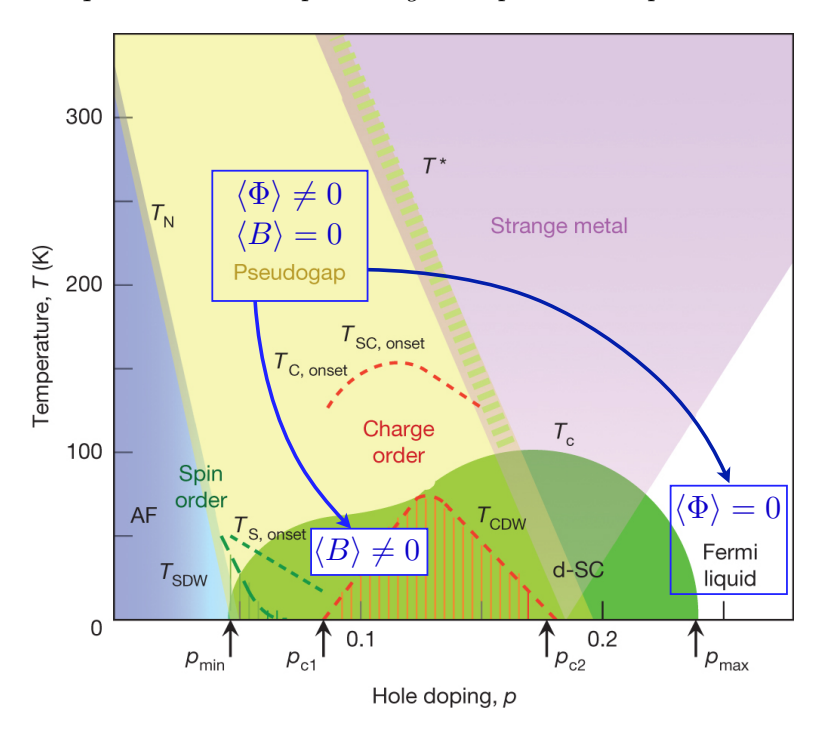


Figure 24. Cuprate phase diagram from Ref. [1]. Annotations in blue have been added. In Section 7 we consider the transition from the FL\* pseudogap to the Fermi liquid focusing on the Higgs field  $\Phi$ , while setting B=0. The transition from the pseudogap to the d-SC was discussed in Section 5 as a theory of the dynamics of B, while setting  $\Phi$  to a non-zero constant which determined the magnitude of the pseudogap.

# observed properties [58, 59].

We begin by motivating the model appropriate for the cuprates, and mention generalizations to other materials later. To this end, we present the phase diagram of Fig. 1 again in Fig. 24, but now with annotations updated with reference to the ancilla theory in Fig. 16. In Section 5 we have considered the low temperature fate of the  $FL^*$  pseudogap associated with condensation of the Higgs field B. In this analysis, we treated  $\Phi$  simply as a c-number constant. In this section,  $\Phi$  and B will exchange roles. In considering the transition from FL\* to FL in Fig. 13 and Fig. 24, we consider the dynamics of the  $\Phi$  field, and the fermions in the top two layers in Fig. 16. In FL\*, we can safely set B = 0 (apart for some thermal fluctuations which were needed in Section 5.3). In the FL phase of Fig. 13, we see that the  $f_1$  fermions of the middle layer form a trivial rung-singlet state with the f fermions in the bottom layer: this confinement of  $f_1$  and f is not associated with B, but by the confinement of another gauge field [112, 113, 117]. Consequently, it is safe to ignore B in the quantum criticality of the FL\* to FL transition [112, 113]. So we will only consider the  $\Phi$  boson here, along with the  $c_{\alpha}$  and  $f_1$  fermions in the top two layers. This is the approximation in which the inversion mapping to the Kondo lattice in Fig. 14 becomes exact.

We therefore consider the T > 0 quantum criticality of the FL\* to FL transition sketched in Fig. 25, associated with the Higgs transition in  $\Phi$ . We could study this using

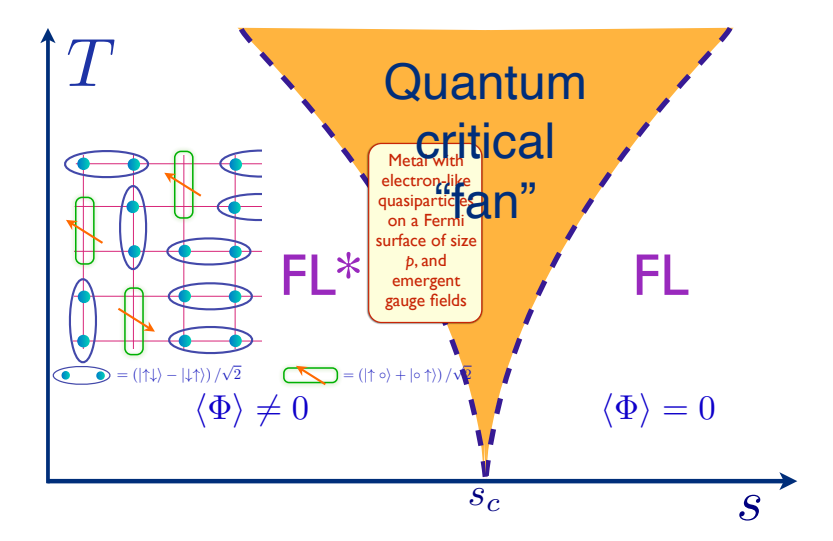


Figure 25. Schematic phase diagram of a metal with a fermion volume changing transition without a broken symmetry on either side of the transition. When spatial disorder is included, Griffiths effects lead to a quantum critical 'foot' on the FL side, which is reviewed elsewhere [66].

the 'Kondo breakdown' dynamic mean field theories [44, 45, 46, 47, 48, 49, 50, 51, 52, 53, 54, 55, 56, 57], which map the transition to SYK-type Green's functions studied in Section 6. However, here we will instead treat the spatial dimensionality seriously, and focus on the low energy, long-wavelength structure. Spatially random couplings play a crucial role in such an analysis, and lead to new Griffiths effects associated with the 'foot' of strange metal behavior [64, 65, 66]. But, we do not discuss such Griffiths effects here, and focus on the disorder-average theory.

At the mean-field level the FL\* to FL transition is described by  $\mathcal{H}_{KLmf}$  in Eq. (4.3). We now include spatial dependence in all fields, allow for quenched spatial disorder, and obtain the (universal) Lagrangian

$$\mathcal{L}_{\Phi} = \sum_{\mathbf{k}} c_{\mathbf{k}\alpha}^{\dagger} \left( \frac{\partial}{\partial \tau} + \varepsilon(\mathbf{k}) \right) c_{\mathbf{k}\alpha} + \sum_{\mathbf{k}} f_{1\mathbf{k}\alpha}^{\dagger} \left( \frac{\partial}{\partial \tau} + \varepsilon_{1}(\mathbf{k}) \right) f_{1\mathbf{k}\alpha}$$

$$+ \int d^{2}\mathbf{r} \left\{ s |\Phi(\mathbf{r})|^{2} + \left[ g + \mathbf{g}'(\mathbf{r}) \right] c_{\alpha}^{\dagger}(\mathbf{r}) f_{1\alpha}(\mathbf{r}) \Phi(\mathbf{r}) + \text{H.c.}$$

$$+ K |\nabla_{\mathbf{r}} \Phi(\mathbf{r})|^{2} + u |\Phi(\mathbf{r})|^{4} + \mathbf{v}(\mathbf{r}) c_{\alpha}^{\dagger}(\mathbf{r}) c_{\alpha}(\mathbf{r}) \right\}.$$

$$(7.6)$$

We are using the convention that quenched random variables (with no dynamics and a fixed, random dependence on r) are colored in red. There should also be a gauge field associated with Eq. (4.4) in Eq. (7.6), but we have dropped it as is does not significantly modify the critical behavior [164, 148]. The dispersions  $\varepsilon(\mathbf{k})$  and  $\varepsilon_1(\mathbf{k})$  arise from the  $t_{ij}$  and  $t_{1ij}$  in Eq. (4.3), s is the tuning parameter in Fig. 25, and we have added various in an effective action for  $\Phi$ .

The most common form of spatial disorder in studies of metallic transport is a random potential from impurities, and this realized by v(r). This spatial disorder is

averaged over after assuming it is uncorrelated at different points in space

$$\overline{v(\mathbf{r})} = 0$$
 ,  $\overline{v(\mathbf{r})v(\mathbf{r}')} = v^2 \delta(\mathbf{r} - \mathbf{r}')$ . (7.7)

One of the main new points made in Refs. [164, 58], as we will see in Section 7.2, is that random potential disorder is also not sufficient to produce a strange metal, and the effects of spatial randomness in the interactions [148] must also be considered. Spatial disorder in the Kondo exchange interaction  $J_K$  in Eq. (4.1) translates into the spatially random Yukawa coupling  $g'(\mathbf{r})$  which we take to obey the disorder average

$$\overline{g'(\mathbf{r})} = 0$$
 ,  $\overline{g'(\mathbf{r})g'(\mathbf{r}')} = g'^2 \delta(\mathbf{r} - \mathbf{r}')$ . (7.8)

In the underlying electronic model, the exchange  $J_K \sim t^2/U$ , where t is some hopping—so randomness in t (which is a form of random potential disorder) translates to randomness in  $J_K$ , and hence in the Yukawa coupling. We can also see that upon integrating out the fermions, the coupling  $g'(\mathbf{r})$  generates spatial randomness in s. The latter is usually identified as 'Harris disorder', associated with spatial randomness in the position of the phase transition. But as long as we are in a self-averaging regime, the lesson from the WES-SYK model is that it is more convenient to keep the randomness in the Yukawa coupling. Moreover, we can transfer random mass disorder to random Yukawa coupling disorder simply by rescaling  $\Phi$ : so keeping it in  $g'(\mathbf{r})$  is equivalent to working in the boson eigenstates of the random mass term. At very low energies, the random mass does eventually lead to boson localization and the new physics [64, 65, 66] of the 'foot', but we do not discuss that further here.

The properties of this strange metal theory will be determined by directly extending the methods used to solve the WES-SYK model. This extension can be viewed as simply solving the equations in Fig. 23, while using the propagators in  $\mathcal{L}_{\Phi}$ . Alternatively, a fictitious flavor index on all fields ranging over N values can be introduced and the large N limit taken, assuming couplings are random in this flavor space. This method yields a G- $\Sigma$ -D- $\Pi$  theory which is a direct generalization of Eq. (6.16) to Green's functions that are bilocal in both space and time

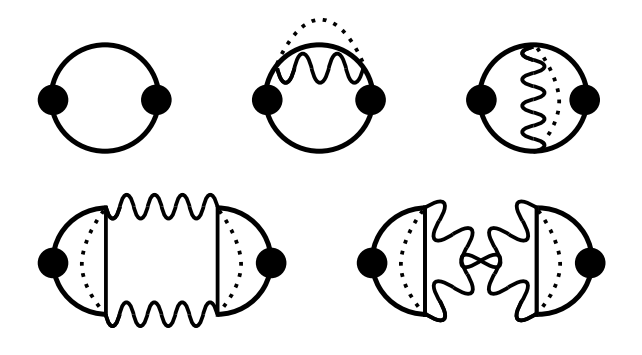
$$\mathcal{Z} = \int \mathcal{D}G \, \mathcal{D}\Sigma \, \mathcal{D}D \, \mathcal{D}\Pi \exp(-NS_{\text{all}})$$

$$S_{\text{all}} = -\ln \det(\partial_{\tau} + \varepsilon(\boldsymbol{k}) - \mu + \Sigma) + \frac{1}{2} \ln \det(-\partial_{\tau}^{2} + \boldsymbol{q}^{2} + m_{b}^{2} - \Pi)$$

$$+ \int d\tau d^{2}r \int d\tau' d^{2}r' \left[ -\Sigma(\tau', \boldsymbol{r}'; \tau, \boldsymbol{r})G(\tau, \boldsymbol{r}; \tau', \boldsymbol{r}') + \frac{1}{2}\Pi(\tau', \boldsymbol{r}'; \tau, \boldsymbol{r})D(\tau, \boldsymbol{r}; \tau', \boldsymbol{r}') + \frac{g^{2}}{2}G(\tau, \boldsymbol{r}; \tau', \boldsymbol{r}')G(\tau', \boldsymbol{r}'; \tau, \boldsymbol{r})D(\tau, \boldsymbol{r}; \tau', \boldsymbol{r}') + \frac{v^{2}}{2}G(\tau, \boldsymbol{r}; \tau', \boldsymbol{r}')G(\tau', \boldsymbol{r}'; \tau, \boldsymbol{r})\delta(\boldsymbol{r} - \boldsymbol{r}')$$

$$+ \frac{g'^{2}}{2}G(\tau, \boldsymbol{r}; \tau', \boldsymbol{r}')G(\tau', \boldsymbol{r}'; \tau, \boldsymbol{r})D(\tau, \boldsymbol{r}; \tau', \boldsymbol{r}')\delta(\boldsymbol{r} - \boldsymbol{r}') \right] . \tag{7.9}$$

For compactness of notation and analysis, we have assumed that the c and  $f_1$  fermions Green's functions are both equal to G, but it is not difficult to treat the more general



+ all ladders and bubbles.....

Figure 26. Diagrams for the conductivity for the theory  $\mathcal{L}_c + \mathcal{L}_v + \mathcal{L}_{\phi}$ .

case. Note that the spatially random couplings lead to an additional  $\delta(\mathbf{r} - \mathbf{r}')$  in their contributions arising from the disorder averages in Eqs. (7.7) and (7.8). The saddle point of Eq. (7.9) leads to equations for the Green's functions which can also be derived from Fig. 23:

$$\Sigma(\tau, \mathbf{r}) = g^{2}D(\tau, \mathbf{r})G(\tau, \mathbf{r}) + \mathbf{v}^{2}[G(\tau, \mathbf{r})\delta^{2}(\mathbf{r}) + g'^{2}G(\tau, \mathbf{r})D(\tau, \mathbf{r})\delta^{2}(\mathbf{r}),$$

$$\Pi(\tau, \mathbf{r}) = -g^{2}G(-\tau, -\mathbf{r})G(\tau, \mathbf{r}) - g'^{2}G(-\tau, \mathbf{r})G(\tau, \mathbf{r})\delta^{2}(\mathbf{r}),$$

$$G(i\omega, \mathbf{k}) = \frac{1}{i\omega - \varepsilon(\mathbf{k}) + \mu - \Sigma(i\omega, \mathbf{k})},$$

$$D(i\Omega, \mathbf{q}) = \frac{1}{\Omega^{2} + \mathbf{q}^{2} + m_{b}^{2} - \Pi(i\Omega, \mathbf{q})}.$$

$$(7.10)$$

We also need an equation to determine the boson mass  $m_b$ : this is determined by the Hartree contribution from the u term in Eq. (7.6) [165].

This is a good point to note the importance of the elastic scattering term v(r). This broadens the Fermi surfaces, and so effects from Fermi surface nesting or 'hotspots' are quenched. This is a key reason for the universality of  $L_{\Phi}$ , which applies to symmetry breaking transitions too, along with the non-symmetry breaking FL\*-FL transition we are considering. This is also the reason the difference in dispersion between c and  $f_1$  is mostly not important, and has been neglected above. However, the particle-hole asymmetry of the FL\*-FL transition is important for the thermopower, and we comment on this near Eq. (7.14).

Before discussing the solution of Eq. (7.10), the computation of response functions of fermion bilinears, such as the conductivity, is described. These can be obtained by inserting external sources into Eq. (7.9) and then taking the variational derivatives with respect to them. This leads to the graphs shown in Fig. 26, which have to evaluated with fully renormalized Green's functions.

The following subsections discuss the solutions of the equations in Eq. (7.10) and Fig. 26 for the cases without and with spatial randomness.

## 7.2. No spatial randomness

The solution of Eq. (7.10) with  $g \neq 0$ , but g' = 0 and v = 0, is considered. This corresponds to the quantum phase transition without disorder, and has been much studied in the literature. At the quantum critical point, Eq. (7.10) yields a non-Fermi liquid form for the fermion Green's function, and a Landau-damped form for the boson Green's function [166, 165]

$$\Sigma(i\omega, \mathbf{k}) \sim -i \operatorname{sgn}(\omega) |\omega|^{2/3}, \quad G(i\omega, \mathbf{k}) = \frac{1}{i\omega - \varepsilon(\mathbf{k}) - \Sigma(i\omega, \mathbf{k})}$$

$$D(i\Omega, \mathbf{q}) = \frac{1}{\Omega^2 + \mathbf{q}^2 + \gamma |\Omega|/q}, \qquad (7.11)$$

The fermion Green's function has a sharp Fermi surface in momentum space, and k in Eq. (7.11) is assumed to be close to the Fermi surface. But G is diffusive in frequency space, indicating the absence of well-defined fermionic quasiparticles.

However, an important point is that essentially none of this non-Fermi liquid structure feeds into the conductivity, which remains very similar to that of a Fermi liquid [167, 168, 169, 164, 170, 171] with the form:

$$\sigma(\omega) \sim \frac{1}{-i\omega} + |\omega|^0 + \cdots \quad (\omega^{-2/3} \text{ term has vanishing co-efficient})$$
 (7.12)

There has been a claim [172] of a  $\omega^{-2/3}$  contribution to the conductivity, but its coefficient vanishes after evaluation of all the graphs in Fig. 26 [170, 164]. This cancellation can be understood as a consequence of Kohn's theorem [173], which states that in a Galilean-invariant system only the first term of the right-hand-side of Eq. (7.12) is non-zero. A Galilean-invariant system is not considered here, but all contributions to the possible  $\omega^{-2/3}$  term arise from long-wavelength processes in the vicinity of patches of the Fermi surface, and these patches can be embedded in a system which is Galilean-invariant also at higher energies.

### 7.3. With spatial randomness

The absence of the  $\omega^{-2/3}$  term in Eq. (7.12) is a strong indication that the resolution of the strange metal problem cannot come from a clean system. There can be umklapp processes which dissipate momentum, but these require special features of the Fermi surface to survive at low momentum. A theory with only potential scattering disorder as in Eq. (7.7), i.e.  $g \neq 0$ ,  $v \neq 0$ , but g' = 0, is also not sufficient [164, 174]: it leads to marginal Fermi-liquid behavior in the electron self energy, but no strange metal behavior in transport. So for a generic and universal theory of strange metals, the influence of disorder with g, g', and v all non-zero should be considered. The solution of Eq. (7.10) yields a boson Green's function which has a diffusive form at the critical point [175]

$$D(i\Omega, \mathbf{q}) \sim \frac{1}{\mathbf{q}^2 + \gamma |\Omega|}.$$
 (7.13)

This is a good point to mention, in passing, a special feature of the FL\*-FL transition, not shared by phase transitions of two-dimensional metals with symmetry

breaking order parameters. The  $\Phi$  propagator of the FL\*-FL transition is sensitive to particle-hole asymmetry, as it also carries electrical charge (for  $\mathcal{L}_{\Phi}$ , the asymmetry requires  $\varepsilon(\mathbf{k}) \neq \varepsilon_1(\mathbf{k})$ ). This allows a more general form for the boson propagator than Eq. (7.13) [148, 60]

$$D(i\Omega, \mathbf{q}) \sim \frac{1}{\mathbf{q}^2 + \gamma |\Omega| - i\bar{\gamma}\Omega}$$
 (7.14)

The  $\bar{\gamma}$  term is responsible for the singular thermopower response, as discussed in Ref. [60], and this connects to observations on Fermi volume changing transitions in cuprates [61, 62] and heavy-fermion compounds [63].

Inserting Eq. (7.13) or (7.14) into the fermion Green's function gives a marginal Fermi liquid form [175, 58]

$$G(\omega) \sim \frac{1}{\omega \frac{m^*(\omega)}{m} - \varepsilon(\mathbf{k}) + i\left(\frac{1}{\tau_e} + \frac{1}{\tau_{\rm in}(\omega)}\right) \operatorname{sgn}(\omega)}$$

$$\frac{1}{\tau_e} \sim \mathbf{v^2} \quad ; \quad \frac{1}{\tau_{\rm in}(\omega)} \sim \left(\frac{g^2}{\mathbf{v^2}} + \mathbf{g'^2}\right) |\omega| \quad ; \quad \frac{m^*(\omega)}{m} \sim \frac{2}{\pi} \left(\frac{g^2}{\mathbf{v^2}} + \mathbf{g'^2}\right) \ln(\Lambda/\omega) \,.$$

The expressions in the second line are schematic, and show only the dependence upon g, g' and v without numerical constants. This result matches the photoemission observations in Eq. (7.3) for  $\alpha = 1/2$ . Note that there are two distinct contributions to the singular  $|\omega|$  electron inelastic scattering rate  $1/\tau_{\rm in}$ : one from the combination of impurity scattering v with the spatially uniform interaction g [175], and the other from the spatially random interaction g' [148, 58].

Inserting these solutions for the Green's functions into the action in Eq. (7.9), gives a  $T \ln(1/T)$  specific heat [165].

Turning to the evaluation of the conductivity graphs in Fig. 26, the key property of the strange metal, the conductivity, is given by [148, 58]

$$\sigma(\omega) \sim \frac{1}{\frac{1}{\tau_{\text{trans}}(\omega)} - i\omega \frac{m_{\text{trans}}^*(\omega)}{m}}$$
 (7.16)

$$\frac{1}{\tau_{\text{trans}}(\omega)} \sim v^2 + g'^2 |\omega| \quad ; \quad \frac{m_{\text{trans}}^*(\omega)}{m} \sim \frac{2g'^2}{\pi} \ln(\Lambda/\omega) \tag{7.17}$$

This expression shows that the residual resistivity  $\rho_0$  at T=0 is determined by the elastic scattering rate  $1/\tau_e \sim v^2$ , as in a disordered Fermi liquid. The inelastic processes lead to a frequency and temperature dependence which matches precisely with the observational form in Eq. (7.2). An important feature is that of the two processes contributing to the electron inelastic scattering rate  $1/\tau_{\rm in}$  in Eq. (7.15), only one contributes to the inelastic transport rate  $1/\tau_{\rm trans}$ . The processes involving the spatially uniform interaction g and the impurity potential v cancel out in the computation of the conductivity from Fig. 26, and only those involving the spatially random interaction g' survive [58]. A consequence of this cancellation is that the constant  $\alpha$  in Eq. (7.5) approaches  $\alpha = \pi/2$  for the quasiparticle  $m^*$  in the limit  $g' \gg g$  [165], and decreases from this value as g is increased [58].

To summarize, the conductivity of the theory  $\mathcal{L}_{\Phi}$  yields the strange metal conductivity in Eq. (7.1), with  $\rho_0 \sim v^2$  and  $A \sim g'^2$ . Note that the value of g does not make a direct difference to the value of the linear-T resistivity, although it does affect the marginal Fermi liquid behavior of the electron self energy, as noted in Eq. (7.15). It is also notable that the residual resistivity and linear-T resistivity slope are determined by different sources of disorder: those in Eqs. (7.7) and (7.8) respectively. This distinction should be important in understanding trends in observations [176, 177].

We note that a full numerical solution of Eq. (7.10) at g = 0 has been presented by Li et al. [59], including results for the conductivity and the onset of superconductivity.

The key role of spatial randomness in the Yukawa coupling in this theory implies a prediction: correlated electron systems will not exhibit low T strange metal behavior in sufficiently clean samples. Evidence in support of this prediction has appeared in recent experiments on graphene: while twisted bilayer graphene has a strange metal phase [178], the much cleaner system of rhombohedral trilayer graphene does not [179].

Finally, note that a recent computation [180] of shot noise in the g'-v model yields results in agreement with observations [181]. The g'-v model has also been used to study non-linear optical response [182], and there are interesting connections to recent observations [183]

# Acknowledgments

This research was supported by NSF Grant DMR-2245246 and by the Simons Collaboration on Ultra-Quantum Matter which is a grant from the Simons Foundation (651440, S. S.).

# References

- [1] B. Keimer, S.A. Kivelson, M.R. Norman, S. Uchida and J. Zaanen, From quantum matter to high-temperature superconductivity in copper oxides, Nature 518 (2015) 179.
- [2] D.J. Scalapino, A common thread: The pairing interaction for unconventional superconductors, Reviews of Modern Physics 84 (2012) 1383 [1207.4093].
- [3] T. Senthil, S. Sachdev and M. Vojta, Fractionalized Fermi Liquids, Phys. Rev. Lett. 90 (2003) 216403 [cond-mat/0209144].
- [4] T. Senthil, M. Vojta and S. Sachdev, Weak magnetism and non-Fermi liquids near heavy-fermion critical points, Phys. Rev. B 69 (2004) 035111 [cond-mat/0305193].
- [5] A. Paramekanti and A. Vishwanath, Extending Luttinger's theorem to Z₂ fractionalized phases of matter, Phys. Rev. B 70 (2004) 245118 [cond-mat/0406619].
- [6] P. Bonderson, M. Cheng, K. Patel and E. Plamadeala, Topological Enrichment of Luttinger's Theorem, arXiv e-prints (2016) [1601.07902].
- [7] M. Christos, Z.-X. Luo, H. Shackleton, Y.-H. Zhang, M.S. Scheurer and S. Sachdev, A model of d-wave superconductivity, antiferromagnetism, and charge order on the square lattice, Proc. Nat. Acad. Sci. 120 (2023) e2302701120 [2302.07885].
- [8] C. Wang, A. Nahum, M.A. Metlitski, C. Xu and T. Senthil, Deconfined quantum critical points: symmetries and dualities, Phys. Rev. X 7 (2017) 031051 [1703.02426].
- [9] N. Read and S. Sachdev, Valence-bond and spin-Peierls ground states of low-dimensional quantum antiferromagnets, Phys. Rev. Lett. 62 (1989) 1694.

- [10] N. Read and S. Sachdev, Spin-Peierls, valence-bond solid, and Néel ground states of low-dimensional quantum antiferromagnets, Phys. Rev. B 42 (1990) 4568.
- [11] T. Senthil, A. Vishwanath, L. Balents, S. Sachdev and M.P.A. Fisher, Deconfined Quantum Critical Points, Science 303 (2004) 1490 [cond-mat/0311326].
- [12] T. Senthil, L. Balents, S. Sachdev, A. Vishwanath and M.P.A. Fisher, Quantum criticality beyond the Landau-Ginzburg-Wilson paradigm, Phys. Rev. B 70 (2004) 144407 [cond-mat/0312617].
- [13] I. Affleck and J.B. Marston, Large-n limit of the Heisenberg-Hubbard model: Implications for high-T<sub>c</sub> superconductors, Phys. Rev. B 37 (1988) 3774.
- [14] I. Affleck, Z. Zou, T. Hsu and P.W. Anderson, SU(2) gauge symmetry of the large-U limit of the Hubbard model, Phys. Rev. B 38 (1988) 745.
- [15] E. Dagotto, E. Fradkin and A. Moreo, SU(2) gauge invariance and order parameters in strongly coupled electronic systems, Phys. Rev. B 38 (1988) 2926.
- [16] P.W. Anderson, The Resonating Valence Bond State in La<sub>2</sub>CuO<sub>4</sub> and Superconductivity, Science 235 (1987) 1196.
- [17] F.C. Zhang, C. Gros, T.M. Rice and H. Shiba, A renormalised Hamiltonian approach for a resonant valence bond wavefunction, Superconductor Science and Technology 1 (1988) 36 [cond-mat/0311604].
- [18] G. Kotliar and J. Liu, Superexchange mechanism and d-wave superconductivity, Phys. Rev. B 38 (1988) 5142.
- [19] X.-G. Wen and P.A. Lee, Theory of Underdoped Cuprates, Phys. Rev. Lett. 76 (1996) 503 [cond-mat/9506065].
- [20] D.A. Ivanov and T. Senthil, Projected wave functions for fractionalized phases of quantum spin systems, Phys. Rev. B 66 (2002) 115111 [cond-mat/0204043].
- [21] P.A. Lee, N. Nagaosa and X.-G. Wen, Doping a Mott insulator: Physics of high-temperature superconductivity, Rev. Mod. Phys. 78 (2006) 17 [cond-mat/0410445].
- [22] M. Chiao, R.W. Hill, C. Lupien, L. Taillefer, P. Lambert, R. Gagnon and P. Fournier, Low-energy quasiparticles in cuprate superconductors: A quantitative analysis, Phys. Rev. B 62 (2000) 3554 [cond-mat/9910367].
- [23] S. Chatterjee and S. Sachdev, Fractionalized Fermi liquid with bosonic chargens as a candidate for the pseudogap metal, Phys. Rev. B 94 (2016) 205117 [1607.05727].
- [24] M. Christos and S. Sachdev, Emergence of nodal Bogoliubov quasiparticles across the transition from the pseudogap metal to the d-wave superconductor, npj Quantum Materials 9 (2024) 4 [2308.03835].
- [25] M.K. Chan, K.A. Schreiber, O.E. Ayala-Valenzuela, E.D. Bauer, A. Shekhter and N. Harrison, Observation of the Yamaji effect in a cuprate superconductor, arXiv e-prints (2024) arXiv:2411.10631 [2411.10631].
- [26] R.K. Kaul, A. Kolezhuk, M. Levin, S. Sachdev and T. Senthil, Hole dynamics in an antiferromagnet across a deconfined quantum critical point, Phys. Rev. B 75 (2007) 235122 [cond-mat/0702119].
- [27] J. Schmalian, D. Pines and B. Stojković, Weak Pseudogap Behavior in the Underdoped Cuprate Superconductors, Phys. Rev. Lett. 80 (1998) 3839 [cond-mat/9708238].
- [28] J. Schmalian, D. Pines and B. Stojković, Microscopic theory of weak pseudogap behavior in the underdoped cuprate superconductors: General theory and quasiparticle properties, Phys. Rev. B 60 (1999) 667 [cond-mat/9804129].
- [29] M. Ye and A.V. Chubukov, Crucial role of thermal fluctuations and vertex corrections for the magnetic pseudogap, Phys. Rev. B 108 (2023) L081118 [2306.05489].
- [30] E.K. Kokkinis and A.V. Chubukov, Pseudogap in electron-doped cuprates: thermal precursor to magnetism, arXiv e-prints (2025) arXiv:2505.11727 [2505.11727].
- [31] S.E. Sebastian and C. Proust, Quantum Oscillations in Hole-Doped Cuprates, Annual Review of Condensed Matter Physics 6 (2015) 411 [1507.01315].

- [32] P.M. Bonetti, M. Christos and S. Sachdev, Quantum oscillations in the hole-doped cuprates and the confinement of spinons, Proceedings of the National Academy of Sciences 121 (2024) e2418633121 [2405.08817].
- [33] M.R. Norman, H. Ding, M. Randeria, J.C. Campuzano, T. Yokoya, T. Takeuchi, T. Takahashi, T. Mochiku, K. Kadowaki, P. Guptasarma and D.G. Hinks, *Destruction of the Fermi surface in underdoped high-T<sub>c</sub> superconductors, Nature* 392 (1998) 157 [cond-mat/9710163].
- [34] K.M. Shen, F. Ronning, D.H. Lu, F. Baumberger, N.J.C. Ingle, W.S. Lee, W. Meevasana, Y. Kohsaka, M. Azuma, M. Takano, H. Takagi and Z.-X. Shen, Nodal Quasiparticles and Antinodal Charge Ordering in Ca<sub>2-x</sub>Na<sub>x</sub>CuO<sub>2</sub>Cl<sub>2</sub>, Science 307 (2005) 901.
- [35] H.-B. Yang, J.D. Rameau, Z.-H. Pan, G.D. Gu, P.D. Johnson, H. Claus, D.G. Hinks and T.E. Kidd, Reconstructed Fermi Surface of Underdoped Bi<sub>2</sub>Sr<sub>2</sub>CaCu<sub>2</sub>O<sub>8+δ</sub> Cuprate Superconductors, Phys. Rev. Lett. 107 (2011) 047003 [1008.3121].
- [36] S. Kunisada, S. Isono, Y. Kohama, S. Sakai, C. Bareille, S. Sakuragi, R. Noguchi, K. Kurokawa, K. Kuroda, Y. Ishida, S. Adachi, R. Sekine, T.K. Kim, C. Cacho, S. Shin, T. Tohyama, K. Tokiwa and T. Kondo, Observation of small Fermi pockets protected by clean CuO<sub>2</sub> sheets of a high-T<sub>c</sub> superconductor, Science 369 (2020) 833 [2008.07784].
- [37] K. Kurokawa, S. Isono, Y. Kohama, S. Kunisada, S. Sakai, R. Sekine, M. Okubo, M.D. Watson, T.K. Kim, C. Cacho, S. Shin, T. Tohyama, K. Tokiwa and T. Kondo, *Unveiling phase diagram of the lightly doped high-T<sub>c</sub> cuprate superconductors with disorder removed, Nature Communications* 14 (2023) 4064 [2307.07684].
- [38] S. Smit, M. Bluschke, P. Moen, N. Heinsdorf, E. Zavatti, G. Bellomia, S. Giuli, S.K.Y. Dufresne, C.T. Suen, V. Zimmermann, C. Au-Yeung, S. Zhdanovich, J.I. Dadap, M. Zonno, S. Gorovikov, H. Lee, C.-T. Kuo, J.-S. Lee, D. Song, S. Ishida, H. Eisaki, B. Keimer, M. Michiardi, I.S. Elfimov, G. Levy, D.J. Jones, M. Capone and A. Damascelli, Enhanced coherence and layer-selective charge order in a trilayer cuprate superconductor, arXiv e-prints (2025) arXiv:2506.01448 [2506.01448].
- [39] Y. He, Y. Yin, M. Zech, A. Soumyanarayanan, M.M. Yee, T. Williams, M.C. Boyer, K. Chatterjee, W.D. Wise, I. Zeljkovic, T. Kondo, T. Takeuchi, H. Ikuta, P. Mistark, R.S. Markiewicz, A. Bansil, S. Sachdev, E.W. Hudson and J.E. Hoffman, Fermi Surface and Pseudogap Evolution in a Cuprate Superconductor, Science 344 (2014) 608 [1305.2778].
- [40] K. Fujita, C.K. Kim, I. Lee, J. Lee, M.H. Hamidian, I.A. Firmo, S. Mukhopadhyay, H. Eisaki, S. Uchida, M.J. Lawler, E.A. Kim and J.C. Davis, Simultaneous Transitions in Cuprate Momentum-Space Topology and Electronic Symmetry Breaking, Science 344 (2014) 612 [1403.7788].
- [41] H. Pandey, M. Christos, P.M. Bonetti, R. Shanker, S. Sharma and S. Sachdev, Thermal SU(2) lattice gauge theory for the pseudogap and the transition to d-wave superconductivity in the cuprates, arXiv e-prints (2025) arXiv:2507.05336 [2507.05336].
- [42] J.-X. Zhang and S. Sachdev, Vortex structure in a d-wave superconductor obtained by a confinement transition from the pseudogap metal, Phys. Rev. B 110 (2024) 235120 [2406.12964].
- [43] J.E. Hoffman, E.W. Hudson, K.M. Lang, V. Madhavan, H. Eisaki, S. Uchida and J.C. Davis, A Four Unit Cell Periodic Pattern of Quasi-Particle States Surrounding Vortex Cores in Bi<sub>2</sub>Sr<sub>2</sub>CaCu<sub>2</sub>O<sub>8+δ</sub>, Science 295 (2002) 466 [cond-mat/0201348].
- [44] D. Chowdhury, A. Georges, O. Parcollet and S. Sachdev, Sachdev-Ye-Kitaev models and beyond: Window into non-Fermi liquids, Reviews of Modern Physics 94 (2022) 035004 [2109.05037].
- [45] A.M. Sengupta, Spin in a fluctuating field: The Bose(+Fermi) Kondo models, Phys. Rev. B 61 (2000) 4041 [cond-mat/9707316].
- [46] Q. Si, S. Rabello, K. Ingersent and J.L. Smith, Locally critical quantum phase transitions in strongly correlated metals, Nature 413 (2001) 804 [cond-mat/0011477].
- [47] Q. Si, S. Rabello, K. Ingersent and J.L. Smith, Local fluctuations in quantum critical metals, Phys. Rev. B 68 (2003) 115103 [cond-mat/0202414].

- [48] L. Zhu and Q. Si, Critical local-moment fluctuations in the Bose-Fermi Kondo model, Phys. Rev. B 66 (2002) 024426 [cond-mat/0204121].
- [49] Q. Si, J.H. Pixley, E. Nica, S.J. Yamamoto, P. Goswami, R. Yu and S. Kirchner, Kondo Destruction and Quantum Criticality in Kondo Lattice Systems, Journal of the Physical Society of Japan 83 (2014) 061005 [1312.0764].
- [50] A.M. Sengupta and A. Georges, Non-Fermi-liquid behavior near a T=0 spin-glass transition, Phys. Rev. B **52** (1995) 10295 [cond-mat/9504120].
- [51] S. Burdin, A. Georges and D.R. Grempel, Coherence Scale of the Kondo Lattice, Phys. Rev. Lett. 85 (2000) 1048 [cond-mat/0004043].
- [52] S. Burdin, D.R. Grempel and A. Georges, Heavy-fermion and spin-liquid behavior in a Kondo lattice with magnetic frustration, Phys. Rev. B 66 (2002) 045111 [cond-mat/0107288].
- [53] L. de Leo, M. Civelli and G. Kotliar, T=0 Heavy-Fermion Quantum Critical Point as an Orbital-Selective Mott Transition, Phys. Rev. Lett. 101 (2008) 256404 [0804.3314].
- [54] A. Gleis, S.-S.B. Lee, G. Kotliar and J. von Delft, Emergent Properties of the Periodic Anderson Model: A High-Resolution, Real-Frequency Study of Heavy-Fermion Quantum Criticality, Physical Review X 14 (2024) 041036 [2310.12672].
- [55] A. Gleis, S.-S.B. Lee, G. Kotliar and J. von Delft, Dynamical Scaling and Planckian Dissipation Due to Heavy-Fermion Quantum Criticality, Phys. Rev. Lett. 134 (2025) 106501 [2404.14079].
- [56] Y.-Y. Chang, K. Van Nguyen, K. Remund and C.-H. Chung, A mechanism for quantum-critical Planckian metal phase in high-temperature cuprate superconductors, Reports on Progress in Physics 88 (2025) 048001 [2406.14858].
- [57] Y.-Y. Chang, K. Van Nguyen, K. Remund and C.-H. Chung, Theory of universal Planckian metal in t-J model: application for high-Tc cuprate superconductors, arXiv e-prints (2025) arXiv:2506.15552 [2506.15552].
- [58] A.A. Patel, H. Guo, I. Esterlis and S. Sachdev, Universal theory of strange metals from spatially random interactions, Science 381 (2022) 790 [2203.04990].
- [59] C. Li, D. Valentinis, A.A. Patel, H. Guo, J. Schmalian, S. Sachdev and I. Esterlis, Strange Metal and Superconductor in the Two-Dimensional Yukawa-Sachdev-Ye-Kitaev Model, Phys. Rev. Lett. 133 (2024) 186502 [2406.07608].
- [60] P. Lunts, A.A. Patel and S. Sachdev, Thermopower across Fermi-volume-changing quantum phase transitions without translational symmetry breaking, arXiv e-prints (2024) arXiv:2412.15330 [2412.15330].
- [61] C. Collignon, A. Ataei, A. Gourgout, S. Badoux, M. Lizaire, A. Legros, S. Licciardello, S. Wiedmann, J.Q. Yan, J.S. Zhou, Q. Ma, B.D. Gaulin, N. Doiron-Leyraud and L. Taillefer, Thermopower across the phase diagram of the cuprate La<sub>1.6-x</sub>Nd<sub>0.4</sub>Sr<sub>x</sub>CuO<sub>4</sub>: Signatures of the pseudogap and charge density wave phases, Phys. Rev. B 103 (2021) 155102 [2011.14927].
- [62] A. Gourgout, G. Grissonnanche, F. Laliberté, A. Ataei, L. Chen, S. Verret, J.-S. Zhou, J. Mravlje, A. Georges, N. Doiron-Leyraud and L. Taillefer, Seebeck Coefficient in a Cuprate Superconductor: Particle-Hole Asymmetry in the Strange Metal Phase and Fermi Surface Transformation in the Pseudogap Phase, Phys. Rev. X 12 (2022) 011037.
- [63] Z.-Y. Cao, H. Wang, C.-K. Park, T.B. Park, H. Jang, S. Seo, S.-I. Kim and T. Park, Thermoelectric signature of quantum criticality in the heavy-fermion superconductor CeRhIn<sub>5</sub>, arXiv e-prints (2024) arXiv:2408.13604 [2408.13604].
- [64] A.A. Patel, P. Lunts and S. Sachdev, Localization of overdamped bosonic modes and transport in strange metals, Proceedings of the National Academy of Science 121 (2024) e2402052121 [2312.06751].
- [65] A.A. Patel, P. Lunts and M.S. Albergo, Strange metals and planckian transport in a gapless phase from spatially random interactions, arXiv e-prints (2024) arXiv:2410.05365 [2410.05365].
- [66] S. Sachdev, The foot, the fan, and the cuprate phase diagram: Fermi-volume-changing quantum

- phase transitions, Physica C 633 (2025) 1354707 [2501.16417].
- [67] J.A. Hoyos, C. Kotabage and T. Vojta, Effects of Dissipation on a Quantum Critical Point with Disorder, Phys. Rev. Lett. 99 (2007) 230601 [0705.1865].
- [68] R.A. Cooper, Y. Wang, B. Vignolle, O.J. Lipscombe, S.M. Hayden, Y. Tanabe, T. Adachi, Y. Koike, M. Nohara, H. Takagi, C. Proust and N.E. Hussey, Anomalous Criticality in the Electrical Resistivity of La<sub>2-x</sub>Sr<sub>x</sub>CuO<sub>4</sub>, Science 323 (2009) 603.
- [69] R.L. Greene, P.R. Mandal, N.R. Poniatowski and T. Sarkar, The Strange Metal State of the Electron-Doped Cuprates, Annual Review of Condensed Matter Physics 11 (2020) 213 [1905.04998].
- [70] J. Radaelli, O.J. Lipscombe, M. Zhu, J.R. Stewart, A.A. Patel, S. Sachdev and S.M. Hayden, Critical spin fluctuations across the superconducting dome in La<sub>2-x</sub>Sr<sub>x</sub>CuO<sub>4</sub>, arXiv e-prints (2025) arXiv:2503.13600 [2503.13600].
- [71] D.P. Arovas and A. Auerbach, Functional integral theories of low-dimensional quantum Heisenberg models, Phys. Rev. B 38 (1988) 316.
- [72] S. Sachdev and R. Jalabert, Effective lattice models for two-dimensional antiferromagnets, Modern Physics Letters B 04 (1990) 1043.
- [73] J. Alicea, Monopole quantum numbers in the staggered flux spin liquid, Phys. Rev. B **78** (2008) 035126 [0804.0786].
- [74] X.-Y. Song, Y.-C. He, A. Vishwanath and C. Wang, From spinon band topology to the symmetry quantum numbers of monopoles in Dirac spin liquids, Phys. Rev. X 10 (2020) 011033 [1811.11182].
- [75] Y. Ran and X.-G. Wen, Continuous quantum phase transitions beyond Landau's paradigm in a large-N spin model, cond-mat/0609620.
- [76] A.G. Abanov and P.B. Wiegmann, Theta terms in nonlinear sigma models, Nucl. Phys. B 570 (2000) 685 [hep-th/9911025].
- [77] J. Lee and S. Sachdev, Wess-Zumino-Witten Terms in Graphene Landau Levels, Phys. Rev. Lett. 114 (2015) 226801 [1411.5684].
- [78] A. Tanaka and X. Hu, Many-Body Spin Berry Phases Emerging from the π-Flux State: Competition between Antiferromagnetism and the Valence-Bond-Solid State, Phys. Rev. Lett. 95 (2005) 036402 [cond-mat/0501365].
- [79] T. Senthil and M.P.A. Fisher, Competing orders, nonlinear sigma models, and topological terms in quantum magnets, Phys. Rev. B 74 (2006) 064405 [cond-mat/0510459].
- [80] Z. Zhou, L. Hu, W. Zhu and Y.-C. He, SO(5) Deconfined Phase Transition under the Fuzzy-Sphere Microscope: Approximate Conformal Symmetry, Pseudo-Criticality, and Operator Spectrum, Physical Review X 14 (2024) 021044 [2306.16435].
- [81] A. Nahum, P. Serna, J.T. Chalker, M. Ortuño and A.M. Somoza, Emergent SO(5) Symmetry at the Néel to Valence-Bond-Solid Transition, Phys. Rev. Lett. 115 (2015) 267203 [1508.06668].
- [82] F. Ferrari and F. Becca, Gapless spin liquid and valence-bond solid in the J<sub>1</sub>-J<sub>2</sub> Heisenberg model on the square lattice: Insights from singlet and triplet excitations, Phys. Rev. B 102 (2020) 014417 [2005.12941].
- [83] Y. Nomura and M. Imada, Dirac-Type Nodal Spin Liquid Revealed by Refined Quantum Many-Body Solver Using Neural-Network Wave Function, Correlation Ratio, and Level Spectroscopy, Physical Review X 11 (2021) 031034 [2005.14142].
- [84] B.-B. Chen, X. Zhang, Y. Wang, K. Sun and Z.Y. Meng, Phases of (2+1)D SO(5) Nonlinear Sigma Model with a Topological Term on a Sphere: Multicritical Point and Disorder Phase, Phys. Rev. Lett. 132 (2024) 246503 [2307.05307].
- [85] W.-Y. Liu, D. Poilblanc, S.-S. Gong, W.-Q. Chen and Z.-C. Gu, Tensor network study of the spin-1/2 square-lattice J<sub>1</sub>-J<sub>2</sub>-J<sub>3</sub> model: Incommensurate spiral order, mixed valence-bond solids, and multicritical points, Phys. Rev. B 109 (2024) 235116 [2309.13301].
- [86] S.M. Chester and N. Su, Bootstrapping Deconfined Quantum Tricriticality, Phys. Rev. Lett. 132 (2024) 111601 [2310.08343].

- [87] J. Takahashi, H. Shao, B. Zhao, W. Guo and A.W. Sandvik, SO(5) multicriticality in two-dimensional quantum magnets, arXiv e-prints (2024) arXiv:2405.06607 [2405.06607].
- [88] M. Christos, H. Shackleton, S. Sachdev and Z.-X. Luo, Deconfined quantum criticality of nodal d -wave superconductivity, Néel order, and charge order on the square lattice at half-filling, Physical Review Research 6 (2024) 033018 [2402.09502].
- [89] F.F. Assaad, M. Imada and D.J. Scalapino, Quantum Transition between an Antiferromagnetic Mott Insulator and  $d_{x^2-y^2}$  Superconductor in Two Dimensions, Phys. Rev. Lett. 77 (1996) 4592 [cond-mat/9609034].
- [90] X.Y. Xu and T. Grover, Competing Nodal d-Wave Superconductivity and Antiferromagnetism, Phys. Rev. Lett. 126 (2021) 217002 [2009.06644].
- [91] J.M. Luttinger, Fermi Surface and Some Simple Equilibrium Properties of a System of Interacting Fermions, Phys. Rev. 119 (1960) 1153.
- [92] M. Oshikawa, Topological Approach to Luttinger's Theorem and the Fermi Surface of a Kondo Lattice, Phys. Rev. Lett. 84 (2000) 3370 [cond-mat/0002392].
- [93] D.V. Else, R. Thorngren and T. Senthil, Non-Fermi Liquids as Ersatz Fermi Liquids: General Constraints on Compressible Metals, Physical Review X 11 (2021) 021005 [2007.07896].
- [94] S. Sachdev, Quantum Phases of Matter, Cambridge University Press, Cambridge, UK, 1 ed. (2023).
- [95] N. Read and D.M. Newns, A new functional integral formalism for the degenerate Anderson model, Journal of Physics C: Solid State Physics 16 (1983) L1055.
- [96] P. Coleman, New approach to the mixed-valence problem, Phys. Rev. B 29 (1984) 3035.
- [97] A. Auerbach and K. Levin, Kondo Bosons and the Kondo Lattice: Microscopic Basis for the Heavy Fermi Liquid, Phys. Rev. Lett. 57 (1986) 877.
- [98] A.J. Millis and P.A. Lee, Large-orbital-degeneracy expansion for the lattice Anderson model, Phys. Rev. B 35 (1987) 3394.
- [99] M. Punk, A. Allais and S. Sachdev, A quantum dimer model for the pseudogap metal, Proc. Nat. Acad. Sci. 112 (2015) 9552 [1501.00978].
- [100] R.K. Kaul, Y.B. Kim, S. Sachdev and T. Senthil, Algebraic charge liquids, Nature Physics 4 (2008) 28 [0706.2187].
- [101] Y. Qi and S. Sachdev, Effective theory of Fermi pockets in fluctuating antiferromagnets, Phys. Rev. B 81 (2010) 115129 [0912.0943].
- [102] B. Lau, M. Berciu and G.A. Sawatzky, High-Spin Polaron in Lightly Doped CuO<sub>2</sub> Planes, Phys. Rev. Lett. 106 (2011) 036401 [1010.1867].
- [103] E.G. Moon and S. Sachdev, Underdoped cuprates as fractionalized Fermi liquids: Transition to superconductivity, Phys. Rev. B 83 (2011) 224508 [1010.4567].
- [104] B. Lau, M. Berciu and G.A. Sawatzky, Computational approach to a doped antiferromagnet: Correlations between two spin polarons in the lightly doped CuO<sub>2</sub> plane, Phys. Rev. B 84 (2011) 165102 [1107.4141].
- [105] M. Punk and S. Sachdev, Fermi surface reconstruction in hole-doped t-J models without long-range antiferromagnetic order, Phys. Rev. B 85 (2012) 195123 [1202.4023].
- [106] F. Grusdt, M. Kánasz-Nagy, A. Bohrdt, C.S. Chiu, G. Ji, M. Greiner, D. Greif and E. Demler, Parton Theory of Magnetic Polarons: Mesonic Resonances and Signatures in Dynamics, Physical Review X 8 (2018) 011046 [1712.01874].
- [107] C.S. Chiu, G. Ji, A. Bohrdt, M. Xu, M. Knap, E. Demler, F. Grusdt, M. Greiner and D. Greif, String patterns in the doped Hubbard model, Science 365 (2019) 251 [1810.03584].
- [108] F. Grusdt, E. Demler and A. Bohrdt, Pairing of holes by confining strings in antiferromagnets, SciPost Physics 14 (2023) 090 [2210.02321].
- [109] H. Schlömer, U. Schollwöck, A. Bohrdt and F. Grusdt, Kinetic-to-magnetic frustration crossover and linear confinement in the doped triangular t - J model, Phys. Rev. B 110 (2024) L041117 [2305.02342].
- [110] J.H. Nyhegn, K. Knakkergaard Nielsen, L. Balents and G.M. Bruun, Spin-charge bound states

- and emerging fermions in a quantum spin liquid, arXiv e-prints (2025) arXiv:2507.02508 [2507.02508].
- [111] A. Nikolaenko, J. von Milczewski, D.G. Joshi and S. Sachdev, Spin density wave, Fermi liquid, and fractionalized phases in a theory of antiferromagnetic metals using paramagnons and bosonic spinons, Phys. Rev. B 108 (2023) 045123 [2211.10452].
- [112] Y.-H. Zhang and S. Sachdev, From the pseudogap metal to the Fermi liquid using ancilla qubits, Physical Review Research 2 (2020) 023172 [2001.09159].
- [113] Y.-H. Zhang and S. Sachdev, Deconfined criticality and ghost Fermi surfaces at the onset of antiferromagnetism in a metal, Phys. Rev. B 102 (2020) 155124 [2006.01140].
- [114] T. Müller, R. Thomale, S. Sachdev and Y. Iqbal, Polaronic correlations from optimized ancilla wave functions for the Fermi-Hubbard model, Proceedings of the National Academy of Science 122 (2025) e2504261122 [2408.01492].
- [115] H. Shackleton and S. Zhang, Emergent polaronic correlations in doped spin liquids, arXiv e-prints (2024) arXiv:2408.02190 [2408.02190].
- [116] B. Zhou, H.-K. Jin and Y.-H. Zhang, Variational wavefunction for Mott insulator at finite U using ancilla qubits, arXiv e-prints (2024) arXiv:2409.07512 [2409.07512].
- [117] A. Nikolaenko, M. Tikhanovskaya, S. Sachdev and Y.-H. Zhang, Small to large Fermi surface transition in a single band model, using randomly coupled ancillas, Phys. Rev. B 103 (2021) 235138 [2103.05009].
- [118] E. Mascot, A. Nikolaenko, M. Tikhanovskaya, Y.-H. Zhang, D.K. Morr and S. Sachdev, Electronic spectra with paramagnon fractionalization in the single-band Hubbard model, Phys. Rev. B 105 (2022) 075146 [2111.13703].
- [119] K.M. Shen, F. Ronning, D.H. Lu, F. Baumberger, N.J.C. Ingle, W.S. Lee, W. Meevasana, Y. Kohsaka, M. Azuma, M. Takano, H. Takagi and Z.-X. Shen, Nodal Quasiparticles and Antinodal Charge Ordering in Ca<sub>2-x</sub>Na<sub>x</sub>CuO<sub>2</sub>Cl<sub>2</sub>, Science 307 (2005) 901.
- [120] B. Vignolle, A. Carrington, R.A. Cooper, M.M.J. French, A.P. Mackenzie, C. Jaudet, D. Vignolles, C. Proust and N.E. Hussey, Quantum oscillations in an overdoped high-T<sub>c</sub> superconductor, Nature 455 (2008) 952.
- [121] L. Zhang and J.-W. Mei, Quantum oscillation as diagnostics of pseudogap state in underdoped cuprates, Europhysics Letters 114 (2016) 47008 [1411.2098].
- [122] Y. Fang, G. Grissonnanche, A. Legros, S. Verret, F. Laliberté, C. Collignon, A. Ataei, M. Dion, J. Zhou, D. Graf, M.J. Lawler, P.A. Goddard, L. Taillefer and B.J. Ramshaw, Fermi surface transformation at the pseudogap critical point of a cuprate superconductor, Nature Physics 18 (2022) 558 [2004.01725].
- [123] M. Le Tacon, G. Ghiringhelli, J. Chaloupka, M.M. Sala, V. Hinkov, M.W. Haverkort, M. Minola, M. Bakr, K.J. Zhou, S. Blanco-Canosa, C. Monney, Y.T. Song, G.L. Sun, C.T. Lin, G.M. De Luca, M. Salluzzo, G. Khaliullin, T. Schmitt, L. Braicovich and B. Keimer, Intense paramagnon excitations in a large family of high-temperature superconductors, Nature Physics 7 (2011) 725 [1106.2641].
- [124] H.C. Robarts, M. Barthélemy, K. Kummer, M. García-Fernández, J. Li, A. Nag, A.C. Walters, K.J. Zhou and S.M. Hayden, Anisotropic damping and wave vector dependent susceptibility of the spin fluctuations in La<sub>2-x</sub>Sr<sub>x</sub>CuO<sub>4</sub> studied by resonant inelastic x-ray scattering, Phys. Rev. B 100 (2019) 214510 [1908.03086].
- [125] F. Ferrari and F. Becca, Spectral signatures of fractionalization in the frustrated Heisenberg model on the square lattice, Phys. Rev. B 98 (2018) 100405 [1805.09287].
- [126] S. Sachdev, Quantum statistical mechanics of the Sachdev-Ye-Kitaev model and charged black holes, International Journal of Modern Physics B 38 (2024) 2430003 [2304.13744].
- [127] L.E. Anderson, A. Laitinen, A. Zimmerman, T. Werkmeister, H. Shackleton, A. Kruchkov, T. Taniguchi, K. Watanabe, S. Sachdev and P. Kim, Magneto-Thermoelectric Transport in Graphene Quantum Dot with Strong Correlations, Phys. Rev. Lett. 132 (2024) 246502 [2401.08050].

- [128] A. Georges, O. Parcollet and S. Sachdev, Quantum fluctuations of a nearly critical Heisenberg spin glass, Phys. Rev. B 63 (2001) 134406 [cond-mat/0009388].
- [129] S. Sachdev, Bekenstein-Hawking Entropy and Strange Metals, Phys. Rev. X 5 (2015) 041025 [1506.05111].
- [130] A. Kitaev and S.J. Suh, The soft mode in the Sachdev-Ye-Kitaev model and its gravity dual, Journal of High Energy Physics 05 (2018) 183 [1711.08467].
- [131] J. Maldacena and D. Stanford, Remarks on the Sachdev-Ye-Kitaev model, Phys. Rev. D 94 (2016) 106002 [1604.07818].
- [132] S. Sachdev and J. Ye, Gapless spin-fluid ground state in a random quantum Heisenberg magnet, Phys. Rev. Lett. 70 (1993) 3339 [cond-mat/9212030].
- [133] O. Parcollet and A. Georges, Non-Fermi-liquid regime of a doped Mott insulator, Phys. Rev. B 59 (1999) 5341 [cond-mat/9806119].
- [134] D. Chowdhury, A. Georges, O. Parcollet and S. Sachdev, Sachdev-Ye-Kitaev models and beyond: Window into non-Fermi liquids, Rev. Mod. Phys. 94 (2022) 035004 [2109.05037].
- [135] J.S. Cotler, G. Gur-Ari, M. Hanada, J. Polchinski, P. Saad, S.H. Shenker, D. Stanford, A. Streicher and M. Tezuka, Black Holes and Random Matrices, JHEP 05 (2017) 118 [1611.04650].
- [136] D. Bagrets, A. Altland and A. Kamenev, Power-law out of time order correlation functions in the SYK model, Nucl. Phys. B 921 (2017) 727 [1702.08902].
- [137] D. Stanford and E. Witten, Fermionic Localization of the Schwarzian Theory, Journal of High Energy Physics 10 (2017) 008 [1703.04612].
- [138] Y. Gu, A. Kitaev, S. Sachdev and G. Tarnopolsky, Notes on the complex Sachdev-Ye-Kitaev model, Journal of High Energy Physics **02** (2020) 157 [1910.14099].
- [139] W. Fu, D. Gaiotto, J. Maldacena and S. Sachdev, Supersymmetric Sachdev-Ye-Kitaev models, Phys. Rev. D 95 (2017) 026009 [1610.08917].
- [140] L. Pauling, The Structure and Entropy of Ice and of Other Crystals with Some Randomness of Atomic Arrangement, Journal of the American Chemical Society 57 (1935) 2680.
- [141] J. Maldacena, S.H. Shenker and D. Stanford, A bound on chaos, JHEP 08 (2016) 106 [1503.01409].
- [142] J. Murugan, D. Stanford and E. Witten, More on Supersymmetric and 2d Analogs of the SYK Model, JHEP 08 (2017) 146 [1706.05362].
- [143] A.A. Patel and S. Sachdev, Critical strange metal from fluctuating gauge fields in a solvable random model, Phys. Rev. B 98 (2018) 125134 [1807.04754].
- [144] E. Marcus and S. Vandoren, A new class of SYK-like models with maximal chaos, JHEP **01** (2019) 166 [1808.01190].
- [145] Y. Wang, Solvable Strong-coupling Quantum Dot Model with a Non-Fermi-liquid Pairing Transition, Phys. Rev. Lett. 124 (2020) 017002 [1904.07240].
- [146] I. Esterlis and J. Schmalian, Cooper pairing of incoherent electrons: an electron-phonon version of the Sachdev-Ye-Kitaev model, Phys. Rev. B 100 (2019) 115132 [1906.04747].
- [147] Y. Wang and A.V. Chubukov, Quantum Phase Transition in the Yukawa-SYK Model, Phys. Rev. Res. 2 (2020) 033084 [2005.07205].
- [148] E.E. Aldape, T. Cookmeyer, A.A. Patel and E. Altman, Solvable theory of a strange metal at the breakdown of a heavy Fermi liquid, Phys. Rev. B 105 (2022) 235111 [2012.00763].
- [149] W. Wang, A. Davis, G. Pan, Y. Wang and Z.Y. Meng, Phase diagram of the spin-1/2 Yukawa-Sachdev-Ye-Kitaev model: Non-Fermi liquid, insulator, and superconductor, Phys. Rev. B 103 (2021) 195108 [2102.10755].
- [150] D. Valentinis, G.A. Inkof and J. Schmalian, Correlation between phase stiffness and condensation energy across the non-Fermi to Fermi-liquid crossover in the Yukawa-Sachdev-Ye-Kitaev model on a lattice, Phys. Rev. Res. 5 (2023) 043007 [2302.13134].
- [151] D. Valentinis, G.A. Inkof and J. Schmalian, BCS to incoherent superconductivity crossovers in the Yukawa-SYK model on a lattice, arXiv e-prints (2023) [2302.13138].

- [152] H. Hosseinabadi, S.P. Kelly, J. Schmalian and J. Marino, Thermalization of Non-Fermi Liquid Electron-Phonon Systems: Hydrodynamic Relaxation of the Yukawa-SYK Model, arXiv e-prints (2023) [2306.03898].
- [153] S.A. Hartnoll and A.P. Mackenzie, Colloquium: Planckian dissipation in metals, Rev. Mod. Phys. 94 (2022) 041002 [2107.07802].
- [154] X.-Y. Song, C.-M. Jian and L. Balents, Strongly Correlated Metal Built from Sachdev-Ye-Kitaev Models, Phys. Rev. Lett. 119 (2017) 216601 [1705.00117].
- [155] A.A. Patel, J. McGreevy, D.P. Arovas and S. Sachdev, Magnetotransport in a model of a disordered strange metal, Phys. Rev. X 8 (2018) 021049 [1712.05026].
- [156] D. Chowdhury, Y. Werman, E. Berg and T. Senthil, Translationally invariant non-Fermi liquid metals with critical Fermi-surfaces: Solvable models, Phys. Rev. X 8 (2018) 031024 [1801.06178].
- [157] M.R. Norman and A.V. Chubukov, *High-frequency behavior of the infrared conductivity of cuprates*, *Phys. Rev. B* **73** (2006) 140501 [cond-mat/0511584].
- [158] B. Michon, C. Berthod, C.W. Rischau, A. Ataei, L. Chen, S. Komiya, S. Ono, L. Taillefer, D. van der Marel and A. Georges, Reconciling scaling of the optical conductivity of cuprate superconductors with Planckian resistivity and specific heat, Nature Communications 14 (2023) 3033 [2205.04030].
- [159] T.J. Reber, X. Zhou, N.C. Plumb, S. Parham, J.A. Waugh, Y. Cao, Z. Sun, H. Li, Q. Wang, J.S. Wen, Z.J. Xu, G. Gu, Y. Yoshida, H. Eisaki, G.B. Arnold and D.S. Dessau, A unified form of low-energy nodal electronic interactions in hole-doped cuprate superconductors, Nature Communications 10 (2019) 5737.
- [160] C.M. Varma, P.B. Littlewood, S. Schmitt-Rink, E. Abrahams and A.E. Ruckenstein, Phenomenology of the normal state of Cu-O high-temperature superconductors, Phys. Rev. Lett. 63 (1989) 1996.
- [161] J.A.N. Bruin, H. Sakai, R.S. Perry and A.P. Mackenzie, Similarity of Scattering Rates in Metals Showing T-Linear Resistivity, Science 339 (2013) 804.
- [162] A. Legros, S. Benhabib, W. Tabis, F. Laliberté, M. Dion, M. Lizaire, B. Vignolle, D. Vignolles, H. Raffy, Z.Z. Li, P. Auban-Senzier, N. Doiron-Leyraud, P. Fournier, D. Colson, L. Taillefer and C. Proust, *Universal T-linear resistivity and Planckian dissipation in overdoped cuprates*, Nature Physics 15 (2019) 142 [1805.02512].
- [163] G. Grissonnanche, Y. Fang, A. Legros, S. Verret, F. Laliberté, C. Collignon, J. Zhou, D. Graf, P.A. Goddard, L. Taillefer and B.J. Ramshaw, *Linear-in temperature resistivity from an isotropic Planckian scattering rate*, Nature 595 (2021) 667 [2011.13054].
- [164] H. Guo, A.A. Patel, I. Esterlis and S. Sachdev, Large-N theory of critical Fermi surfaces. II. Conductivity, Phys. Rev. B 106 (2022) 115151 [2207.08841].
- [165] I. Esterlis, H. Guo, A.A. Patel and S. Sachdev, Large N theory of critical Fermi surfaces, Phys. Rev. B 103 (2021) 235129 [2103.08615].
- [166] P.A. Lee, Gauge field, Aharonov-Bohm flux, and high-T<sub>c</sub> superconductivity, Phys. Rev. Lett. **63** (1989) 680.
- [167] H.K. Pal, V.I. Yudson and D.L. Maslov, Resistivity of non-Galilean-invariant Fermi- and non-Fermi liquids, Lithuanian Journal of Physics and Technical Sciences 52 (2012) 142 [1204.3591].
- [168] D.L. Maslov and A.V. Chubukov, Optical response of correlated electron systems, Reports on Progress in Physics 80 (2017) 026503 [1608.02514].
- [169] A.V. Chubukov and D.L. Maslov, Optical conductivity of a two-dimensional metal near a quantum critical point: The status of the extended Drude formula, Phys. Rev. B 96 (2017) 205136 [1707.07352].
- [170] Z.D. Shi, D.V. Else, H. Goldman and T. Senthil, Loop current fluctuations and quantum critical transport, SciPost Phys. 14 (2023) 113 [2208.04328].
- [171] H. Guo, D. Valentinis, J. Schmalian, S. Sachdev and A.A. Patel, Cyclotron resonance and

- quantum oscillations of critical Fermi surfaces, arXiv e-prints (2023) [2308.01956].
- [172] Y.B. Kim, A. Furusaki, X.-G. Wen and P.A. Lee, Gauge-invariant response functions of fermions coupled to a gauge field, Phys. Rev. B 50 (1994) 17917 [cond-mat/9405083].
- [173] W. Kohn, Cyclotron Resonance and de Haas-van Alphen Oscillations of an Interacting Electron Gas, Phys. Rev. 123 (1961) 1242.
- [174] T.C. Wu, Y. Liao and M.S. Foster, Quantum interference of hydrodynamic modes in a dirty marginal Fermi liquid, Phys. Rev. B 106 (2022) 155108 [2206.01762].
- [175] B.I. Halperin, P.A. Lee and N. Read, Theory of the half-filled Landau level, Phys. Rev. B 47 (1993) 7312.
- [176] T.R. Chien, Z.Z. Wang and N.P. Ong, Effect of Zn impurities on the normal-state Hall angle in single-crystal YBa<sub>2</sub>Cu<sub>3-x</sub>Zn<sub>x</sub>O<sub>7- $\delta$ </sub>, Phys. Rev. Lett. **67** (1991) 2088.
- [177] J. Gopalakrishnan, C. Shivakumara and V. Manivannan, Superconducting thallium cuprates obtained by substitution of copper for thallium in the double-thallium layer cuprate (Tl2212), Materials Research Bulletin 29 (1994) 369.
- [178] Y. Cao, D. Chowdhury, D. Rodan-Legrain, O. Rubies-Bigorda, K. Watanabe, T. Taniguchi, T. Senthil and P. Jarillo-Herrero, Strange Metal in Magic-Angle Graphene with near Planckian Dissipation, Phys. Rev. Lett. 124 (2020) 076801 [1901.03710].
- [179] H. Zhou, T. Xie, T. Taniguchi, K. Watanabe and A.F. Young, Superconductivity in rhombohedral trilayer graphene, Nature 598 (2021) 434 [2106.07640].
- [180] A. Nikolaenko, S. Sachdev and A.A. Patel, Theory of shot noise in strange metals, Physical Review Research 5 (2023) 043143 [2305.02336].
- [181] L. Chen, D.T. Lowder, E. Bakali, A.M. Andrews, W. Schrenk, M. Waas, R. Svagera, G. Eguchi, L. Prochaska, Y. Wang, C. Setty, S. Sur, Q. Si, S. Paschen and D. Natelson, Shot noise in a strange metal, Science 382 (2023) 907 [2206.00673].
- [182] S. Kryhin, S. Sachdev and P.A. Volkov, Strong non-linear response of strange metals, arXiv e-prints (2024) arXiv:2403.00062 [2403.00062].
- [183] D. Chaudhuri, D. Barbalas, F. Mahmood, J. Liang, R. Romero, III, A. Legros, X. He, H. Raffy, I. Bozovic and N.P. Armitage, Planckian dissipation, anomalous high temperature THz non-linear response and energy relaxation in the strange metal state of the cuprate superconductors, arXiv e-prints (2025) arXiv:2503.15646 [2503.15646].